

Proposal
for the
Wide Angle Shower Apparatus
(WASA)
at COSY-Jülich
”WASA at COSY”

Jülich, October 5, 2004

Corresponding authors:

Bo Höistad (bo.hoistad@tsl.uu.se)
James Ritman (j.ritman@fz-juelich.de)

Preprint version. The figures in here have reduced size and, thus, reduced quality. The original proposal can be accessed at <http://www.fz-juelich.de/ikp/wasa>.

Released October 5, 2004
Revised October 11, 2004

H.-H. Adam¹, M. Bashkanov², U. Bechstedt³, J. Bisplinghoff⁴,
D. Bogoslovski⁵, A. Bondar⁶, B. Borasoy⁴, M. Büscher³, K.-Th. Brinkmann⁷,
P. Brylski⁸, H. Calén⁹, F. Cappellaro¹⁰, V. Chernyshev¹¹, H. Clement²,
R. Czyżykiewicz⁸, E. Doroshkevich², C. Ekström⁹, W. Erven¹², G. Fäldt¹⁰,
P. Fedorets^{3,11}, K. Fransson⁹, H. Freiesleben⁷, A. Gillitzer³, F. Goldenbaum³,
D. Gotta³, V. Yu. Grishina¹³, D. Grzonka³, Yu. Gurov¹⁴, L. Gustafsson¹⁰,
J. Haidenbauer³, C. Hanhart³, M. Hartmann³, P. Hawranek⁸, V. Hejny³,
B. Höistad¹⁰, G. Ivanov⁵, M. Jacewicz¹⁰, M. Janusz⁸, L. Jarczyk⁸,
T. Johansson¹⁰, B. Kamys⁸, B. Karlsson¹⁰, G. Kemmerling¹², O. Khakimova²,
A. Khoukaz¹, K. Kilian³, S. Kistryn⁸, P. Klaja⁸, V. Kleber^{3,15}, H. Kleines¹²,
S. Kliczewski¹⁶, D. Kolev¹⁷, V.I. Komarov⁵, L. Komogorova⁵,
L. Kondratyuk¹¹, M. Kravcikova¹⁸, F. Kren², S. Krewald³, E. Kuhlmann⁷,
P. Kulessa³, S. Kullander¹⁰, A. Kupsc⁹, A. Kuznetsov⁵, M. Lesiak⁸,
P.J. Lieb¹⁹, H. Machner³, A. Magiera⁸, P. Marciniewski⁹, B. Martemyanov¹¹,
G. Martinska²⁰, V. Matveev¹¹, B. Morosov⁵, P. Moskal⁸, U.-G. Meißner^{3,4},
T. Mersmann¹, H.-P. Morsch³, M. Nekipelov³, A. Nikitin⁵, K. Nünighoff³,
W. Oelert³, H. Ohm³, C. Pauly²¹, H. Pettersson¹⁰, Y. Petukhov⁵,
C. Piskor-Ignatowicz⁸, P. Podkopal⁸, A. Povtoreyko⁵, J. Przerwa⁸, K. Pysz¹⁶,
J. Ritman³, E. Roderburg³, R. Ruber⁹, Z. Rudy⁸, T. Rozek³, S. Schadmand³,
K. Schönning¹⁰, W. Scobel²¹, T. Sefzick³, V. Serdyuk⁵, E. Shabalin¹¹,
R. Shafigullin¹⁴, A. Sibirtsev^{3,4}, M. Siemaszko²², I. Sitnik⁵, R. Siudak¹⁶,
B. Shwartz⁶, V. Sidorov⁶, T. Skorodko², M. Śmiechowicz^{3,8}, J. Smyrski⁸,
V. Sopov¹¹, J. Stepaniak²³, H. Ströher³, A. Szczurek¹⁶, A. Täschner¹,
P. Thörngren Engblom¹⁰, V. Tikhomirov⁵, R. Tsenov¹⁷, A. Turowiecki²⁴,
M. Ulicny²⁰, J. Urban²⁰, Yu. Uzikov⁵, P. Vlasov³, G.J. Wagner²,
U. Wiedner¹⁰, P. Winter³, P. Wintz³, A. Wirzba³, M. Wolke³, A. Wrońska⁸,
P. Wüstner¹², S. Wycech²³, J. Zabierowski²³, W. Zipper²², J. Zlomanczuk¹⁰,
P. Zupranski²³, K. Zvoll¹², I. Zychor²³

¹Institut für Kernphysik, Westfälische Wilhelms-Universität Münster, Germany

²Physikalisches Institut, Universität Tübingen, Germany

³Institut für Kernphysik, Forschungszentrum Jülich, Germany

⁴Helmholtz-Institut für Strahlen- und Kernphysik, Rheinische Friedrich-Wilhelms-Universität Bonn, Germany

⁵Joint Institute for Nuclear Research, Dubna, Russia

⁶Budker Institute of Nuclear Physics, Novosibirsk, Russia

⁷Institut für Kern- und Teilchenphysik, Technische Universität Dresden, Germany

⁸Institute of Physics, Jagiellonian University, Cracow, Poland

⁹The Svedberg Laboratory, Uppsala University, Sweden

¹⁰Department of Radiation Sciences, Uppsala University, Sweden

¹¹Institute of Theoretical and Experimental Physics, Moscow, Russia

¹²Zentralinstitut für Elektronik, Forschungszentrum Jülich, Germany

¹³Institute for Nuclear Research, Russian Academy of Sciences, Moscow, Russia

¹⁴Moscow Engineering Physics Institute, Moscow, Russia

¹⁵Institut für Kernphysik, Universität zu Köln, Germany

¹⁶Institute of Nuclear Physics, Polish Academy of Sciences, Cracow, Poland

¹⁷Faculty of Physics, St. Kliment Ohridski University of Sofia, Bulgaria

¹⁸Technical University Kosice, Kosice, Slovakia

¹⁹Physics Department, George Mason University, Fairfax (VA), USA

²⁰University of P.J. Safárik, Kosice, Slovakia

²¹Institut für Experimentalphysik, Universität Hamburg, Germany

²²Institute of Physics, University of Silesia, Katowice, Poland

²³The Andrzej Soltan Institute of Nuclear Studies, Świerk, Warsaw and Łódź, Poland

²⁴Institute of Experimental Physics, Warsaw University, Warsaw, Poland

Executive Summary

The document at hand describes the physics case, the key experiments proposed and the technical solution for the project “WASA at COSY”, which concerns the transfer of the WASA pellet-target and detector system from CELSIUS (TSL, Uppsala, Sweden) to COSY (FZJ, Jülich, Germany) and its installation at an internal target position.

WASA at COSY will provide unique scientific possibilities for research in hadron physics with hadronic probes, since it combines:

- COSY with its (phase-space cooled, polarized) proton and deuteron beams with energies sufficient to cover the strange quark sector including ϕ -mesons
- WASA, a close to 4π detector for both photons and charged particles

Since both COSY and WASA are operational devices, the time needed to install and commission it is short: it is anticipated that the physics program will start at the end of 2006.

The physics that will be investigated comprises:

Symmetries and symmetry breaking:

The fundamental theories of physics are based on symmetry, yet: our world is filled with asymmetry (T.D. Lee).

Finding and studying symmetries and symmetry violations in hadronic reactions will help to better understand the strong interaction. Hadron beams are particularly well suited for such investigations due to the spin- and isospin filter mechanism. In addition, it is even conceivable to search for physics beyond the Standard Model.

Hadron structure and interactions:

That [intermediate distance] scale is the richest phenomenologically, and is certainly the crux region to understand ... what QCD is really about. And at the heart of the subject is the hadron spectrum, in particular the spectrum built from light quarks. (...) Without question, there is a great need ... for a new round of experiments, especially utilizing hadron beams (J.D. Bjorken).

Finding and further investigating specific hadronic bound systems will — together with corresponding progress in theory — provide a more fundamental insight into how nature makes hadrons.

The proposal concentrates on the study of symmetry breaking as the primary objective, in particular in η and η' -decays and meson production. In addition, the potential of further studies is discussed.

An experienced and enthusiastic community of more than one hundred scientists from all over Europe and abroad has started to work for “WASA at COSY” to become a reality and is looking forward to exploit its scientific potential.

Contents

1	Introduction	1
2	Physics case	3
2.1	Primary objective:	
	Symmetries and symmetry breaking	3
2.1.1	Decays of η and η' mesons	3
2.1.2	Isospin violation in $\vec{d}d \rightarrow \alpha\pi^0$	7
2.2	Additional objectives:	
	Exotic and cryptoexotic hadron resonances	9
2.2.1	Mixing of the scalar mesons $a_0/f_0(980)$	10
2.2.2	Hyperon resonances	13
2.2.3	Pentaquarks	16
3	Key experiments	18
3.1	Not-so-rare η' decays	18
3.2	$a_0^+(980)$ production in $pp \rightarrow d\pi^+\eta$	21
3.3	Pentaquarks	25
3.4	Isospin violation in $\vec{d}d \rightarrow \alpha\pi^0$	29
3.5	a_0^0 - f_0 mixing in $pn \rightarrow d\pi^0\eta$ and $dd \rightarrow \alpha\pi^0\eta$	32
3.6	Study of hyperon resonances	32
3.7	Rare and very rare η and η' decays	34
4	Experimental facility	40
4.1	Cooler Synchrotron COSY	40
4.2	The WASA detector	41
4.2.1	Pellet target	41
4.2.2	Forward detector	43
4.2.3	Central detector	48
4.3	Modifications	58
4.3.1	Forward detector (FD)	58
4.3.2	Central detector (CD)	59
4.3.3	Cost estimates	61
4.3.4	DAQ- and Trigger-System	61
5	Project plan	67

1 Introduction

Hadron physics is concerned with one of the most difficult but also most fascinating problems in contemporary physics. It is commonly accepted that the underlying theory, Quantum Chromo Dynamics (QCD), is correct. However, very little is known about the solution of this non-linear quantum field theory in the regime of small and moderate energy scales pertinent to the matter surrounding us. QCD is characterized by two particular phenomena, confinement and chiral symmetry breaking. QCD is formulated in terms of colored quarks and gluons. These fundamental particles have never been observed as free states but only in composite systems, so called hadrons, i.e. they are confined within colorless mesons, baryons and, possibly, exotics. Furthermore, in the sector of the light up, down and strange quarks, QCD possesses an approximate chiral symmetry, which is not observed in nature but rather broken spontaneously with the appearance of almost massless Goldstone bosons. These can be identified with the lowest octet of pseudoscalar mesons. Such broken symmetries also play an important role in phenomenon of superconductivity or the Higgs mechanism, which is believed to lead to the creation masses of the quarks and leptons. The consequences of the dynamical and also the explicit chiral symmetry violation through the current quark masses in QCD can be systematically explored with effective field theory. Presumably related to these phenomena is the generation of hadron masses in QCD, e.g. the proton and the neutron are much heavier than the current quarks they are made of. In the energy regime considered here, the interaction between the quarks and gluons is highly non-linear and also non-perturbative, excluding the use of standard perturbative methods as applied e.g. in Quantum Electro Dynamics or QCD at high energies, where asymptotic freedom is the dominant feature of the theory. A deeper understanding of the structure and dynamics of hadrons, in particular their excitation spectrum, as derived from QCD would explore one of the last *terrae incognitae* of the Standard Model.

To understand complex systems such as hadrons, a variety of complementary experimental and theoretical studies are mandatory. The WASA detector at COSY offers a unique possibility to deepen our understanding of aspects connected with QCD in the non-perturbative regime through a precise study of symmetry breakings and very specific investigations of hadron structure. The η and η' decays, that vanish in the limit of equal quark masses, allow us to explore the explicit isospin symmetry breaking in QCD.

It is well established that isospin violating quark mass effects are often masked by electromagnetic corrections and thus such studies require the detection of neutral decay particles. A textbook example for this is the threshold photo-production of neutral pions off protons which has so clearly revealed the chiral loops inherent to the spontaneous chiral symmetry breaking of QCD. Through the same quark mass term of QCD, such quark mass effects also appear in systems of a few nucleons, so that dd collisions producing ${}^4\text{He}$ plus neutral Goldstone bosons at COSY energies offer yet another tool to explore this area - also because only now theoretical tools are becoming available that allow a model-independent analysis of these processes. Furthermore, precision measurements of rare η and η' decays can be used to get new limits on the breaking of the fundamental C , P and T symmetries, or combinations thereof. In addition,

reactions involving the η' might also offer insight into the elusive glue through the anomaly.

The spontaneous chiral symmetry breaking is believed to be at the heart of the mass generation in QCD. Still, this issue cannot be separated from the question: what kind of hadrons are really generated in QCD? In the course of the last year, the paradigm of the constituent quark model, i.e. the hadrons are either quark-antiquark or three quark states, has been challenged by many experiments. However, a definite picture concerning the nature of e.g. the light scalar mesons, the $a_0(980)$, $f_0(980)$, etc., the $\Lambda(1405)$ or the pentaquark, the $\Theta^+(1540)$, has not yet emerged. Evidently, if one does not understand the nature of these states and others, a true comprehension of confinement can not be achieved. WASA at COSY is capable to contribute significantly to test the models which are offered to explain these states through the precise measurements of decay chains or the coupling to other hadrons. It should be stressed that all these proposed experiments will be *precision measurements*, because only accurate data will allow to test and constrain the theory. With the advent of effective field theory methods, supplemented by coupled channel analyses, the theoretical tools of the required precision are available to analyze the data in a model-independent way, reflecting the change of paradigm in the foundations in this area of theoretical physics, that in the past has been dominated by model building. Moreover, lattice gauge theory offers prospects to confront certain observables, in particular spectroscopic issues, with ab initio calculations. A very close contact between experiment and theory is foreseen and indispensable to achieve progress in the field of hadron physics.

In this document it is proposed to perform high precision measurements of several hadronic reactions to confront the theoretical predictions sketched above. In particular, investigations of symmetry breaking in the decay of the η and η' mesons and isospin violation in the reaction $\bar{d}d \rightarrow \alpha\pi^0$ are seen to be very promising for this purpose. The combination of the detector system WASA and the COSY accelerator facility perfectly matches the requirements needed to measure these reactions. The beam energy range, the phase space cooling and the availability of (polarized) proton and deuteron beams at COSY are essential aspects for high luminosity measurements with low background of these processes. The WASA detector provides nearly full solid angle coverage for both charged and neutral particles, which is needed to for kinematically complete measurements of the multiparticle final states. Furthermore, the usage of frozen pellets of liquid hydrogen and deuterium as the target minimizes background from secondary reactions but at the same time allows high luminosity conditions. Since the development and construction of a detector system fulfilling these requirements requires a number of years, the transfer of an existing detector like WASA to COSY for these measurements will greatly reduce the lead-time until physics output can be expected.

To summarize: The challenge of hadron physics is not only to gain an understanding of QCD in the non-perturbative regime, e.g. to explain the mechanism underlying confinement, but also the possibility of unhooking the foundations of the Standard Model at low energies. The understanding of the structure of matter is intimately linked to the structure and dynamics of hadrons. Thus, hadron physics plays a central role in the whole building of physics. This is the area of research where WASA at COSY can contribute significantly as will be demonstrated in the following sections.

2 Physics case

2.1 Primary objective: Symmetries and symmetry breaking

The degrees of freedom within the Standard Model are leptons and quarks for the matter fields and gluons, photons and the weak gauge bosons. However, at low and intermediate energies only the leptons and photons play a role as dynamical degrees of freedom: W^\pm and Z^0 are too heavy and quarks and gluons are trapped inside composite objects (hadrons, glueballs, and possibly exotics). The mechanisms behind this process are confinement and spontaneous breakdown of chiral symmetry. However, through its symmetries the underlying theory is still visible. If a symmetry is spontaneously broken, there is no obvious connection between the excitation spectrum and the symmetry. The currents are still conserved and, as a consequence, the interactions of the hadrons at low energies are largely constrained. The same holds true in the presence of a small explicit symmetry breaking: in nature the chiral symmetry is broken by the non-vanishing quark masses. We will discuss in the following examples, where a study of symmetries and symmetry breaking patterns in hadronic systems allows to get insights on symmetries and symmetry breaking patterns of QCD.

2.1.1 Decays of η and η' mesons

Isospin symmetry forbidden decays $\eta(\eta') \rightarrow 3\pi$ are sensitive to isospin symmetry breaking (ISB) due to the light quark mass difference $\Delta m = m_d - m_u$, and provide an approach complementary to ISB estimates from pseudoscalar meson masses and production processes (see section 2.1.2 and [1–3]). ISB effects in these decay channels can be associated directly with Δm , since electromagnetic effects are expected to be small [4,5]. Moreover, the ratio of symmetry breaking and allowed η' decays to 3π and $\eta 2\pi$, respectively, is directly proportional to the square of Δm (see Ref. [6] and section 3.1):

Mixing between isospin eigenstates $|\tilde{\pi}^0\rangle$ and $|\tilde{\eta}\rangle$ occurs due to the non-vanishing matrix element of the quark mass contribution to the QCD Hamiltonian density $\mathcal{H}_m = m_u u\bar{u} + m_d d\bar{d} + m_s s\bar{s}$

$$\langle \tilde{\pi}^0 | \mathcal{H}_m | \tilde{\eta} \rangle = \frac{1}{\sqrt{6}} \langle (u\bar{u} - d\bar{d}) | \mathcal{H}_m | (u\bar{u} + d\bar{d} - s\bar{s}) \rangle = -\frac{1}{\sqrt{6}} \Delta m, \quad (1)$$

where SU(3) meson wave functions and a pseudoscalar singlet–octet mixing angle $\Theta_{ps} \approx -19.5^\circ$ have been employed [7]. The mixing angle $\Theta_{\pi\eta}$ for the physical states π^0 and η is related to Δm by [6, 8, 9]:

$$\begin{pmatrix} \pi^0 \\ \eta \end{pmatrix} = \begin{pmatrix} \cos \Theta_{\pi\eta} & \sin \Theta_{\pi\eta} \\ -\sin \Theta_{\pi\eta} & \cos \Theta_{\pi\eta} \end{pmatrix} \begin{pmatrix} \tilde{\pi}^0 \\ \tilde{\eta} \end{pmatrix}; \quad \sin \Theta_{\pi\eta} = \frac{\sqrt{3} \Delta m}{4(m_s - \hat{m})} \quad (2)$$

with the average light quark mass $\hat{m} = (m_u + m_d)/2$.

Measuring the ratios of isospin symmetry breaking $\eta' \rightarrow 3\pi$ decays with respect to the allowed $\eta 2\pi$ modes

$$\mathcal{R}_1 = \frac{\Gamma(\eta' \rightarrow \pi^0 \pi^0 \pi^0)}{\Gamma(\eta' \rightarrow \eta \pi^0 \pi^0)}; \quad \mathcal{R}_2 = \frac{\Gamma(\eta' \rightarrow \pi^0 \pi^+ \pi^-)}{\Gamma(\eta' \rightarrow \eta \pi^+ \pi^-)}, \quad (3)$$

the π - η mixing angle in this approach can be determined in η' decays from

$$\mathcal{R}_i = P_i \sin^2 \Theta_{\pi\eta}, \quad (4)$$

with P_i denoting phase space factors [6].

The energy dependence of hadronic decays of η and η' to pseudoscalars, i.e. $\eta(\eta') \rightarrow 3\pi$ and $\eta' \rightarrow \eta\pi\pi$, is contained in the Dalitz plot distribution of the decay products. Some of the published results obtained for slope parameters of the Dalitz plots for $\eta \rightarrow 3\pi$ [10–17] are not in agreement with each other and with theoretical predictions [18, 19]. In particular, the predicted slope parameter for the neutral decay is excluded by the most recent published data [17]. Preliminary results on both charged and neutral 3π decay modes from a high statistics measurement at the KLOE facility have recently been reported [20]. The energy dependence of hadronic decays $\eta' \rightarrow \eta 2\pi$ and $\eta' \rightarrow 3\pi$ is discussed in the ChPT framework in more detail in [19, 21]. The presently available data with highest statistics on the $\eta 2\pi$ decay mode are still inconclusive, whether Dalitz plot distributions deviate from phase space. For the $\eta' \rightarrow 3\pi$ decay, no experimental data on the Dalitz plot parameters are presently available.

Hadronic decay modes also constrain the interpretation of the scalar meson nonet: Isovector $a_0(980)$ exchange is found to dominate $\eta' \rightarrow \eta 2\pi$ [19, 22], and the experimental data are used to fix unknown scalar–pseudoscalar–pseudoscalar couplings [22]. In comparison to $\eta \rightarrow 3\pi$ decays, exchange diagrams involving $f_0(980)$ and $a_0(980)$ are expected to have a stronger influence in η' decays to the 3π channel, since the exchange particles are much closer to the mass shell [23]. The axial U(1) anomaly prevents the pseudoscalar singlet η_0 from being a Goldstone boson. The dominant contribution to the mass of the singlet state arises from the divergence of the singlet axial current, that acquires an additional term with the gluonic field strength tensor and, consequently, does not vanish in the chiral limit. Since the physical states η and η' are mixtures of the octet and singlet fields, η_8 and η_0 , respectively, the η' cannot be disentangled from the η and a proper study of η' physics requires to account for the η as well. Precision data on decays of η and η' allow to probe a variety of aspects of low-energy hadron dynamics. Experimental results can be compared with model-independent calculations of chiral perturbation theory (ChPT) with a clear theoretical connection to QCD. Two-photon decays in the η - η' system allows ChPT predictions to be tested, particularly its extension to the U(3) framework including the axial U(1) anomaly.

Radiative decays $\eta(\eta') \rightarrow 2\gamma$ and $\eta(\eta') \rightarrow \pi^+\pi^-\gamma$ test parameters of the QCD triangle and box anomalies. Two-photon decays $\eta(\eta') \rightarrow \gamma\gamma$ provide insight into the axial $U_A(1)$ anomaly of QCD, since they are determined by the pseudoscalar singlet and octet couplings to the divergences of the relevant axial-vector currents and the singlet–octet mixing angle Θ_{ps} (see section 3.7 and [24]). The latter can be constrained from radiative decays of vector (V) and pseudoscalar (P) mesons in $V(P) \rightarrow P(V)\gamma$ processes, i.e. from η' by the $\rho\gamma$ and $\omega\gamma$ decay modes. A model framework to conclude about the glue content of the η' is discussed in [25]. The two-photon decays of η and η' are furthermore well suited to confirm the number of colors in the low-energy hadronic sector to be $N_c = 3$ [26, 27]. Within a few weeks, the available statistics for radiative η' decays could be increased by two orders of magnitude at the WASA facility (Table 1).

Theoretically, the anomalous behavior of the effective action under chiral transformations is reproduced by the Wess–Zumino–Witten term of the effective Lagrangian [28, 29] which yields the major contribution to the decays $\eta(\eta') \rightarrow \gamma\gamma$. The $\pi^+\pi^-\gamma$ mode is dominated by $\eta' \rightarrow \rho\gamma$. However, the amplitude of the non-resonant $\eta' \rightarrow \pi^+\pi^-\gamma$ decay is determined both by parameters of the AVV (axialvector–vector–vector) triangle anomaly, that can be derived from radiative decays as discussed above, and by the AAAV box anomaly [28, 30–34]. On the basis of the presently available statistics, non-resonant contributions have not been unequivocally extracted (see Ref. [35, 36] and section 3.1).

Dalitz decays $\eta(\eta') \rightarrow \gamma\gamma^* \rightarrow \gamma l^+ l^-$ with $l = e, \mu$, where a time-like virtual photon converts to a lepton pair, probe the transition form factor, i.e. the electromagnetic properties of η and η' in terms of the spatial distribution of meson charge with the $l^+ l^-$ invariant mass corresponding to the four-momentum squared of the virtual photon (theoretical approaches for η decays are discussed in [33, 37]). The available data for $\eta' \rightarrow \gamma l^+ l^-$ consist of 33 ± 7 $\mu^+\mu^-\gamma$ events [38, 39]. Thus, a detailed analysis of the leptonic mass spectrum is presently not possible due to the lack of statistics. Significant progress could be made using the WASA facility at COSY (section 3.7).

The decays $\eta(\eta') \rightarrow l^+ l^- l^+ l^-$ into lepton pairs address decays via two off-shell photons and indicate whether double vector meson dominance is realized in nature. The coupling to two virtual photons is substantial for the real part of the decay amplitude to a single lepton pair, but also an important issue in kaon decays, and for the hadronic contribution to the anomalous magnetic moment of the muon [40, 41]. The corresponding $\eta\gamma^*\gamma^*$ form factor has neither been measured in the time-like nor in the space-like region (see section 3.1), a recent theoretical investigation is presented in [33].

The dominant mechanism in the leptonic decay $\eta \rightarrow e^+e^-$, which is forbidden to proceed via a single photon intermediate state, is a fourth order electromagnetic process with two virtual photons [39, 42]. The decay is additionally suppressed by helicity factors m_e/m_η at the γe^+e^- vertices. A very low branching ratio $5 \cdot 10^{-9}$ [43, 44], predicted by the Standard Model, makes the decay sensitive to contributions from non-conventional effects that would significantly increase the branching ratio (section 3.7).

The observation of CP or C violating rare decays might hint at effects from new physics beyond the Standard Model: The single conversion decay $\eta \rightarrow \pi^+\pi^-e^+e^-$ allows to search for CP violation in flavor-conserving processes beyond the Cabbibo–Kobayashi–Maskawa (CKM) mechanism [46, 47], which are not constrained by limits on the neutron electric dipole moment. A recently proposed CP violating mechanism from an interference between magnetic and electric decay amplitudes can induce a sizable linear photon polarization in the $\eta \rightarrow \pi^+\pi^-\gamma$ decay [48, 49]. The photon polarization is accessible in the associated conversion decay $\eta \rightarrow \pi^+\pi^-e^+e^-$ as an asymmetry in the angular distribution between the $\pi^+\pi^-$ and e^+e^- production planes. Similarly, this method was used to measure CP violating effects in the K^0 system in the decay $K_L \rightarrow \pi^+\pi^-e^+e^-$ [50], with an asymmetry reported as large as 14%. The

Table 1: Counting rate estimates including detector efficiencies for η (η') decays with WASA at COSY based on a luminosity of $10^{32} \text{ cm}^{-2} \text{ s}^{-1}$, with a $20 \mu\text{b}$ (300 nb) cross section in $pp \rightarrow pp\eta$ (η') at $2.250 \text{ GeV}/c$ ($3.350 \text{ GeV}/c$) beam momentum.

	Decay mode	Branching fraction Γ_i/Γ_{tot} [45]	Existing data [events]	Counting rate [evts/day]
η (semi)-leptonic	$e^+e^-\pi^+\pi^-$	$4. \frac{+14.0}{-2.7} \cdot 10^{-4}$	5	7000 ¹
	$e^+e^-e^+e^-$	$< 6.9 \cdot 10^{-5}$	-	450 ²
	e^+e^-	$< 7.7 \cdot 10^{-5}$	-	1/6 ³
	$\pi^0e^+e^-$	$< 4. \cdot 10^{-5}$	-	1/15 – 1/2 ⁴
η' hadronic	$\pi^+\pi^-\eta$	$44.3 \pm 1.5 \%$	8200	18000
	$\pi^0\pi^0\eta$	$20.9 \pm 1.2 \%$	5400	14500
	$3\pi^0$	$1.56 \pm 0.26 \cdot 10^{-3}$	130	145
	$\pi^+\pi^-\pi^0$	$< 5. \%$	-	85 ⁵
η' radiative	$\rho^0\gamma$	$29.5 \pm 1.0 \%$	9550	44000 ⁶
	$\omega\gamma$	$3.03 \pm 0.31 \%$	160	1200
	$\gamma\gamma$	$2.12 \pm 0.14 \%$	2767	17100
η' semi-leptonic	$\mu^+\mu^-\gamma$	$1.04 \pm 0.26 \cdot 10^{-4}$	33	15
	$e^+e^-\gamma$	$< 9. \cdot 10^{-4}$	-	45 ⁷

corresponding asymmetry for $\eta \rightarrow \pi^+\pi^-e^+e^-$ is expected to be at a level of 10^{-3} – 10^{-2} (see section 3.1 and [48, 49]).

A variety of decays, e.g. η (η') $\rightarrow \pi^0\pi^0\gamma$, η (η') $\rightarrow 3\pi^0\gamma$, η (η') $\rightarrow 3\gamma$, and $\eta' \rightarrow e^+e^-\pi^0$ (η) or $\eta \rightarrow e^+e^-\pi^0$ probe C-invariance, for which only moderate experimental limits exist. For the latter decays to the $e^+e^-\pi^0$ mode the dominant Standard Model — i.e. C conserving — mechanism is an intermediate state with two photons $\gamma^*\gamma^*\pi^0$ resulting in a branching ratio of $0.2 - 1.3 \cdot 10^{-8}$ [52–54] for the η decay. If C invariance is violated, the intermediate $\gamma^*\pi^0$ state with one virtual photon can contribute, increasing the branching ratio with respect to the Standard Model prediction (section 3.7).

The move of the WASA facility to COSY offers the possibility to extend the programs both on η decays at CELSIUS and on η' production dynamics at COSY. Until the end of the present data taking period at KLOE in the middle of 2005, an integral luminosity of 2000 pb^{-1} is anticipated (presently 500 pb^{-1}), corresponding to $8 \cdot 10^7$ and $4 \cdot 10^5$ fully reconstructed η and η' events, respectively, from $\phi \rightarrow \eta$ (η') γ events [56]. The KLOE data will significantly improve the presently available data set. However, the total anticipated statistics from KLOE can be reached with WASA at COSY in a period of 1 to 10 days, accord-

¹assuming the theoretical estimate of $3 \cdot 10^{-4}$ for the branching ratio [51]

²assuming $\Gamma(\eta \rightarrow e^+e^-e^+e^-)/\Gamma_{tot} = 2.52 \cdot 10^{-5}$ [51]

³Standard Model estimate $\Gamma(\eta \rightarrow e^+e^-)/\Gamma_{tot} = 5 \cdot 10^{-9}$ from $\eta \rightarrow \mu^+\mu^-$ [43, 44]

⁴Standard Model estimates $\Gamma(\eta \rightarrow \pi^0e^+e^-)/\Gamma_{tot} = 0.2 - 1.3 \cdot 10^{-8}$ [52–54]

⁵assuming $\Gamma(\eta' \rightarrow \pi^+\pi^-\pi^0) \approx \Gamma(\eta' \rightarrow 3\pi^0)$, see [19]

⁶including $\eta' \rightarrow \pi^+\pi^-\gamma$

⁷assuming $\Gamma(\eta' \rightarrow e^+e^-\gamma)/\Gamma_{tot} \approx 3 \cdot 10^{-4}$ [55]

ing to the rate estimates given in table 1, which take into account acceptance and reconstruction efficiency of the existing experimental setup of the WASA facility. Considering these future developments we concentrate on specific rare and not-so-rare decays.

Together with the decay data, new and important information will be gained on the η' -nucleon interaction. Because of the special features of the η' outlined above, this is a system of interest by itself. In addition, it is well known that final state interactions that occur subsequent to short range processes are universal. As a consequence the η' -nucleon interaction is the same in $pp \rightarrow pp\eta'$ as in $B \rightarrow \eta'pX$. Thus, the measurement of the former reaction will provide necessary information to interpret the latter one that will eventually be measured at the B factories and might shed light on the dynamics of charmless B decays [57].

2.1.2 Isospin violation in $\vec{d}d \rightarrow \alpha\pi^0$

Within the standard model there are only two sources of isospin violation, namely the electro-magnetic interaction and the differences in the masses of the lightest quarks [1,2]. Especially in situations where we are able to disentangle these two sources, the observation of isospin violation in hadronic reactions is a direct window to quark mass ratios [2,3] — quark masses themselves are not directly observable and additional information is necessary to assign a scale to these fundamental parameters of the standard model (see e.g. [58]).

Already in 1977 Weinberg predicted a huge effect (up to 30% difference in the scattering lengths for $p\pi^0$ and $n\pi^0$) of isospin violation in π^0N scattering [1]. Also the impact of soft photons was studied systematically [59–62]. Since scattering experiments with neutral pions are not feasible, in Ref. [63] it was suggested to use NN induced pion production instead⁹. The authors demonstrated that a charge symmetry breaking (CSB)¹⁰ πN seagull term (the Weinberg term), required by chiral symmetry, should be even more relevant for $A_{fb}(pn \rightarrow d\pi^0)$ — the forward-backward asymmetry in $pn \rightarrow d\pi^0$ — than $\pi - \eta$ mixing, previously believed to completely dominate this CSB observable [65].

Interest in CSB in hadronic reactions was revived recently with the successful completion of experiments for $A_{fb}(pn \rightarrow d\pi^0)$ [67] as well as $dd \rightarrow \alpha\pi^0$ ([66], see Fig. 1) close to the pion threshold. A large collaboration has formed to perform the corresponding calculations within effective field theory. First results are presented in [68]. The studies show that the relative importance of the various charge symmetry breaking effects is very different for the two reactions and a consistent investigation of both should help to further disentangle the leading CSB matrix elements.

However, open questions will remain. It is the main result of Ref. [68] that, within a plane wave calculation, the Weinberg term is suppressed due to selection rules in the reaction $dd \rightarrow \alpha\pi^0$. Thus, the lowest order that gives finite contributions is next-to-next-to leading order (NNLO). At this order there are several diagrams contributing and only a NNNLO contribution will really prove that there is a convergence in the series for this particular reaction. However, there is one more important test for the approach that will be used for the

⁹The π^0p scattering length might also be measurable in polarized neutral pion photoproduction at threshold [64].

¹⁰Charge symmetry is fulfilled, if the amplitudes are invariant under a 180 degree rotation in isospin space. CSB is thus a subclass of isospin breaking effects.

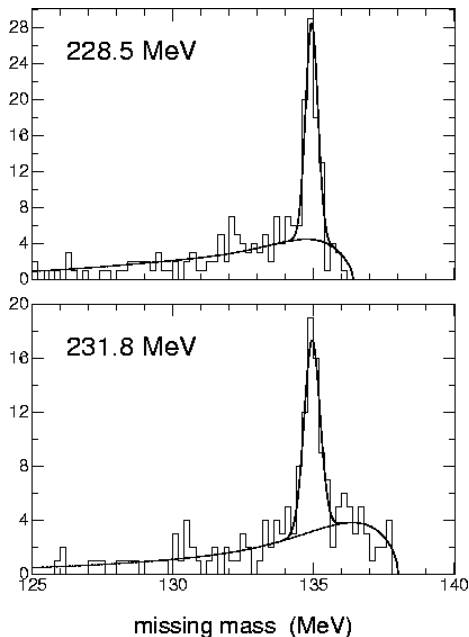


Figure 1: Experimental missing-mass spectra ($dd \rightarrow \alpha X$) from Ref. [66] revealing a clean pion peak. The smooth curves show a reproduction of the data using a Gaussian peak and a continuum. The corresponding cross sections are $\sigma = (12.7 \pm 2.2)\text{pb}$ and $\sigma = (15.1 \pm 3.1)\text{pb}$ for the lower and higher energy, respectively. The data are consistent with pure s -waves contributions.

analysis of the recent CSB experiments, namely, once the parameters are fixed the p -waves in $dd \rightarrow \alpha\pi^0$ can be predicted parameter free to leading and next-to-leading order. The IUCF experiment [66] was consistent with purely s -waves contributing. Thus, the same experiment at somewhat higher energies (but still well below the Δ region, e.g. at $Q \approx 60$ MeV) is urgently called for.

The Bose symmetry of the initial wave function strongly limits the number of allowed partial waves. As a consequence, for s -wave as well as p -wave production only a single partial wave is allowed, namely ${}^3P_0 \rightarrow s$ and ${}^5D_1 \rightarrow p$. Thus, they do not interfere in any unpolarized measurement. It would therefore be very important to measure the unpolarized total cross section as well as polarized differential observables. In addition, the analyzing powers are given by the imaginary parts of interference terms and thus would provide an important test of the initial state interaction, the ingredient to the calculations that is controlled to the smallest extent. In a plane wave treatment the analyzing powers would vanish identically.

In a further step, CSB effects involving the Δ isobar and purely nucleonic ones can be disentangled taking data in the Δ regime as well ($Q \approx 160$ MeV). This will not only be an additional important cross check of the analysis carried out previously, but gives in addition quite direct access to matrix elements difficult to get at from other experiments. However, in order to study the different partial waves polarized differential observables are as important as for the lower energy.

It is important to stress that CSB studies for few-nucleon systems can be based on recent developments in effective field theories [69–73], thus allowing for a model-independent analysis of the data.

2.2 Additional objectives: Exotic and cryptoexotic hadron resonances

The study of hadron resonances and their decays is one important approach to obtain information about quark dynamics in the non-perturbative regime of QCD. The experiments performed at the proton-antiproton storage ring LEAR (Crystal Barrel) and at the new generation of experiments in electron-positron colliders (BaBar, Belle, BES, CLEO) have found new mesons which challenge the traditional interpretation of mesons as quark-antiquark states [74, 75]. In particular, new meson candidates with the quantum numbers $J^{PC} = 1^{-+}$ cannot be generated by $q\bar{q}$ states [76, 77]. Because of this feature these states are called exotics. With the recent evidence for the existence of the so called pentaquark Θ^+ a first baryon candidate was added to this list. In addition, in the hadron spectrum there are several states with quantum numbers consistent with the quark model. However, some of their other properties are not. These states are called cryptoexotics. Both mesons, like the well known a_0 and f_0 , as well as baryons like the $\Lambda(1405)$, are discussed in the literature as candidates for this class of states. However, it is clear that additional experimental information is needed to verify or falsify these conjectures. Hadronic probes provide an experimental tool complementary to electromagnetic excitations because of different spin- and isospin selectivities. In the following we elaborate why WASA is particularly suited to investigate those exotic and cryptoexotic resonances.

In the *meson sector* the controversial states that are within the COSY energy range are the scalar-isoscalar $f_0(980)$ and the scalar-isovector $a_0(980)$. Although QCD can in principle be treated explicitly in the low momentum-transfer regime using lattice techniques [78], those are not yet in the position to make quantitative statements about light scalar states ($J^P=0^+$). Alternatively, QCD inspired models, which use effective degrees of freedom, are to be used. The constituent quark model is one of the most successful in this respect (see e.g. Ref. [79–84]). This approach treats the lightest scalar resonances $a_0/f_0(980)$ as conventional $q\bar{q}$ states. However, they have also been identified with $K\bar{K}$ molecules [85–89] or compact $qq\bar{q}\bar{q}$ states [90–92]. It has even been suggested that at masses below 1.0 GeV/c² a full nonet of 4-quark states might exist [93].

As in the reaction $dd \rightarrow \alpha\pi^0$, with WASA at COSY we can use the isospin selectivity in the $dd \rightarrow \alpha X$ transition, to model independently access the isospin-violating a_0 - f_0 mixing: the total cross section for the reaction $dd \rightarrow \alpha(\pi^0\eta)$ was shown to be directly proportional to the square of the mixing matrix element with the influence of other isospin violating effects being suppressed by one order of magnitude [94]. There is the additional possibility to extract the phase of the mixing matrix element from the forward-backward asymmetry in $pn \rightarrow da_0^0/f_0$. Both measurements will reveal independent new information about the structure of the light scalar mesons, in particular about their $K\bar{K}$ -meson content.

In the *baryon sector*, several facilities have obtained evidence for a new baryon resonance, the Θ^+ , which has achieved a three-star status in the Particle Data Group [45]. If ultimately confirmed with convincing statistics, this resonance will have a large impact on the field. The Θ^+ has positive strangeness which can only be generated by an antistrange quark as a building block of the resonance and therefore cannot be accommodated by a three quark structure. The width of the Θ^+ is unexpectedly small: while direct determinations of the width can only

give upper limits of the order of 10 MeV/c² due to limited energy resolution, indirect analysis point to a width of less than 1 MeV/c² [95–98]. Jaffe and Jain have recently pointed out the limitations such a small width imposes on the possibilities to generate the Θ^+ dynamically in the K N channel or as a Castillejo-Dalitz-Dyson pole [99].

Theorists have pointed out the possible existence of pentaquark states with narrow widths due to the formation of colored clusters about thirty years ago [100]. Recent theoretical work has focussed on the diquark degree of freedom [101]. Though the clustering of colored diquarks provides a qualitative explanation of the small width of the Θ^+ , explicit dynamical calculation require fine-tuning of the model [102]. Combining the colored diquark degree of freedom with chiral symmetry, however, produces hadrons which are stable and do not couple to the kaon-nucleon degree of freedom in the chiral limit [103–105].

The production of the Θ^+ via the reaction $pd \rightarrow p\Lambda\Theta^+$ allows access to a pure isospin $I = 0$ combination $\Lambda\Theta^+$ in the final state. This allows to obtain information complementary to the proton-proton reaction which produces the Θ^+ starting from a pure isospin $I = 1$ state.

It is well established that if there is one exotic there should be many and it is the corresponding multiplet structure that encodes essential information on the underlying substructures.

The $N^*(1710)$ has been assumed to be a member of the pentaquark antidecuplet and predictions for the branching into various decay channels have been published [106] awaiting experimental tests.

The Roper resonance, $N(1440)$, has been studied already with WASA at CELSIUS. The Roper is not a manifestly exotic state, but its broad width and small mass have caused many experimental and theoretical investigations of its structure. In the Jaffe-Wilczek diquark scenario, the Roper may be related to the Θ^+ .

In addition, the $\Lambda(1405)$ has been a candidate for a non-triplet quark structure and thus for a crypto exotic for a long time. Recent work within unitarized chiral perturbation theory suggests that the $\Lambda(1405)$ is made of two overlapping resonances with different flavor structure. This calls for detailed investigations of the decay channels as a function of the excitation energy.

Recently, the ANKE collaboration has found evidence for a hyperon $Y(1475)$ (see Fig.5 in section 2.2.2) which is not predicted by any known quark model. The PDG gives a one-star status to a surmised $\Sigma(1480)$.

2.2.1 Mixing of the scalar mesons $a_0/f_0(980)$

Both, the (isospin $I=1$) a_0 - and the ($I=0$) f_0 -resonances can decay into $K\bar{K}$, whereas in the non-strange sector the decays are into different final states according to their isospin, $a_0^\pm \rightarrow (\pi^\pm\eta)_{I=1}$, $a_0^0 \rightarrow (\pi^0\eta)_{I=1}$ and $f_0 \rightarrow (\pi^0\pi^0)_{I=0}$ or $(\pi^+\pi^-)_{I=0}$. Thus, only the non-strange decay channels have defined isospin and allow one to (model independently) discriminate between the two mesons. It is also only by measuring the non-strange decay channels that isospin violating effects can be investigated. Such measurements can be carried out with WASA at COSY for π^0 - or η -meson identification, while the strange decay channels $a_0/f_0 \rightarrow K_S K_S$ might be measured in parallel. Measurements of the $K\bar{K}$ final state with at least one charged kaon have already been performed at COSY

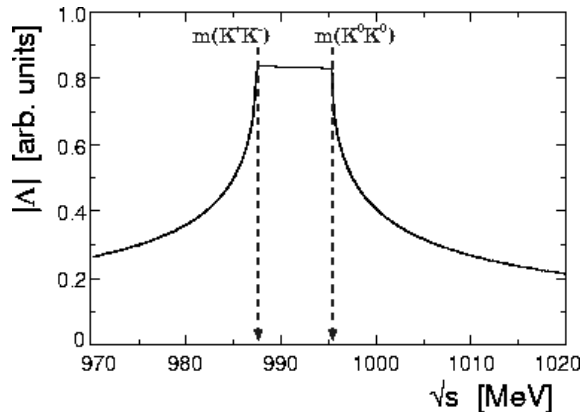


Figure 2: Modulus of the leading term of the mixing amplitude Λ defined in Eq. (5). The two kinks occur at the K^+K^- (at 987.35 MeV) and the \bar{K}^0K^0 (995.34 MeV) threshold respectively.

using magnetic spectrometers. The main results of these experiments and their implications on the proposed measurements are described below.

In 1979 Achasov and collaborators [107] pointed out that between the charged and neutral kaon thresholds the leading term to the a_0 - f_0 mixing amplitude is dominated by the unitary cut of the intermediate two-kaon system. It was demonstrated, that the leading piece of the a_0 - f_0 mixing amplitude can be written as

$$\Lambda = \langle f_0 | T | a_0 \rangle = i g_{f_0 K \bar{K}} g_{a_0 K \bar{K}} \sqrt{s} (p_{K^0} - p_{K^+}) + \mathcal{O}\left(\frac{p_{K^0}^2 - p_{K^+}^2}{s}\right), \quad (5)$$

where the effective coupling constants are defined through $\Gamma_{xK\bar{K}} = g_{xK\bar{K}}^2 p_K$. This \sqrt{s} dependence of Λ is depicted in Fig. 2. Here, electromagnetic effects between the kaons were neglected as in [107].

As demonstrated in a recent compilation [108], the values for $g_{a_0 K \bar{K}}$ and $g_{f_0 K \bar{K}}$ range from 0.224 to 0.834 and from 1.31 to 2.84, respectively — depending on the Flatté parameterization of measured $\pi\pi$ and $\pi\eta$ spectra. It has also been shown in Ref. [108] that the coupling of a physical particle to mesons carries information about the nature of that particle, as was shown by Weinberg for the deuteron case [109]. Based on the existing data, the authors of Ref. [108] conclude that both the a_0 and f_0 have significant mesonic ($K\bar{K}$) components, however, more quantitative statements require a better knowledge of $g_{a_0/f_0 K \bar{K}}$, which could be obtained from an accurate measurement of Λ .

In addition, since Λ (as defined in eq. 5) is essentially the overlap of the wavefunctions of a_0 and f_0 , it is expected that also that part of the mixing amplitude that does not stem from kaons will reveal new insights into the structure of the light scalar mesons.

A $pp \rightarrow dX$ reaction must lead to a_0^+ ($I=1$) production, a $pn \rightarrow dX$ interaction is not isospin selective and both the a_0^0 and f_0 may be produced ($I=0, 1$), whereas the $dd \rightarrow \alpha X$ reaction — neglecting the small isospin violating contributions which are the final goal of the proposed experimental program — is a filter for the f_0 ($I=0$) resonance, since the initial deuterons and the α particle in

the final state have isospin $I=0$ (“isospin filter”). Since at COSY it is possible to manipulate the initial isospin one can thus selectively produce the a_0 or f_0 resonances and can identify observables that vanish in the absence of isospin violation [3, 110]. The idea behind the proposed experiments is the same as behind recent measurements of isospin violation in the reactions $np \rightarrow d\pi^0$ [67] and $dd \rightarrow \alpha\pi^0$ [66]. However, the interpretation of the signal from the scalar mesons is much simpler as compared to the pion case. Since the a_0 and the f_0 are rather narrow overlapping resonances, the a_0 - f_0 mixing in the final state is enhanced by more than an order of magnitude compared to isospin violation in the production operator (i.e. “direct” isospin violating $dd \rightarrow \alpha a_0$ production) and should, e.g., give the dominant contribution to the isospin violating effect via the reaction chain $dd \rightarrow \alpha f_0 (I=0) \rightarrow \alpha a_0^0 (I=1) \rightarrow \alpha(\pi^0\eta)$ [94].

The $dd \rightarrow \alpha(\pi^0\eta)$ reaction seems to be most promising for the extraction of isospin violating effects. Any observation of $\pi^0\eta$ production in this particular channel is a direct indication of isospin violation, however, the cross section $d\sigma/dm$ will be given by the product of the mixing amplitude $\Lambda(m)$ and the $dd \rightarrow \alpha f_0$ production operator. It is therefore compulsory to determine the latter in an independent measurement in order to extract the mixing amplitude. A corresponding experiment aiming at the measurement of the $dd \rightarrow \alpha(K^+K^-)_{I=l=0}$ cross section is foreseen for winter 2004/05 at ANKE [111]. These data, together with the information on the $dd \rightarrow \alpha(\pi^0\eta)$ reaction from WASA will allow one to determine Λ independently.

In analogy to the measurement of isospin violation in the reaction $np \rightarrow d\pi^0$, it has been predicted that the measurement of angular asymmetries (i.e. forward-backward asymmetry in the da_0 c.m.s.) also allows to extract the a_0 - f_0 mixing amplitude [112–114]. It was stressed in Ref. [113] that — in contrast to the $np \rightarrow d\pi^0$ experiment where the forward-backward asymmetry was found to be as small as 0.17% [67] — the reaction $pn \rightarrow d\pi^0\eta$ is subject to a kinematical enhancement. As a consequence, the effect is predicted to be significantly larger in the a_0/f_0 case. The numbers range from some 10% [113] to a few factors [112] and, thus, should easily be observable. It has been pointed out in Ref. [114] that the analyzing power of the reaction $\bar{p}n \rightarrow d\pi^0\eta$ also carries information about the a_0 - f_0 mixing amplitude. This quantity can be measured at COSY as well.

An experimental program has already been started at COSY which aims at exclusive data on a_0/f_0 production close to the $K\bar{K}$ threshold from pp [115–117], pn [118], pd [118, 119] and dd [111, 120] interactions. The reactions $pp \rightarrow ppK^+K^-$ and $pd \rightarrow {}^3\text{He}K^+K^-$ have been measured at COSY-11 [115, 116] and MOMO [119], respectively, at excitation energies up to $Q = 56$ MeV above the $K\bar{K}$ threshold. However, mainly due to the lack of precise angular distributions, the contribution of the a_0/f_0 to $K\bar{K}$ production remains unclear for these reactions. At ANKE, the reaction $pp \rightarrow dK^+\bar{K}^0$ has been measured exclusively (by reconstructing the \bar{K}^0 from the measured dK^+ missing mass) at beam momenta of $p=3.46$ and 3.65 GeV/c ($Q=46$ and 103 MeV). The differential spectra for the lower beam momentum are shown in Fig. 3 [121]. The background of misidentified events at ANKE is less than 10% which is crucial for the partial-wave analysis. This analysis reveals that the $K^+\bar{K}^0$ pairs are mainly (83%) produced in a relative S -wave (dashed line in Fig. 3), presumably via the a_0^+ channel [121]. Based on model calculations for the $pp \rightarrow dK^+\bar{K}^0$ reaction the authors of Ref. [122] draw the conclusion that for $Q < 100$ MeV the $K\bar{K}$ pair production proceeds dominantly via the a_0^+ -resonance. Limits on the \bar{K}^0d

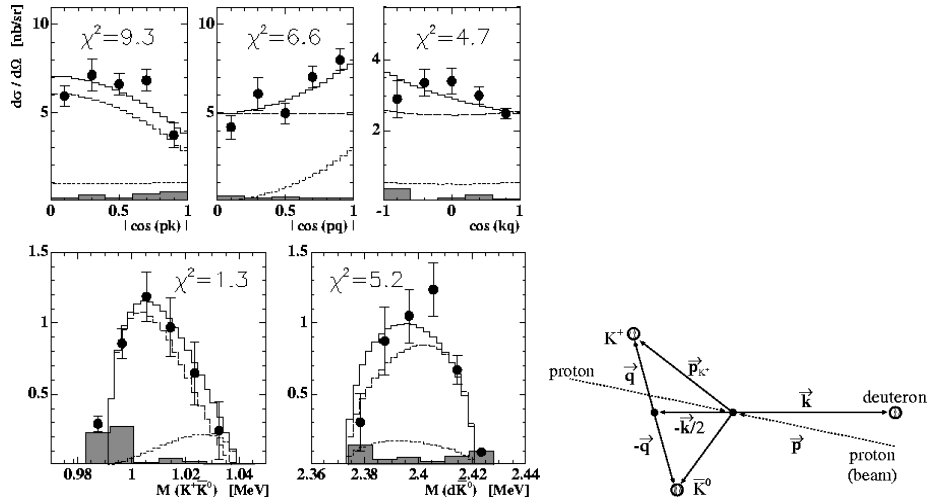


Figure 3: ANKE data for the reaction $p(3.46 \text{ GeV}/c)p \rightarrow dK^+\bar{K}^0$ [121]. The shaded areas correspond to the systematic uncertainties of the acceptance correction. The dashed (dotted) line corresponds to $K^+\bar{K}^0$ -production in a relative S -(P -) wave and the solid line is the sum of both contributions. For definition of the vectors p , q and k in the cms of the reaction $pp \rightarrow dK^+\bar{K}^0$ see right hand part of the figure. Angular distributions with respect to the beam direction \vec{p} have to be symmetric around 90° since the two protons in the entrance channel are indistinguishable.

scattering length have been obtained in Ref. [123]. For a further discussion of scalar mesons in these reactions see e.g. Ref. [124].

Data on the reaction $p(3.46 \text{ GeV}/c)p \rightarrow d\pi^+X$ have been obtained at ANKE in parallel to the kaon data. In contrast to the latter, where the spectra are almost background free, the $pp \rightarrow d\pi^+\eta$ signal is on top of a huge multi-pion background [125]. This demonstrates the need for a photon detector supplying active π^0 - or η -meson identification. With such a detector one may expect data of a quality comparable to what is shown in Fig. 3 also for the non-strange decay channels.

2.2.2 Hyperon resonances

Compared to the spectrum of nucleon resonances, the excitation modes of hyperons (Λ, Σ) are much less known. The lowest excitations listed in Ref. [126] are the $\Lambda(1405)$ $J^P = \frac{1}{2}^-$ isospin singlet and the $\Sigma(1385)$ $J^P = \frac{3}{2}^+$ isospin triplet states, well accessible in proton-nucleon collisions at COSY. The study of the $\Lambda(1405)$ state is particularly interesting since this resonance has still not been understood in its nature, its spin and isospin assignment is based on indirect arguments only. In the quark model the $\Lambda(1405)$ is interpreted as a state with orbital excitation. However, three well established quark models with entirely different residual interaction (gluon exchange [127], meson exchange [128], and t'Hooft instanton induced interaction [129]) have difficulties in reproducing the mass of the $\Lambda(1405)$. All models [127–129] find a degeneracy of the computed

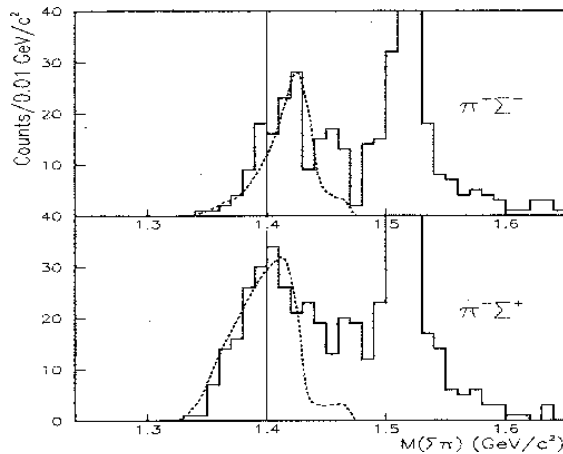


Figure 4: Invariant mass spectra for $\pi^+\Sigma^-$ and $\pi^-\Sigma^+$ as observed in the $p(\gamma, K^+\pi)\Sigma$ reaction at SPring-8/LEPS [144].

$\Lambda(1405)$ with the $J^P = \frac{3}{2}^-$ $\Lambda(1520)$ resonance in contrast to the observation. A similar problem is also manifest in very recent lattice QCD calculations where an extrapolation to the physical pion mass results in a too high value for the $\Lambda(1405)$ mass [130].

On the other hand, since long time the $\Lambda(1405)$ has been interpreted as a $\bar{K}N$ quasi-bound state [131–133], later on substantiated by the consideration of chiral symmetry [134, 135]. Recent work in the framework of unitarized chiral effective field theories has pointed out that the structure of the $\Lambda(1405)$ is extremely sensitive to the breaking of the $SU(3)$ symmetry [136–139]. Ref. [139] finds two poles of the scattering matrix close to the nominal $\Lambda(1405)$ resonance, one of which couples more strongly to $\pi\Sigma$ states and the other one mostly to $\bar{K}N$ states. As an experimentally observable consequence, peak structures with different invariant mass distributions are expected in photon and hadron induced reactions that populate the $\Lambda(1405)$ resonance [139].

The experimental information available on the $\Lambda(1405)$ and $\Sigma(1385)$ resonances is primarily based on studies of K^- proton collisions in bubble chambers [140–143]. In this entrance channel the resonances are only observable through the decay of higher-lying Λ^* and Σ^* resonances.

Recently photon-induced hyperon resonance production with a statistics of ≈ 100 events in the $\Lambda(1405)/\Sigma(1385)$ region was observed at SPring-8 [144], showing different spectral shapes in $\Sigma^+\pi^-$ and $\Sigma^-\pi^+$ final states. Based on arguments given in Ref. [145], this was interpreted as an indication for a meson-baryon nature of the $\Lambda(1405)$ [144] (see Fig. 4).

In view of the limited quality of the existing data and the lack of proton induced studies, it is important to investigate the nature of the $\Lambda(1405)$ resonance in proton-proton collisions by measuring its spectral shape with good resolution and statistics. This will allow recent theoretical predictions based on the chiral unitarity approach to be tested. In particular, a comparison of the $\Sigma^+\pi^-$ and $\Sigma^-\pi^+$ spectral distribution will reveal a possible resonant behavior of the the $I = 1$ amplitude in this mass region, whereas the $\Sigma^0\pi^0$ distribution provides

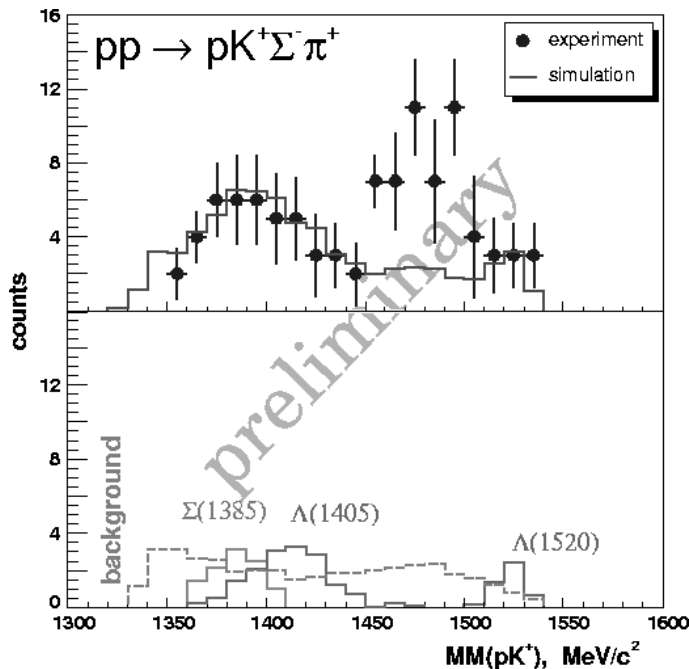


Figure 5: K^+p missing mass spectrum for the reaction $p(3.60 \text{ GeV}/c)p \rightarrow pK^+\Sigma^-\pi^+$ measured at ANKE in comparison with a simulation (upper panel). The simulated K^+p missing mass spectrum decomposes into background from misidentified events and non-resonant $\Sigma^-\pi^+$ production, as well as the known hyperons $\Sigma(1385)$, $\Lambda(1405)$ and $\Lambda(1520)$ decaying into $\Sigma^-\pi^+$ (lower panel).

the true shape of the $I = 0$ resonance according to Ref. [145]. A comparison with the shape of the spectral distribution measured in photo-induced reactions is predicted to reveal the two-pole structure of the resonance [139].

An experimental study of the $\Lambda(1405)$ resonance also delivers information on the $\Sigma(1385)$ resonance as a by-product, since due to their similar pole masses and widths the production of these two resonances can only be disentangled by the complete identification of the final states populated in their decays ($\Lambda(1405) \rightarrow \Sigma\pi$ (100%); $\Sigma(1385) \rightarrow \Lambda\pi$ ($88 \pm 2\%$), $\Sigma\pi$ ($12 \pm 2\%$)). This involves the detection of both charged and neutral pions, and thus a large acceptance detector with charged and neutral particle detection capability like the WASA detector. In particular, photon detection is required for the observation of the decay channel $\Lambda(1405) \rightarrow \Sigma^0\pi^0 \rightarrow (\Lambda\gamma)(\gamma\gamma)$. The identification of this final state is particularly important since it is not populated in the decay of the $\Sigma^0(1385)$ resonance and thus provides direct access to the spectral shape of the $\Lambda(1405)$ resonance. The $\Sigma^0(1385)$ contribution in the charged $\Sigma\pi$ final states ($\Sigma^+\pi^-, \Sigma^-\pi^+$) can be deduced from a measurement of the $\Lambda\pi^0$ final state which is not populated in the $\Lambda(1405)$ decay.

Recent data from ANKE on the reaction $pp \rightarrow pK^+Y^* \rightarrow pK^+\Sigma(1190)^-\pi^+$ measured at a beam momentum of 3.60 GeV/c are consistent with a hyperon resonance Y^* with a mass of 1475 MeV/c² and a width of 45 MeV/c² (see [146])

and Fig. 5). This state is also seen with comparable strength in the charge-conjugate decay channel $Y^* \rightarrow \Sigma(1190)^+\pi^-$ and its production cross section is of the same order as for the $\Lambda(1405)$. Within the above mentioned quark models [127–129] there is no room for an additional Λ or Σ hyperon below ≈ 1600 MeV/c². However, a $\Sigma(1480)$ with a $4q1\bar{q}$ structure has been predicted in Ref. [100] — as the $I = 1$ partner of the $\Lambda(1405)$ in a common multiplet. Further studies are needed in order to confirm the conjecture that the observed enhancement in the K^+p missing mass spectrum originates from a new hyperon resonance. If this interpretation will be supported after further analysis or new measurements, the next step is to determine the isospin of the new hyperon state. This is not possible from the ANKE data but requires a comparison of the possible decay channels $\Sigma^\pm\pi^\mp$, $\Sigma^0\pi^0$, and $\Lambda\pi^0$.

As an additional note, it should be mentioned that the different nature of the $\Lambda(1405)$ and $\Sigma(1385)$ states is also expected to manifest itself in different in-medium properties of these hyperon resonances. In particular, if the meson-baryon picture of the $\Lambda(1405)$ is correct, its medium properties are intimately related to the behavior of antikaons (K^-, \bar{K}^0) in nuclear matter, which is a still unsolved problem, of importance in both hadron physics and astrophysics. A comparative study of $\Lambda(1405)$ and $\Sigma(1385)$ resonance production on nuclear targets allows to investigate the propagation of these hyperon resonances inside the nuclear medium. A better knowledge of the in-medium properties of the $\Lambda(1405)$ (absorption cross section, modification of the spectral shape) will also help to understand the dynamics of antikaons in nuclear matter.

2.2.3 Pentaquarks

Early in 2003, the LEPS Collaboration at the SPring-8 facility in Japan observed a sharp resonance, Θ^+ , at (1.54 ± 0.01) GeV/c² with a width smaller than 25 MeV/c² and a statistical significance of 4.6σ in the reaction $\gamma n \rightarrow K^+K^-n$ [147]. This resonance decays into K^+n , hence carries strangeness $S = +1$. Later, many other groups have claimed the observation of this state [148–158]. In particular, evidence for the Θ^+ has also been seen at the COSY-TOF experiment in the reaction $pp \rightarrow \Sigma^+pK_s$ [159] in the pK_s invariant mass spectrum. While in some experiments detecting a pK_s in the final state the strangeness of the resonance in this system is undefined, in this experiment it is uniquely determined that the observed pK_s system originates from a $S = +1$ state since the full final state with an associated Σ^+ is identified.

Since all known baryons with $B = +1$ carry negative or zero strangeness, such a resonance must have a minimum quark content $uudd\bar{s}$, a structure which is clearly beyond the conventional quark model. This experimental discovery triggered a lot of theoretical activity and up to now over 250 papers appeared trying to interpret this exotic state [160].

There is preliminary evidence that the Θ^+ is an iso-scalar because no enhancement was observed in the pK^+ invariant mass distribution [150, 152, 153, 158]. All the other quantum numbers including its angular momentum and parity remain undetermined. Most of theoretical work postulated its angular momentum to be one half, because of its low mass, but the possibility of $J = 3/2$ still cannot be excluded completely.

It is important to point out that many other experimental groups reported negative results [161–163]. A long list of experiments yielding negative results (still unpublished at the time of the writing) can be found in Ref. [164].

With both positive and null evidence for the Θ^+ from a variety of experiments, it is difficult to conclude whether the Θ^+ exists or not. Furthermore, the theoretical difficulties to explain a possible narrow width, perhaps as small as $1 \text{ MeV}/c^2$, suggest that if the Θ^+ exists, it is very unusual indeed. Guidance from lattice gauge theory is not helpful, as some calculations show evidence for a negative parity resonance, while another indicates positive parity. Furthermore, one does not see a resonance in either parity. So the confirmation of the Θ^+ is of highest importance for which the COSY-TOF collaboration will start an extensive experimental investigation in October 2004.

One should note that the Θ^+ is a member of a multiplet. This calls for the existence for additional unusual states. WASA at COSY with its very good mass resolution and large acceptance can make a decisive contribution to this field by providing high statistics data on the differential cross sections of exotic baryon production in elementary reactions. While there are several elementary reactions with the Θ^+ in the final state within the COSY energy range, the $pd \rightarrow p\Lambda\Theta^+$ reaction is of special interest. Currently this reaction is investigated by the CELSIUS/WASA collaboration close to threshold. This reaction provides access to the pure isospin zero Θ^+ production channel via the subsystem $pn \rightarrow \Theta^+\Lambda$ and thus allows to obtain further and independent insight into the physics of the Θ^+ pentaquark as compared to elementary transitions like $pp \rightarrow \Theta^+\Sigma^+$ (which is pure isospin one). For example, one can obtain additional and complementary information on the parity of the Θ^+ [165] but explore also the Θ^+ production mechanism, which is so far completely unknown.

3 Key experiments

In this chapter several key experiments are presented to address the issues discussed in the previous chapter. After the commissioning phase of WASA at COSY, in which the performance of the detector will be demonstrated, the intention is to carry out the experiments discussed below. The proposed immediate program consists of experiments that are feasible shortly after the initial commissioning of WASA at COSY, and will produce physics results soon. The medium term plans require either extended data taking or improvements of the experimental conditions depending on the experience gained in the initial experiments. The order of the experiments listed below presents a reasonable balance between the physics interest and timeliness of the experimental feasibility.

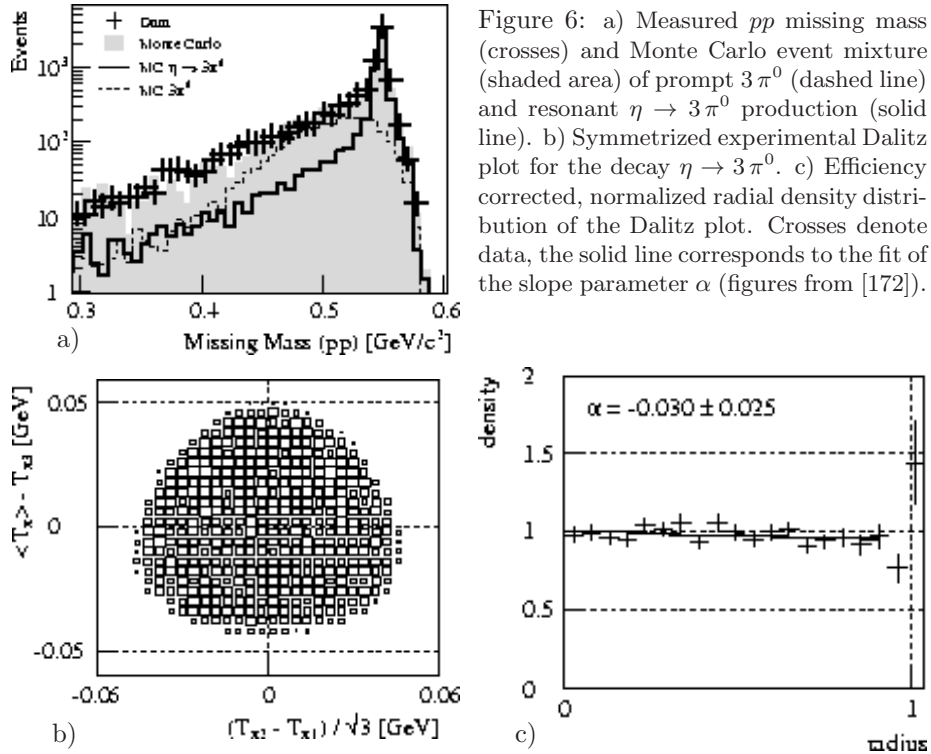
3.1 Not-so-rare η' decays

Isospin symmetry breaking in η' decays. The experiment aims at a precise determination of the ratios of isospin symmetry breaking decays $\eta' \rightarrow 3\pi$ with respect to the isospin allowed $\eta 2\pi$ modes as defined in relation (3) of section 2.1.1 to extract the mixing angle $\Theta_{\pi\eta}$, which is proportional to the light quark mass difference Δm (eq. 2). While only an upper limit is known for $\eta' \rightarrow \pi^0\pi^+\pi^-$ [45], in the neutral decay modes in eq. (3) the ratio \mathcal{R}_1 has been measured with a statistics of ≈ 130 events, leading to $\sin \Theta_{\pi\eta} = 0.023 \pm 0.002$ [166]. However, there is considerable uncertainty in the literature concerning $\sin \Theta_{\pi\eta}$: a value of $\sin \Theta_{\pi\eta} = 0.010$ was extracted using PCAC relations for meson masses and removing electromagnetic contributions [6], in agreement with the estimate in [167]. Further results given in the literature cover a range between 0.013 and 0.014 [168–170], except for $\sin \Theta_{\pi\eta} = 0.034 \pm 0.013$ reported in [171].

With the WASA facility at COSY, in the tagging reaction $pp \rightarrow pp\eta'$ a statistical accuracy of 1% can be achieved for the lowest $\sin \Theta_{\pi\eta}$ estimate within a running time of 12 weeks, improving the precision of the existing experimental value by an order of magnitude (see Table 1). Background influencing the precision of the extracted value is primarily expected from non-resonant 3π production. Although the background will be distributed smoothly in the vicinity of an η' signal in the two proton missing mass, the final precision of the result will depend on the four-momentum resolution achieved for both protons in the forward detector and the decay system. Modifications of the WASA detector setup to ensure a required performance at higher energies are discussed in section 4.3.

With selective central detector trigger conditions on either six neutral particles from the decays $\eta(\pi^0) \rightarrow 2\gamma$ or two neutral and two charged particles, both ratios \mathcal{R}_i can be determined simultaneously. Since the Dalitz plots of the hadronic decay channels are measured completely, the energy dependence of the decays is inherent to the data, and can be used both to test predictions from ChPT, and as a constraint on the the scalar meson sector as discussed in section 2.1.1. The present performance of the WASA detector for the detection of multipion final states is demonstrated in Fig. 6 for a data sample obtained at CELSIUS at a kinetic beam energy of 1360 MeV, i.e. at an excess energy of ≈ 40 MeV with respect to the η production threshold in proton–proton scattering [172].

The experimental pp missing mass spectrum is well reproduced by contributions from $pp \rightarrow pp\eta \rightarrow pp3\pi^0$ and prompt $3\pi^0$ production (fig. 6a). The complete kinematical information is contained in the Dalitz plot for the $\eta \rightarrow 3\pi^0$ decay,



that is shown in its symmetrized form ($\langle T_\pi \rangle - T_{\pi 3}$ vs. $T_{\pi 2} - T_{\pi 1}/\sqrt{3}$) in Fig. 6b. The slope parameter α (fig. 6c), which reflects the strong and energy dependent $\pi\pi$ interaction, is extracted from a linear fit of the normalized radial density distribution [7]. The preliminary value $\alpha = -0.03 \pm 0.025$ is limited by the statistics of 11700 events, but agrees in sign with the result $\alpha = -0.031(4)$ of the Crystal Ball analysis based on 10^6 events [17].

Search for evidence of the box anomaly of QCD in $\eta' \rightarrow \pi^+\pi^-\gamma$ decays.

The experimental signature for the detection of the $\pi^+\pi^-\gamma$ decay mode of the η' consists of two charged and one neutral particle in the central detector, with the η' being tagged from the missing mass with respect to the two protons identified in the forward detector. This signature can be used for a selective trigger condition. Moreover, with the requirement of one γ in the central detector, the experiment trigger for a measurement of the hadronic decays $\eta' \rightarrow \eta(\pi^0)\pi^+\pi^-$ discussed above is a mere subset, i.e. both experiments could run simultaneously.

The experiment aims at measuring the $\pi^+\pi^-$ invariant mass distribution in the decay $\eta' \rightarrow \pi^+\pi^-\gamma$ with high accuracy. One (Two) order(s) of magnitude higher statistics compared to the presently available data can be achieved within a running time of two days (three weeks). Following the experimental technique used in [36] the number of $\eta' \rightarrow \pi^+\pi^-\gamma$ can be determined in each bin of the $\pi^+\pi^-$ invariant mass separately. Consequently, the $\pi^+\pi^-$ spectrum will be background free (Fig. 7).

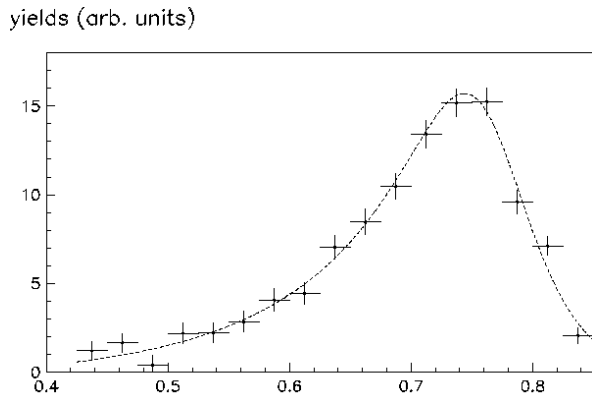


Figure 7: Distribution of the $\pi^+\pi^-$ invariant mass for $\eta' \rightarrow \pi^+\pi^-\gamma$ decays from [36]. Crosses denote experimental data, the dashed line is the result of the fit used to extract box anomaly parameters with a statistical significance of 4σ .

The quantity $E_{\eta'}$ associated with the matrix element of a non-resonant contribution as a consequence of the box anomaly is related at the chiral point to the parameters of the pseudoscalar nonet by one of the Chanowitz relations [30,31]:

$$E_{\eta'}(0) = -\frac{e}{4\pi^2\sqrt{3}} \frac{1}{f_\pi^2} \left[\frac{\sin\Theta_{ps}}{f_8} + \sqrt{2} \frac{\cos\Theta_{ps}}{f_0} \right]. \quad (6)$$

Θ_{ps} denotes the pseudoscalar octet-singlet mixing angle, f_π is the pion leptonic decay constant, and, in analogy, f_0 and f_8 are defined as couplings of the pseudoscalar singlet and octet states η_0 and η_8 to the divergences of the singlet and octet axial-vector currents, respectively. $E_{\eta'}$ can be derived from a fit to the spectrum of the $\pi^+\pi^-$ mass $m_{\pi\pi}$ (Fig. 7 and [36,173,174]) in the $\pi^+\pi^-\gamma$ decay mode of the η' using (for a more sophisticated analysis of this decay, see [34], which should be used in the final analysis)

$$\frac{d\Gamma_{\eta'}}{dm_{\pi\pi}} = \frac{1}{48\pi^3} \left| \frac{2G_\rho(m_{\pi\pi})g_{\eta'\rho\gamma}}{D_\rho(m_{\pi\pi})} + E_{\eta'} \right| k_\gamma^3 q_\pi^3, \quad (7)$$

where k_γ and q_π are the four-momenta of the outgoing γ and π^\pm , $g_{\eta'\rho\gamma}$ denotes the coupling constant for the ρ contribution to the $\pi^+\pi^-\gamma$ decay mode, and $D_\rho(m_{\pi\pi})$ and $G_\rho(m_{\pi\pi})$ are the ρ propagator and its coupling to the $\pi^+\pi^-$ channel.

On the one hand, the extraction of the box anomaly contribution is strongly dependent on the model employed in the description of the ρ . On the other hand, from the two-photon widths of η and η' as described by the Chanowitz equations [30,31] using additional information from radiative $J/\Psi \rightarrow \eta(\eta')\gamma$ decays (AFN relation [175,176]), the parameters of the pseudoscalar nonet are completely determined, and can be used to predict the box anomaly constant $E_{\eta'}$. Consequently, the ρ shape and the box anomaly parameters are closely related to each other — the approach might allow for an alternative approach to extract the ρ line shape in a clean way.

So far, experimentally no consistent picture has been obtained: The box anomaly contribution extracted from the Crystal Barrel data [36] is rather

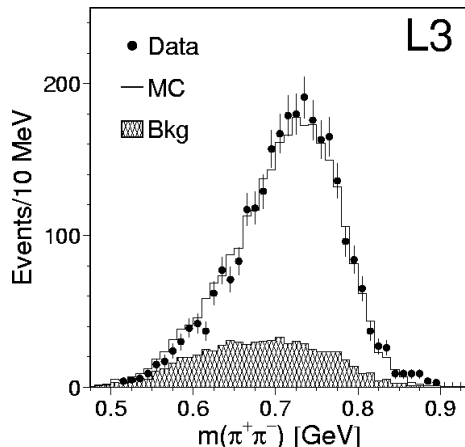


Figure 8: $\pi^+\pi^-$ effective mass distribution in the decay $\eta' \rightarrow \pi^+\pi^-\gamma$ from L3 [35]. Points denote experimental data, the solid line is the best fit result with $m_\rho = 766$ MeV and $\Gamma_\rho = 150$ MeV. The estimated background (shaded area) is mainly attributed to decays of the $a_2(1320)$.

disfavoured (confidence level 3%) by the L3 result (Fig. 8 and [35]), which is consistent with a pure ρ line shape (C.L. 37%). On the other hand, the Crystal Barrel data would require a mass $m_\rho = 790$ MeV when neglecting the anomaly related non-resonant contribution, i.e. 20 MeV above the presently accepted value [45]. In this respect, these two results with the up to now highest statistics are inconsistent.

3.2 $a_0^+(980)$ production in $pp \rightarrow d\pi^+\eta$

a_0^+ -production has first been investigated at COSY by measuring the reaction $pp \rightarrow dK^+\bar{K}^0$ at a beam momentum of $p = 3.46$ GeV/c ($Q = 46$ MeV) with ANKE [121]. The measured total cross section for the $pp \rightarrow dK^+\bar{K}^0$ reaction is $(38 \pm 2 \pm 14)$ nb and, thus, ≈ 1000 events could be collected within five days of beam time using a cluster-jet target ($L = 2.7 \cdot 10^{31}$ cm $^{-2}$ s $^{-1}$ during these measurements). According to the partial-wave analysis the $K^+\bar{K}^0$ pairs are mainly (about 83%) produced in a relative S -wave, i.e. via the a_0^+ channel [121]. This observation is in good agreement with a model prediction [122] for the total a_0^+ -production cross section in pp collisions. This model has also been used to estimate the cross-section ratio for resonant (via the a_0^+) [112, 177] and non-resonant [112, 178] $\pi^+\eta$ production:

$$R_d^{\text{res/nres}} \Big|_{p=3.46\text{GeV}/c} = \frac{\sigma(pp \rightarrow da_0^+)}{\sigma(pp \rightarrow d\pi^+\eta)} \approx 0.3 \dots 0.5. \quad (8)$$

This prediction for $R_d^{\text{res/nres}}$ is in line with data from ANKE for the reaction $pp \rightarrow d\pi^+X$ [179]. Since most of the non-resonant $\pi^+\eta$ pairs are expected at lower invariant masses, we anticipate that the resonant signal can well be identified in case of the $pp \rightarrow d\pi^+\eta$ reaction.

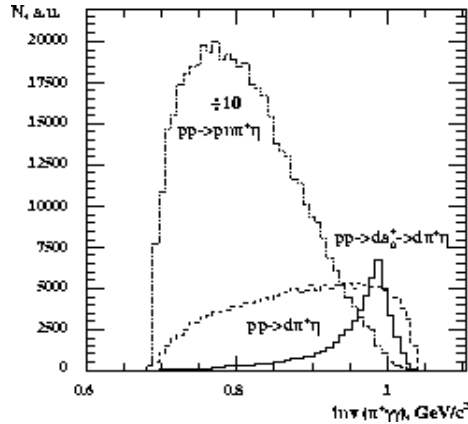


Figure 9: Invariant mass ($\pi^+\eta$) for a_0^+ production in $pp \rightarrow da_0^+ \rightarrow d\pi^+\eta$ and for the two background processes, $pp \rightarrow d\pi^+\eta$ and $pp \rightarrow pn\pi^+\eta$ (downscaled by factor 10).

The model can also be used to estimate $R_{pn}^{\text{res/nres}}$ for the $pp \rightarrow pn\pi^+\eta$ reaction (see Refs. [180,181] for a_0^+ - and Ref. [178] for non-resonant $\pi^+\eta$ production):

$$R_{pn}^{\text{res/nres}} \Big|_{p=3.46\text{GeV}/c} = \frac{\sigma(pp \rightarrow pna_0^+)}{\sigma(pp \rightarrow pn\pi^+\eta)} \approx 0.015 \dots 0.03. \quad (9)$$

Thus $R_{pn}^{\text{res/nres}}$ is expected to be about one order of magnitude smaller than the corresponding ratio $R_d^{\text{res/nres}}$ with deuteron formation in the final state. Therefore, an experimental study of the a_0^+ in pp reactions with WASA requires the identification of the $pp \rightarrow d\pi^+\eta$ reaction, and the $pp \rightarrow pn\pi^+\eta$ reaction will be the most “dangerous” source of background. Consequently, the following simulation calculations focus on the problem of deuteron-vs.-proton discrimination. The reaction $pp \rightarrow da_0^+ \rightarrow d\pi^+\eta$ with subsequent decay $\eta \rightarrow \gamma\gamma$ can be measured with WASA by detecting deuterons in the forward detector (FD) in coincidence with the π^+ and photons in the central detector (CD). The reaction is identified by reconstructing the masses $m(\eta) = m(\gamma\gamma)$ and $m(d) = m.m.(\pi^+\gamma\gamma)$. In order to investigate the acceptance and background suppression the simulations were performed for $a_0^+(980)$ production with a deuteron in the final state and both background reactions using the cross section ratios $\sigma(a_0^+):\sigma(d\pi^+\eta):\sigma(pn\pi^+\eta) = 1.1 \mu\text{b}:3.5 \mu\text{b}:96 \mu\text{b}$ [112,177,178]. Fig. 9 shows the initial ($\pi^+\eta$) invariant mass distributions for these reactions: a Flatté distribution for the $a_0^+(980)$ [177,181], a distribution according to the model in Refs. [178,181,182] for the non-resonant $d\pi^+\eta$, and a phase-space distribution for the non-resonant $pn\pi^+\eta$ production. The WASA acceptance for forward going particles is $\theta \approx 3^\circ \dots 18^\circ$. This acceptance covers about 93% of deuterons from $pp \rightarrow da_0^+$, which are distributed in the range $\theta = 0^\circ \dots 17^\circ$. The acceptance for pions and photons is $\theta \approx 20^\circ \dots 169^\circ$ (for the simulations angles $\theta \approx 20^\circ \dots 143^\circ$ — SEC and SEF, the central and forward part of the calorimeter — were used). The result of the acceptance estimate is shown in the Table 2. For the background reactions the acceptance is smaller due to the wider angular distributions. We have only considered the

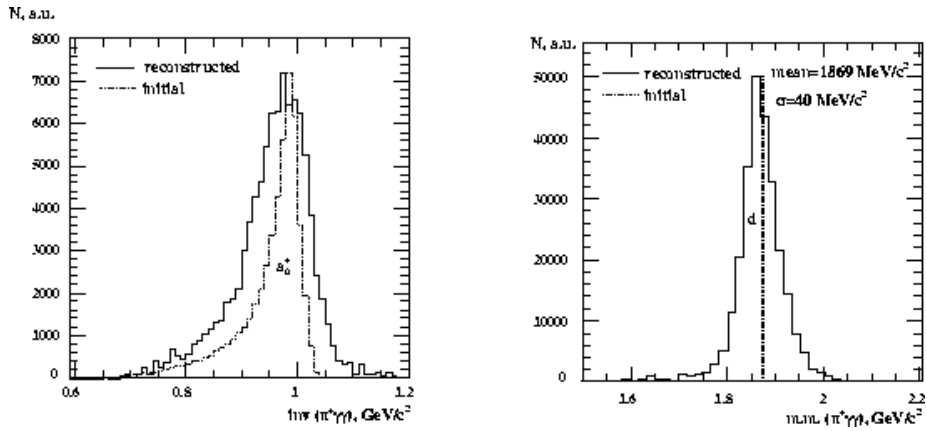


Figure 10: Initial (dotted line) and reconstructed (solid) invariant mass ($\pi^+\gamma\gamma$) (left) and missing mass ($\pi^+\gamma\gamma$) (right) for the reaction $pp \rightarrow da_0^+ \rightarrow d\pi^+\eta$.

decay channel $\eta \rightarrow \gamma\gamma$ since for the other two main decay channels $\eta \rightarrow \pi^+\pi^-\pi^0$ and $\eta \rightarrow 3\pi^0$ the acceptance is two times smaller.

Reaction	Acceptance ($\eta \rightarrow \gamma\gamma$ decay only)
$pp \rightarrow da_0^+ \rightarrow d\pi^+\eta$	0.42
$pp \rightarrow d\pi^+\eta$	0.34
$pp \rightarrow pn\pi^+\eta$	0.32

Table 2: Simulated acceptance of WASA for $a_0^+(980)$ production and the two background processes. Deuterons/protons are detected in the FD ($\theta \approx 3^\circ \dots 18^\circ$), pions and photons in the CD ($\theta \approx 20^\circ \dots 143^\circ$).

In the simulations the π^+ detected in the CD have angular resolution better than $\sigma(\theta) = 0.4^\circ$ (for angles larger than 30°) and momentum resolution between $\sigma(p)/p = 3 \dots 6\%$. For photons in the CD the resolution is $\approx 5^\circ$ (FWHM), due to the crystal sizes in the SEC. The energy resolution varies from 10 MeV (FWHM) for large angles and low initial energies up to 40 MeV (FWHM) for angles less than 30° and initial energies close to 1 GeV. Such resolutions yield $\gamma\gamma$ invariant mass distributions with a FWHM of 43 MeV/c² in the η mass region, which is in agreement with WASA at CELSIUS data [183].

Fig. 10 shows the initial and reconstructed invariant mass ($\pi^+\gamma\gamma$) and missing mass ($\pi^+\gamma\gamma$) for the reaction $pp \rightarrow da_0^+ \rightarrow d\pi^+\eta \rightarrow d\pi^+\gamma\gamma$. Pions and photons detected in coincidence in CD were used for the reconstruction, which provide a ($\pi^+\gamma\gamma$) missing mass resolution of $\sigma = 40$ MeV/c².

The expected background from the reaction $pp \rightarrow pn\pi^+\eta$ is two order higher than the a_0^+ signal. Due to the large momenta of the protons and deuterons they cannot be stopped in the FD and their initial kinetic energy cannot be reconstructed. Moreover, their energy losses are close to minimum ionizing

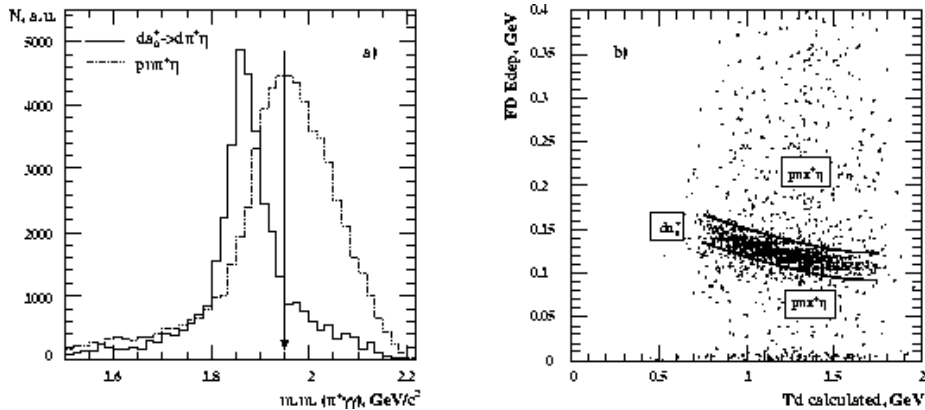


Figure 11: Reconstructed missing mass ($\pi^+\gamma\gamma$) for the reactions $pp \rightarrow da_0^+ \rightarrow d\pi^+\eta$ and $pp \rightarrow pn\pi^+\eta$ (left). The cut is indicated by the arrow. Energy losses in the FD vs. kinetic energy of the deuterons/protons (calculated from the detected π^+ and the two photons assuming that the forward particle is a deuteron). The cut is indicated by the two lines.

and the standard WASA at CELSIUS $\Delta E/E$ method cannot be used for p/d discrimination.

In order to suppress the proton background a set of criteria has been applied. The first cut was applied on the reconstructed ($\pi^+\gamma\gamma$) missing mass, see Fig. 11. The cut at 1.95 GeV suppresses protons by a factor ≈ 1.6 . The two-dimensional distribution energy loss vs. kinetic energy of the forward particle shows a correlation for a_0^+ events, see Fig. 11. Applying a gate with ± 20 MeV around these events, background protons can be suppressed by a factor of ≈ 3.9 .

Another strong criterion for proton suppression is the difference between the measured azimuthal and polar angles of the forward particles and the expected deuteron angles calculated from the π^+ and two photons. For the a_0^+ events these angles coincide within the resolutions of the detector and the reconstruction procedure. For protons from the $pn\pi^+\eta$ events the correlation is much weaker. This is clearly seen in two dimensional plots of measured vs. calculated angles. If one assumes that all forward particles are deuterons, then the real deuterons are seen as lines whereas the protons are smeared out (Fig. 12 (a,b)). Cuts were applied to the difference between measured and calculated azimuthal and polar angles of forward particles (Fig. 12 (c,d)). An azimuthal angle cut of $\pm 20^\circ$ and a polar angle cut of $\pm 2^\circ$ suppresses protons by a factor ≈ 21 .

Taking into account all mentioned cuts and the difference in acceptances the proton suppression factor is $1.3 \times 1.6 \times 3.9 \times 21 \approx 170$. We therefore expect that the non-resonant $pn\pi^+\eta$ events can sufficiently be suppressed without modifications of the existing FD for the higher particle momenta at COSY.

Assuming a luminosity of $L = 10^{31} \text{ cm}^{-2} \text{ s}^{-1}$, an overall efficiency due to detector acceptance, reconstruction algorithms and d/p cuts of ≈ 0.07 , the effect of dead-time and detector efficiencies of ≈ 0.5 and using the cross section estimate from Refs. [112, 177], $\sigma(pp \rightarrow da_0^+ \rightarrow d\pi^+\eta) \times BR(\eta \rightarrow 2\gamma) = 1.1 \mu\text{b} \times 0.393$, the final count rate is $\approx 0.15 \text{ s}^{-1} \approx 90000 \text{ week}^{-1}$.

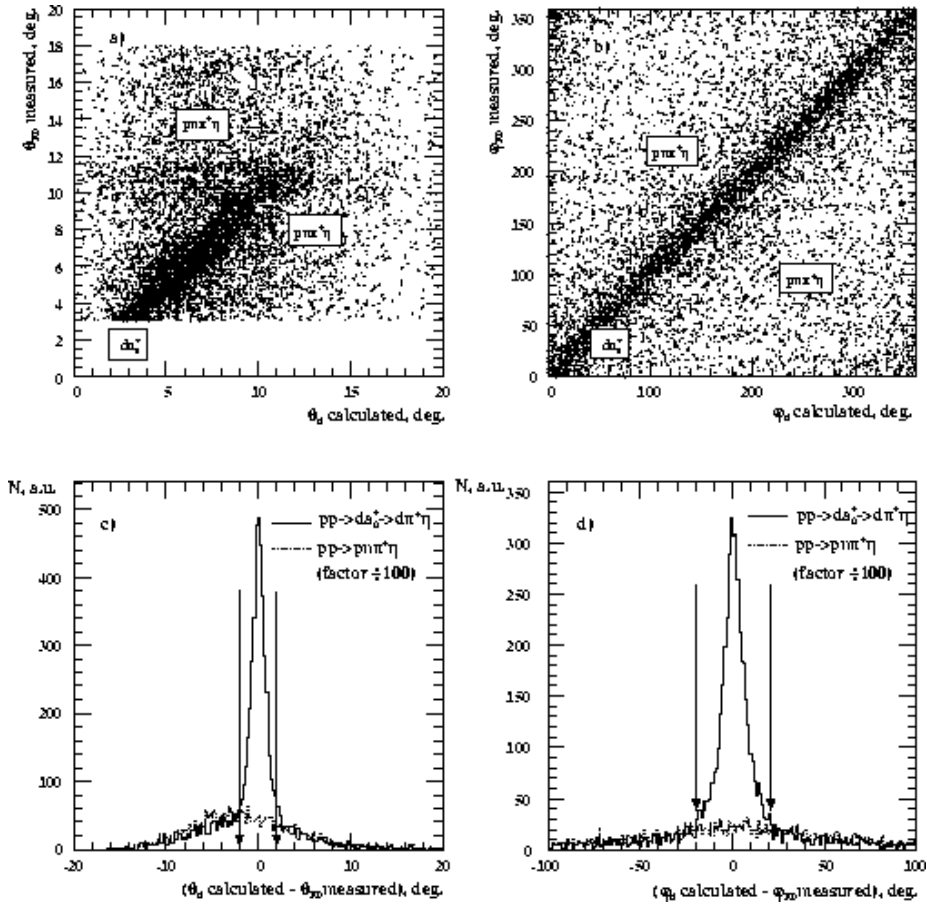


Figure 12: (a,b) Measured vs. calculated forward azimuthal and polar angles assuming that the forward particle is a deuteron. (c,d) Difference between measured and calculated angles of the forward particles. The background $pn\pi^+\eta$ events (dotted line) is downscaled by a factor 100. The cuts are indicated by the arrows.

3.3 Pentaquarks

At present, several experimental groups, including TOF at COSY, are performing high statistics experiments to confirm the existence of the Θ^+ .

Provided the existence of the Θ^+ is confirmed, we will be interested in basic properties of this hadron and details of the production mechanism.

In the following we concentrate on the $pd \rightarrow p\Lambda\Theta^+$ reaction as one example to illustrate the feasibility of high statistics experiments involving both neutral and charged decay products.

Out of the two decay modes of the Θ^+ , the K^0p channel gives the best experimental conditions for being measured in the WASA detector, so we shall here concentrate on this decay branch.

For the Λ there are two important decay modes, $p\pi^-$ and $n\pi^0$ with branching ratios of 63.9% and 35.8%, respectively. The choice of using the charged decay mode to identify the Λ is advantageous due to the following reasons:

- the energy resolution of WASA for charged particles is generally better than for photons,
- the combination of the forward tracker and the MDC provides a clean identification of the Λ by reconstruction of its decay vertex,
- both decay products are measured,
- higher branching ratios as compared to neutral decay modes.

Regarding the kaon decay, half of the events are lost due to K_L^0 having $c\tau = 15.5$ m and thus escaping detection. For the K_S^0 two modes are important, $\pi^+\pi^-$ ($BR = 68.6\%$) and $\pi^0\pi^0$ ($BR = 31.4\%$). Selecting the charged mode has the advantage of higher rate. However, it leads to a final state with six charged particles. It might be difficult to distinguish between the π^- produced in the Λ decay and the K_S^0 decay, which could impair the reconstruction of the Λ . Therefore, the neutral decay mode will be used.

Taking all branching ratios together gives the overall branching ratio, or efficiency of detecting Θ^+ using this particular final state, of $0.5 \times 0.639 \times 0.314 = 0.1$. This final state with four charged particles, π^- and three protons, and the four photons from $\pi^0\pi^0$ provides a well defined trigger as well as favorable analysis conditions.

A rough estimate of the WASA acceptance for the $pd \rightarrow p + \Lambda + \Theta^+ \rightarrow p + p\pi^- + p\gamma\gamma\gamma$ reaction has been obtained using phase space Monte Carlo simulation. The first things needed are the energies and angles of all charged final state particles. They are shown in Fig. 13 below. The proton produced directly is denoted p while those produced in the decays of the Λ and Θ^+ are denoted p_Λ and p_Θ , respectively. It is seen that the maximum energies for p and p_Λ are below 300 MeV, which is the highest energy deposited by protons in the FD. For such protons one may expect a very good energy resolution.

Assuming that reconstruction of the Λ requires the p_Λ proton to be detected in the FD ($2.5^\circ < \theta_{p_\Lambda} < 18^\circ$) and the π^- either in the FD or MDC ($22^\circ < \theta_\pi < 158^\circ$) one finds that this requirement is fulfilled in $\approx 85\%$ of cases. This is roughly the efficiency of the Λ reconstruction, ϵ_Λ . It should be noted that the resolution of the MDC is limited at the forward and backward angles due to a reduced number of wire planes being crossed by the particles. All 17 layers are crossed only for angles between 44° and 134° . For the π^- going into the FD or into this limited angular range of the MDC, the ϵ_Λ is reduced to 55%.

The requirement that the proton p_Θ from Θ^+ enters the FD or the plastic barrel is fulfilled in $\epsilon_{p_\Theta} = 87\%$ of cases.

Finally, the requirement of the four photons (from the K_S^0 decay into $\pi^0\pi^0$) to fall into the angular range of the electromagnetic calorimeter is fulfilled with an efficiency $\epsilon_{4\gamma} = 62\%$. This gives the overall acceptance of $\approx 45\%$ for $\epsilon_\Lambda = 85\%$ and 29% for $\epsilon_\Lambda = 55\%$.

Remembering that the resolution of the WASA detector is far better for charged particles than for photons one would like the Θ^+ mass to be calculated as the missing mass to the reconstructed p , p_Λ and π^- (for π^- only angles will be used,

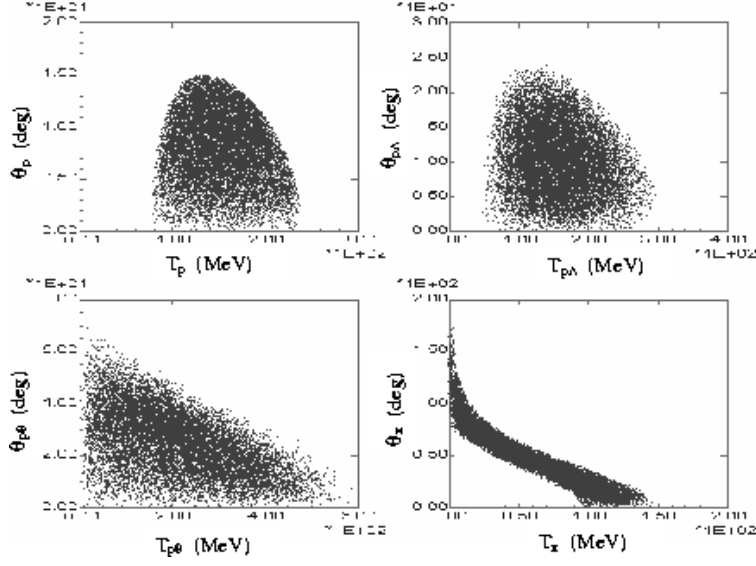


Figure 13: Energy and angular ranges of the four final state charged particles in the reaction $pd \rightarrow p + \Lambda + \Theta^+ \rightarrow p + p\pi^- + p\gamma\gamma\gamma$ at 1360 MeV proton beam energy.

see below). In such a case one has to take into account losses of protons due to nuclear interactions with the detector material, which is expected to reduce the acceptance by roughly a factor of two.

As already mentioned, the Θ^+ mass will be found as the missing mass calculated for the p and p_Λ reconstructed in the FD and π^- either in the FD or MDC. Measurement of the energy and angle of the p proton is straightforward since the reaction vertex is at the known target position. This is not the case for the p_Λ because of the Λ 's $c\tau=7.89$ cm. In order to reconstruct the Λ momentum one has to find the Λ decay vertex using either the forward tracker, when both p_Λ and π^- enter the FD, or the forward tracker and the MDC. Reconstruction of the vertex requires finding two tracks which, together with the target point, are in the same plane. When two tracks fulfilling the above criteria are found, one can calculate the absolute value of the π^- momentum, k , from the condition:

$$(\sqrt{m_\pi^2 + k^2} + E)^2 - (k\hat{u} + \vec{p})^2 = m_\Lambda^2,$$

where E , \vec{p} represent the proton total energy and momentum, \hat{u} is the unit vector representing direction of the presumed π^- and m_Λ is the Λ mass. One should verify that the reconstructed Λ -momentum points to the target area.

A further check is provided by the $\Delta E-E$ method when the pion enters the FD (see Fig. 14) and extracting the momentum from the measurement of the track curvature in the magnetic field, when the pion enters the MDC.

At present the position resolution of the forward tracker amounts to ≈ 2 cm in the x - y plane (perpendicular to the beam) [184] so one can estimate the resolution in angle to be of the order of $\arctan(2/140) \approx 1^\circ$, where 140 cm is the distance between the target position and the FD tracker. For the proton p , the resolution in angle is given by the size of the beam-target overlap and

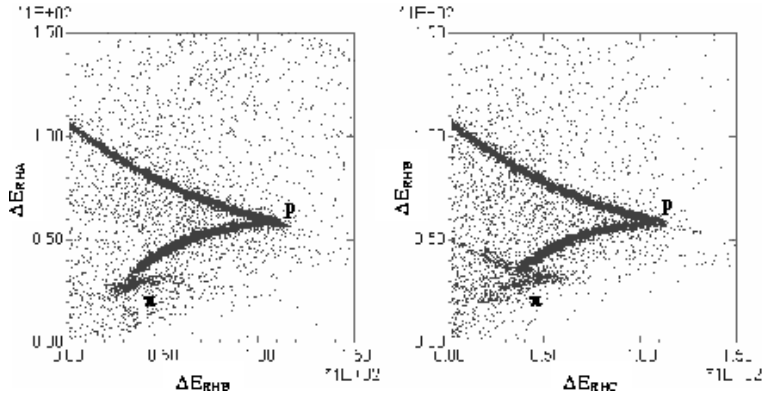


Figure 14: ΔE - E plots for three consecutive layers of the range hodoscope in the FD as obtained in the M-C simulation of the reaction $pd \rightarrow p + \Lambda + \Theta^+ \rightarrow p + p\pi^- + p\gamma\gamma\gamma$ at 1360 MeV proton beam energy.

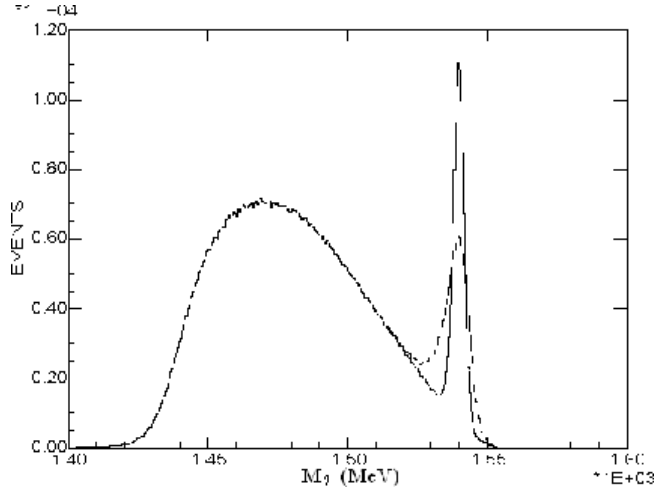


Figure 15: Phase space Monte Carlo simulation of the reaction $p+d \rightarrow p+\Lambda+\Theta^+$ at 1360 MeV beam energy. The Θ^+ peaks are seen on a wide background from non-resonant $p+d \rightarrow p+\Lambda+K^0+p$ reaction, which has been assumed to be 10 stronger than the Θ^+ production. For both peaks the energy resolution for protons has been assumed to be equal to 3% and the π^- angular resolution to amount to 3° . The narrower peak, $\text{FWHM}=4.6 \text{ MeV}/c^2$, corresponds to the proton angular resolution of 1° and for the wider one the resolution of 3° has been assumed. The width obtained in this case amounts to $9.6 \text{ MeV}/c^2$.

accuracy of the FD tracker. For the π^- , which in most cases enters the MDC, one can expect the resolution in θ to be of the order of $\arctan(1/22) = 2.6^\circ$.

A rough estimate of the resolution in M_{Θ^+} can be obtained by smearing the energies of the p , p_Λ and angles of the p , p_Λ and π^- with the experimental resolutions. Taking for the energy resolution 3%, and 1.0° , and 3.0° for the

angular resolution for protons and π^- respectively, leads to the results shown in the Fig. 15 (solid line). The width of the peak at half maximum amounts to $4.5 \text{ MeV}/c^2$, which is nearly five times better than the resolution quoted in Ref. [147]. This is a valuable feature which could improve our knowledge of the true width of the Θ^+ resonance expected to be much smaller than the $20 \text{ MeV}/c^2$ measured in the experiments so far. The wide background seen in the figure corresponds to the phase space simulation of the non-resonant reaction $p + d \rightarrow p + \Lambda + K^0 + p$.

For the Θ^+ cross section of 30 nb , the beam-target luminosity of $10^{31} / \text{cm}^{-2} \text{s}^{-1}$ and the acceptance of 1.5% (with the overall branching ratio of 10% included) one would expect the Θ^+ event rate of $30 \times 10^{-33} \times 10^{31} \times 0.015 \text{ s}^{-1} = 0.0045 \text{ s}^{-1}$ at a beam energy of 1360 MeV . Simulation shows that the detector acceptance depends rather weakly on the beam energy. Thus increasing the beam energy to 1450 MeV would increase the event rate by a factor of ≈ 7 due to the change of the cross section [185]. With a duty factor of 50% obtaining 10^4 events would require less than 200 hours.

3.4 Isospin violation in $\vec{d}d \rightarrow \alpha\pi^0$

Due to the small cross section (a few pb) and the high background from the reaction $dd \rightarrow \alpha X$ the detection and unambiguous identification of the $\alpha\pi^0$ channel is rather difficult. Hence, first attempts to measure this reaction have produced only upper limits (see Ref. [186]). The only positive report at a deuteron energy of 1.1 GeV [187] has been questioned, because the background from the double radiative capture process $dd \rightarrow \alpha\gamma\gamma$ could have been misinterpreted [188]. Consequently, in the recent experiment performed at IUCF [66] the α and the two γ 's have been measured in coincidence to provide a clean signal of $dd \rightarrow \alpha\pi^0$ channel.

At COSY, studies of this reaction were initially proposed for BIG KARL [189]. However, a sufficient background suppression without photon detection would have been hard to achieve. The idea was resubmitted within a proposal for an electromagnetic calorimeter at ANKE [190]. This combination — like WASA — would have provided a clean identification of the forward-going α particle and the π^0 decaying into two photons.

Compared with the latter proposal, the WASA detector provides a similar acceptance for photons ($\Theta = 20^\circ \dots 169^\circ$) but a significantly wider angular acceptance for α particles ($\Theta \approx 3^\circ \dots 18^\circ$). This will allow the extraction of angular distributions starting from $Q \approx 60 \text{ MeV}$ up to and beyond the η threshold (see Fig. 16). In addition, the fully symmetric WASA detector covers the entire azimuthal angular range of 2π and, thus, is well suited to measure polarization observables. The simulations are done for the measurement at $Q = 60 \text{ MeV}$ (studying the development of p -waves).

As indicated previously, the reaction $dd \rightarrow \alpha\pi^0$ will be identified by detecting the α and the decay $\pi^0 \rightarrow \gamma\gamma$ in coincidence. Here, the high energy loss of the α in combination with two neutral hits in the calorimeter provides a very efficient first level trigger. For α momenta above $1 \text{ GeV}/c$ all particles pass the (currently used) Forward Window Counter (FWC) of WASA and are stopped in one of the layers of the Forward Trigger Hodoscope (FTH). Subsequent layers (e.g. of the Forward Range Hodoscope, FRH) can be used as veto layers for

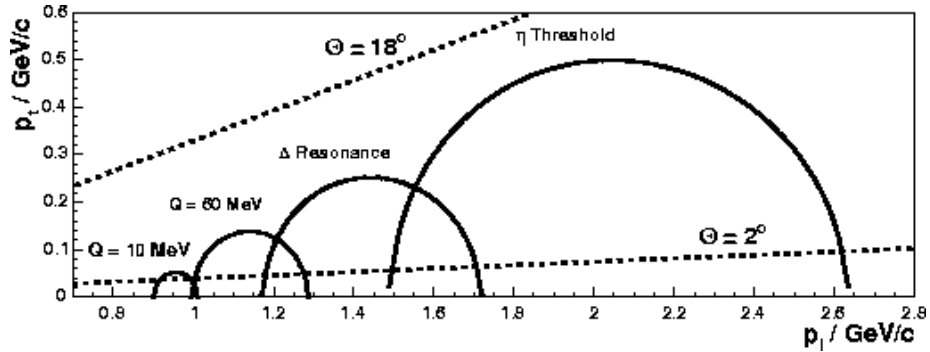


Figure 16: Kinematics of the reaction $dd \rightarrow \alpha\pi^0$ for various Q values. The transverse momentum of the α versus its longitudinal momentum in laboratory is plotted. The lines indicate the azimuthal angle covered by WASA.

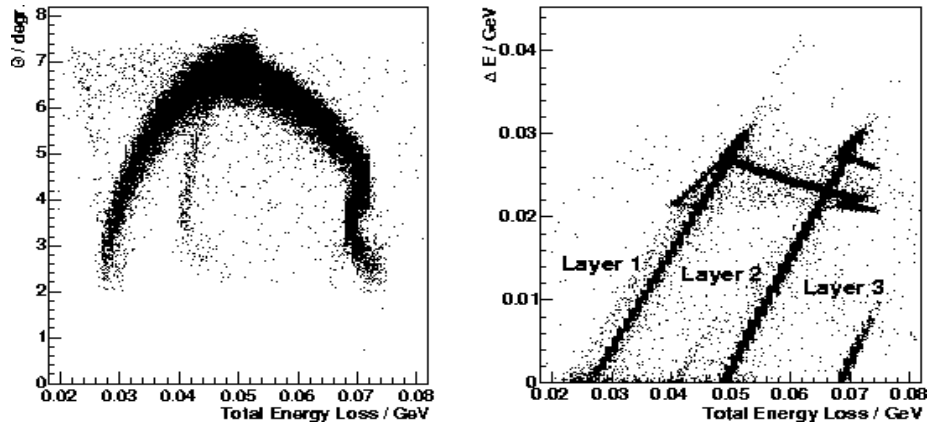


Figure 17: Energy losses of α particles from the reaction $dd \rightarrow \alpha\pi^0$. Left: Reconstructed angle versus total energy loss. Right: Energy loss in the three single layers of the Forward Tracking Hodoscope versus total energy loss.

particles, which are not stopped. Angles are reconstructed by means of the Forward Proportional Chambers (FPC).

Fig. 17 (right side) and Fig. 18 show the energy losses in the individual layers of the tracking hodoscope for α particles as well as for ${}^3\text{He}$ and tritons. While tritons can already be discriminated by these energy loss patterns, ${}^3\text{He}$ is quite similar to α particles¹¹. However, a further reduction of the ${}^3\text{He}$ content can already be done by requiring the correct kinematics as shown in Fig. 17 (left side).

Together with the measured π^0 , the reaction is kinematically over-constrained. Tests on the energy and momentum conservation prevents further particles from being missing. While the standard procedure would be an overall kinematic fit,

¹¹Protons and deuterons are not shown. Their energy loss is — compared with tritons — again smaller and the bands for stopped particles are shifted further to lower energy losses.

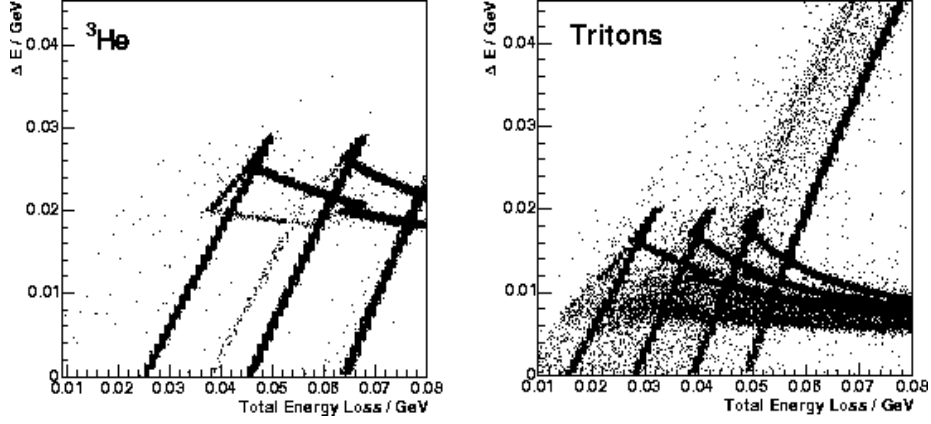


Figure 18: Energy loss in the individual layers versus total energy loss. On the left ${}^3\text{He}$, on the right tritons. While the energy loss pattern for ${}^3\text{He}$ is rather similar to ${}^4\text{He}$, the one for tritons can be used efficiently for particle discrimination.

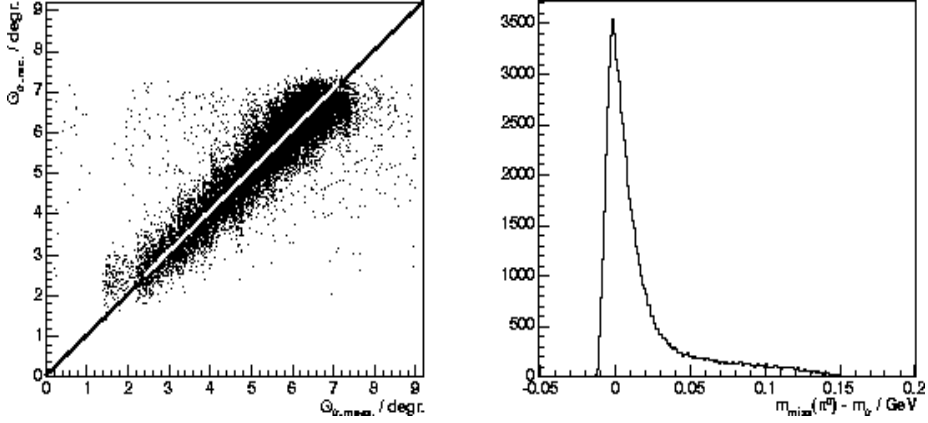


Figure 19: α kinematics reconstructed from measured π^0 . Left: Reconstructed polar angle versus measured polar angle. Right: Reconstructed α missing mass.

Fig. 19 shows — as an example — the correlation between the measured polar angle of the α and the one reconstructed from the pion kinematics as well as the missing mass with only the pion detected.

Taking into account the current geometry of WASA, the combined acceptance for α and π^0 does not vary much and will be $\epsilon_{\text{acc}} \approx 0.5$ for all beam momenta from 1.2 GeV/c up to η threshold. For the following estimates an additional factor of 0.5 is considered representing dead-time corrections, detector- and analysis efficiencies.

Assuming a luminosity of $L = 10^{32} \text{ cm}^{-2} \text{ s}^{-1} = 10^{-4} \text{ s}^{-1} \text{ pb}^{-1}$ the final count rate will be 15 events per week and pb. Since the goal of this experimental

program is to extract differential cross sections, the total yield has to be at least a few hundred events for each beam energy. Using a total cross section of $\sigma \approx 75\text{pb}$ at $Q = 60\text{ MeV}$ (i.e. scaling the IUCF result by s -wave phase space) leads to beam times of about 1 or 2 weeks per measurement. Consequently, although a lower luminosity would still allow to measure one data point within a longer (but still reasonable) beam time, it would hardly be possible to carry out the full experimental program. This program would cover measurements in two different energy ranges, namely at $Q \approx 60\text{ MeV}$ and in the Δ region ($Q \approx 160\text{ MeV}$). However, initially one data point at the lowest beam energy should be measured. It is aimed to run with polarized beam to disentangle the contribution of different partial waves (especially p -waves) as discussed in section 2.1.2. Further runs will then depend on the analysis of these data.

As shown above the reaction $dd \rightarrow \alpha\pi^0$ can be measured with the existing WASA setup without any modifications on the detector system itself. The electronics has to be upgraded: the trigger logic has to be adopted in order to use an efficient energy loss trigger and the data acquisition systems has to be replaced to be able to run at high luminosities (see section 4.3.4).

3.5 a_0^0 - f_0 mixing in $pn \rightarrow d\pi^0\eta$ and $dd \rightarrow \alpha\pi^0\eta$

At a later stage of the experimental program with WASA at COSY the reactions $pn \rightarrow d\pi^0\eta$ and $dd \rightarrow \alpha\pi^0\eta$ will be measured. The main challenges for the identification of the isospin violating effects in these reactions will be:

$pn \rightarrow d\pi^0\eta$: The measurement of this reaction is similar to the pp experiment described in Section 3.2. However, an additional complication comes from the fact that deuterium has to be used as an effective neutron target. The signal for isospin violation in this reaction would be provided from the measurement of the angular forward-backward asymmetry of the $(\pi^0\eta)_{l=0}$ system.

$dd \rightarrow \alpha\pi^0\eta$: This reaction is only possible due to isospin violation and the yield will be rather small. First estimates show that the cross section should be of the order of 100 pb [111]. A better prediction can be obtained from data on the reaction $dd \rightarrow \alpha K^+ K^-$ which are expected from ANKE in winter 2004/05. It is thus suggested to perform these measurements (at lower beam energies, see Sect. 3.4) before the $dd \rightarrow \alpha\pi^0\eta$ reaction will be studied at maximum COSY momentum ($\approx 3.7\text{ GeV}/c$).

3.6 Study of hyperon resonances

In order to understand the nature of the $\Lambda(1405)$ hyperon resonance it is proposed to study $\Lambda(1405)$ production in proton-proton collisions, and in a second step also in proton-nucleus collisions. The primary goal of this study is to measure the $\Lambda(1405)$ production cross section and, in particular, its spectral shape. As a by-product also information on the $\Sigma(1385)$ resonance is obtained.

Due to its large acceptance for both charged particles and photons, the WASA detector allows to investigate all isospin combinations of $\Sigma\pi$ and $\Lambda\pi$ that are populated in hyperon resonance decay subsequent to the production reactions $pp \rightarrow \Lambda(1405)K^+p$ and $pp \rightarrow [\Sigma(1385)K]^+p$. With the use of a deuterium target the implementation of a proton spectator detector close to the interaction

point would be required, in order to allow the full measurement of all particles in the final state (equivalent to pp collisions) also in $pn \rightarrow \Lambda(1405)K^0p$ and $pn \rightarrow [\Sigma(1385)K]^0p$ reactions. Note that the latter reaction also allows to excite the $\Sigma^-(1385)$ state.

The photon detection capability of WASA matches particularly well to the study of the $pp \rightarrow \Lambda(1405)K^+p$ reaction with the decay channel $\Lambda(1405) \rightarrow \Sigma^0\pi^0 \rightarrow (\Lambda\gamma)(\gamma\gamma)$ which is not populated in $\Sigma^0(1385)$ decay, and thus should reflect the $\Lambda(1405)$ spectral distribution in an undisturbed way. Therefore special emphasis should be given to this channel, but as discussed in Sect. 2.2.2 also the $\Sigma^+\pi^-$ and $\Sigma^-\pi^+$ channels deserve investigation in order to extract a possible isovector contribution. For the observed final state in the decay channel $\Lambda(1405) \rightarrow \Sigma^0\pi^0 \rightarrow (\Lambda\gamma)(\gamma\gamma) \rightarrow (p\pi^-\gamma)(\gamma\gamma)$ the expected branching ratio is rather large, and amounts to 21%.

Fig. 20 shows the simulated transverse versus longitudinal momentum distribution for the particles in the final state in this reaction induced by 3.6 GeV/c protons, assuming a pure phase space distribution of the events, and taking into account a $\Lambda(1405)$ Lorentz mass distribution of a full width $\Gamma = 50$ MeV/c². It demonstrates that both protons in the final state, from the primary vertex and from the Λ decay, have a high probability to be emitted into the acceptance of the forward detector, whereas the dominant fraction of the pions will be detected by the central detector of WASA. The K^+ mesons populate both regions of the phase space seen by the central and by the forward detector. Only a small fraction of photons is not covered by the CsI calorimeter acceptance.

In order to add new information to the experimental knowledge of the spectral shapes of the $\Lambda(1405)$ and $\Sigma(1385)$ resonances, the mass resolution has to be clearly better than the widths of these resonances of ≈ 50 MeV/c² and ≈ 40 MeV/c², respectively. The resolution of better than ≈ 10 MeV/c² allowed by the WASA detector is considered to be sufficient for this study. Further improvement of the resolution is possible if new tracking detectors, such as μ -strip silicon arrays, are implemented close to the target. This would allow, in addition to the reduction of non-strange background, to make use of additional kinematic constraints by a precise measurement of tracks including displaced vertex information.

The optimum proton beam energy is given by the requirement that the kinematic limit be at sufficient distance from the pole of the $\Lambda(1405)$ resonance in order to guarantee the undisturbed measurement of its spectral distribution. At energies too close to threshold it may be difficult to disentangle the $\Lambda(1405)$ spectral function and the effect of an energy dependent final state interaction. A reasonable beam momentum is $p_p = 3.6$ GeV/c, well within the COSY momentum range for internal beams, at which the kinematic limit in the Λ^* or Σ^* mass is $M_{max} = 1.53$ GeV, more than 100 MeV/c² above the $\Lambda(1405)$ pole.

The expected hyperon resonance production cross sections are of the order of 1 μ b [191]. With a luminosity $L = 10^{31}$ cm⁻²s⁻¹, assuming 10% overall efficiency, one thus expects approximately 18000 counts per day for the $pp \rightarrow \Lambda(1405)K^+p$ reaction with a $(p\pi^-\gamma)_{\Sigma^0}(\gamma\gamma)_{\pi^0}K^+p$ final state discussed above. In case the cross section and/or efficiencies should be smaller, the maximum design luminosity $L = 2 \cdot 10^{32}$ cm⁻²s⁻¹ of WASA gives room for an increase of the luminosity.

The second part of the program related to comparative studies of the in-medium properties of the $\Lambda(1405)$ and $\Sigma(1385)$ hyperon resonances requires the usage

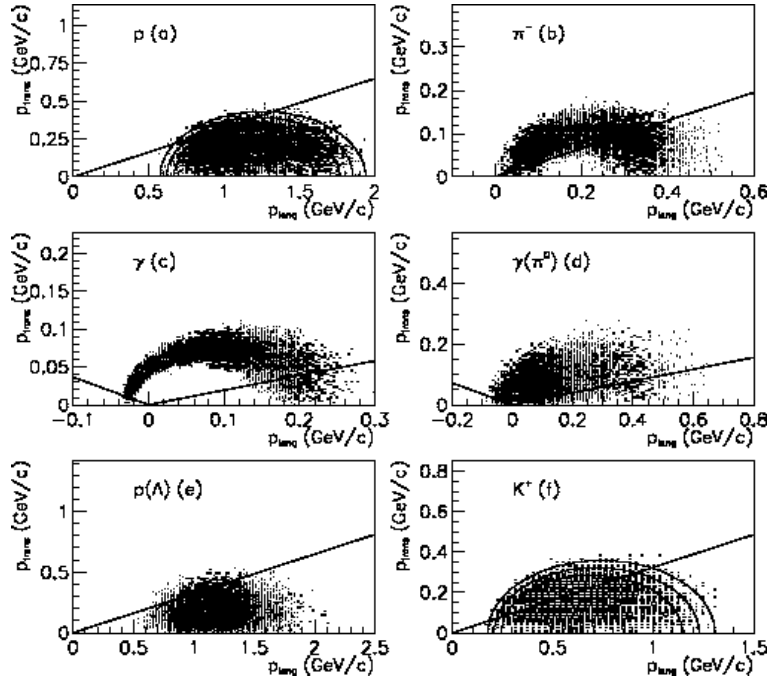


Figure 20: Simulated transverse vs. longitudinal momentum distribution for the final state particles in the reaction $pp \rightarrow \Lambda(1405)pK^+ \rightarrow \Sigma^0\pi^0pK^+ \rightarrow \Lambda\gamma\pi^0pK^+ \rightarrow p^{(e)}\pi^{-(b)}\gamma^{(c)}\gamma\gamma^{(d)}p^{(a)}K^{+(f)}$. The superscripts denote the corresponding panels. The ellipses in panels (a) and (f) show the kinematic limits with $\Lambda(1405)$ production at its pole mass as well as 25 MeV/c² below and above. The straight lines separate the acceptance of the central and the forward spectrometer of WASA.

of nuclear targets, and thus an extension of the existing pellet target to an operation with gases like nitrogen, argon and xenon which still needs to be developed. Furthermore, for these studies additional tracking information close to the target allowing hyperon and K_s identification will be necessary, since a full reconstruction of the final state is not possible with a nuclear target, which results in a loss of kinematic constraints. For this purpose the WASA detector would have to be extended by the implementation of μ -strip silicon detectors in close geometry to the interaction point.

3.7 Rare and very rare η and η' decays

High precision branching ratio for $\eta' \rightarrow \gamma\gamma$. In spite of the large branching ratio this experiment will be performed at a later time since it requires technical modifications to achieve high precision as discussed below. The radiative decay widths of $\eta(\eta') \rightarrow \gamma\gamma$, together with additional information from radiative J/Ψ decays to $\eta(\eta')\gamma$ or from radiative transitions of vector (V) and pseudoscalar (P) mesons in $V \rightarrow P\gamma$ and $P \rightarrow V\gamma$ processes, allow to extract the fundamental constants of the pseudoscalar nonet (see e.g. [24]). The unprecedented statistical

accuracy, that is expected to be feasible for radiative decays using the WASA facility at COSY (see table 1) suggests to increase the precision on branching ratios of radiative decays presently available.

For the decay $\eta' \rightarrow \gamma\gamma$, the statistical accuracy of the branching ratio might be increased by an order of magnitude in a dedicated run of two to three weeks, yielding a statistical error below the percent level. However, to obtain precision values for the branching ratio requires to control the systematic error with comparable accuracy. A suitable experimental approach is described for the decay $\eta \rightarrow \gamma\gamma$ in [192], with a direct measurement of the branching ratio. Thus, all systematic uncertainties related to the "normalization", i.e. the simultaneous measurement of a known branching ratio, are eliminated, and, analogously to [192] the branching ratio is given by

$$\frac{\Gamma(\eta' \rightarrow \gamma\gamma)}{\Gamma_{tot}} = \frac{N(\eta' \rightarrow \gamma\gamma)}{N(pp \rightarrow pp\eta')} \times \left(A_{\eta' \rightarrow \gamma\gamma} \epsilon_{\eta' \rightarrow \gamma\gamma}^{analysis} \epsilon_{\eta' \rightarrow \gamma\gamma}^{electronics} \right), \quad (10)$$

where $A_{\eta' \rightarrow \gamma\gamma}$ denotes the detector acceptance and $\epsilon_{\eta' \rightarrow \gamma\gamma}$ the efficiencies in the analysis and in the electronics to reconstruct and reliably digitize an $\eta' \rightarrow \gamma\gamma$ decay. The precise number of events, background subtraction and (different) efficiency corrections only have to be considered for the $\gamma\gamma$ decay mode. Experimentally, the approach requires to trigger on the pp system associated with η' production, i.e. on two protons in the forward detector. With an estimate of a 50 kHz rate from a trigger on two charged particles in the forward detector at luminosities of $10^{32} \text{ cm}^{-2} \text{ s}^{-1}$, and in view of the attainable event rates for the planned data acquisition system (see section 4.3.4) in the order of 10 kHz a high precision measurement of the $\eta' \rightarrow \gamma\gamma$ branching ratio seems feasible after all, but will require further improvements of the selectivity of the forward detector trigger. Developments have already started for WASA at CELSIUS to implement a missing mass trigger for the $\Delta E/E$ technique by implementing energy reconstruction and angular correction of the energy loss information on the trigger level, and direct branching ratio measurements should become feasible after some experience and development with WASA at COSY.

Double vector meson dominance in $\eta \rightarrow e^+e^-e^+e^-$. Experimentally, the η will be tagged by using the missing mass of the two protons detected in the forward detector. Tracks of electrons and positrons are measured in the Mini Drift Chamber (MDC) inside the super-conducting solenoid, and their energy is determined by means of the CsI calorimeter.

Background from $2\pi^0$ production via $\pi^0\pi^0 \rightarrow e^+e^-e^+e^-\gamma\gamma$ with two undetected γ s can be effectively removed by kinematic cuts. The η decay modes to $e^+e^-\gamma$ ($\Gamma(\eta \rightarrow e^+e^-\gamma)/\Gamma_{tot} = 6.0 \pm 0.8 \cdot 10^{-3}$ [45]) and to 2γ ($\Gamma(\eta \rightarrow \gamma\gamma)/\Gamma_{tot} = 39.43 \pm 0.26\%$ [45]) contribute via photon conversion in the beam tube. Both channels are effectively reduced to a level below 1% by reconstructing the vertices of both e^+e^- pairs [193].

Based on the QED prediction for the branching ratio of $2.52 \cdot 10^{-5}$ [51] and the acceptance of the WASA setup, at a luminosity of $10^{32} \text{ cm}^{-2} \text{ s}^{-1}$ we expect a rate of about $3 \cdot 10^3$ events per week. In a 3-months run one will collect a data sample of 30000 events which will allow for a high statistics measurement of the form factor dependence on the virtual photon masses. In a second phase the data for the decay $\eta \rightarrow e^+e^-e^+e^-$ can be collected together with the $\eta \rightarrow e^+e^-$ experiments.

Search for CP violation in the rare decay $\eta \rightarrow \pi^+\pi^-e^+e^-$. η tagging as well as electron and positron detection will be performed as described in Section 3.1. Electrons are separated from pions using the momentum over energy ratio with an accuracy of $5 \cdot 10^{-3}$. The fraction of misidentified charged leptons has been estimated to be less than $2.5 \cdot 10^{-5}$. From the complete four-momentum information for all four charged decay products, the angle between the $\pi^+\pi^-$ and e^+e^- production planes can be reconstructed.

The major source of background arises from the conversion of photons from the $\eta \rightarrow \pi^+\pi^-\gamma$ decay in the beam tube. With an overall conversion probability of 0.28% the background is important only in the region of small e^+e^- invariant masses below $40 \text{ MeV}/c^2$. In comparison, background from other sources like direct production is negligible.

The experiment can be carried out together with studies of the $\eta \rightarrow e^+e^-e^+e^-$ decay channel (see paragraph above) and statistics of nearly $4 \cdot 10^5$ $\eta \rightarrow \pi^+\pi^-e^+e^-$ events could be obtained, corresponding to an accuracy of $2 \cdot 10^{-3}$ for the asymmetry.

Search for physics beyond the Standard Model in the very rare $\eta \rightarrow e^+e^-$ decay. The experiment aims at reaching a sensitivity that allows to test whether the η decay to the e^+e^- mode occurs at a rate compatible with the Standard Model prediction of $5 \cdot 10^{-9}$ [43, 44], which makes the decay susceptible to contributions from physics beyond the Standard Model, with a present experimental upper limit at $7.7 \cdot 10^{-5}$ [45].

The experimental signature will consist of four charged tracks, with two protons in the reaction $pp \rightarrow pp\eta \rightarrow ppe^+e^-$ tagged in the forward detector and the e^+e^- , with an isotropic distribution in the η rest frame measured in the central detector with magnetic field. In view of the low branching ratio the experiment requires high acceptance and high luminosity, charged particle tracking, and the possibility to reject events with photons by means of an electromagnetic calorimeter, which makes the WASA facility at COSY a unique device for this rare decay channel. The most important physics processes that can contribute to a possible background are the $\eta \rightarrow \gamma e^+e^-$ Dalitz decay, the radiative decay mode $\eta \rightarrow \gamma\gamma$, and prompt e^+e^- production. The continuous spectrum of e^+e^- pairs up to the η mass from the γe^+e^- decay mode ($\Gamma(\eta \rightarrow \gamma e^+e^-)/\Gamma_{tot} = 6.0 \pm 0.8 \cdot 10^{-3}$ [45]) is effectively reduced to a level of less than 10% compared to the $\eta \rightarrow e^+e^-$ signal by rejecting photons in the central detector (Fig. 21).

γ conversion in the material between the interaction point and the plastic barrel (PSB) leads to a background contribution from the $\eta \rightarrow \gamma\gamma$ mode ($\Gamma(\eta \rightarrow \gamma\gamma)/\Gamma_{tot} = 39.43 \pm 0.26\%$ [45]), if both γ s convert asymmetrically in energy. Most of the relevant material is concentrated by the 1.2 mm Be beam-pipe, giving rise to a signal-to-background ratio¹² of 1–2 to 1 in the η mass range (Fig. 21). A statistically significant signal from the rare $\eta \rightarrow e^+e^-$ decay on the level of the Standard Model prediction, as indicated in figure 21, could be obtained in a running time of 2 months. It should be noted, that an appropriate trigger setting will allow to run the experiment in parallel with other η decay studies, and, that already after one hour of beamtime, the experiment can increase the level of sensitivity in comparison to the present upper limit

¹²The background is expected to be reduced further by vertex reconstruction, which is not implemented in the simulations.

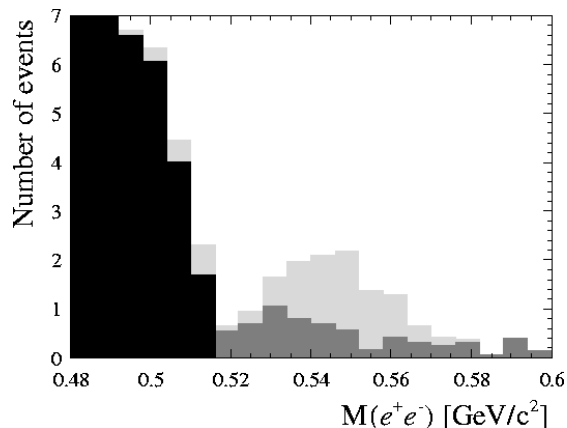


Figure 21: Background contribution from $\eta \rightarrow \gamma e^+ e^-$ (black), $\eta \rightarrow \gamma\gamma$ (dark grey) and sum of the $\eta \rightarrow e^+ e^-$ signal and the two background sources (light grey). The simulation assumes the Standard Model prediction for the branching ratio of $5 \cdot 10^{-9}$ for $\eta \rightarrow e^+ e^-$ and the PDG values for the background channels, scaled to a total of 10^{10} η events produced.

by an order of magnitude. Furthermore, it should be emphasized, that these investigations are only feasible due to the optimization of the WASA setup with respect to the amount of material between the interaction point and the central detector (see section 4.2), to fully exploit the advantages of a windowless internal target.

However, the theoretical and experimental uncertainties for the background from prompt $e^+ e^-$ production in the η mass range are large. Calculations [194] based on the approach described in [195] lead to a signal-to-background ratio for the decay $\eta \rightarrow e^+ e^-$ of 1 to 30 with respect to prompt production. Thus, in order to have a reliable estimate for the prompt production background, it is suggested to prepare the $\eta \rightarrow e^+ e^-$ search by measuring the prompt contribution $pp \rightarrow ppe^+ e^-$ first.

At the same time, since WASA allows for exclusive measurements, this preparatory study can shed light on both the relative strength of different sources of $e^+ e^-$ pairs, and meson and baryon isobar form factors. The first aspect is intimately motivated by the expectation that dileptons carry information from the early stage of heavy ion collisions. Discrepancies between theoretical calculations (see e.g. [196, 197]) and the presently available data for dilepton production in proton-proton and proton-deuteron collisions measured with rather small geometrical acceptance at the DLS spectrometer [198] — especially in the mass range between 0.2 and 0.5 GeV/c^2 — could be verified experimentally using WASA at COSY. Assuming a luminosity of $10^{32} \text{ cm}^{-2} \text{ s}^{-1}$ reasonable statistics of about 10^4 events can be achieved in five days of data taking, i.e. a program of four kinetic beam energies ranging from 1.04 to 2.5 GeV to overlap both with the DLS data and theoretical calculations is feasible within three weeks, and will provide the necessary information for a reliable background estimate from prompt production concerning the search for the rare $\eta \rightarrow e^+ e^-$ decay.

C violation in $\eta \rightarrow \pi^0 e^+ e^-$. The experiment aims at a sensitivity down to the Standard Model prediction for the branching ratio of $0.2 - 1.3 \cdot 10^{-8}$ [52–54], to search for new C-violating effects in the electromagnetic interaction. With a value of $\Gamma(\eta \rightarrow \pi^0 e^+ e^-)/\Gamma_{tot} < 4 \cdot 10^{-5}$ [45] the present upper limit is three orders of magnitude weaker than the theoretical estimate.

Monte Carlo simulations have been carried out to investigate the feasibility of the experiment and background conditions. In conclusion, a search sensitivity of 10^{-9} is possible considering the full background. A sample of ten events from C-conserving mechanisms for the rare decay can be expected after a period of three weeks to five months, depending on the actual value of the branching ratio.

A C-violating admixture at the level of 10^{-3} would already double the $\eta \rightarrow \pi^0 e^+ e^-$ decay rate. However, at present this effect is small compared to the uncertainty in theoretical estimates for the C conserving decay mechanism, which is due to insufficient knowledge of value and structure of the $\eta \rightarrow \pi^0 \gamma \gamma$ amplitude. Consequently, an improved precision in the $\eta \rightarrow \pi^0 \gamma \gamma$ decay rate is important for the interpretation of the experimental result of the proposed study of the $\pi^0 e^+ e^-$ decay mode, and a high statistics study of $\eta \rightarrow \pi^0 \gamma \gamma$ should be carried out simultaneously.

Measurement of the η' transition form factor. With η' tagging by means of two detected protons in the forward detector and the reconstruction of the decay system of the Dalitz conversion decay $\eta' \rightarrow \gamma \gamma^* \rightarrow \gamma e^+ e^-$ in the central detector, the WASA setup is well suited for measuring the η' transition form factor. With the tracking information from the Mini Drift Chamber, the momenta of electron and positron are determined. Thus, the differential cross section

$$\frac{d\sigma}{dq^2} = \left[\frac{d\sigma}{dq^2} \right]_{pointlike} [F(q^2)]^2 \quad (11)$$

with respect to the four-momentum transfer squared q^2 of the time-like virtual photon, which is equal to the invariant mass squared of the $e^+ e^-$ pair, can be measured, and the transition form factor $F(q^2)$ can be extracted. The form factor is usually fitted with the simplest pole-type formula

$$F(q^2) = \frac{1}{1 - \frac{q^2}{\Lambda^2}} \approx 1 + \frac{q^2}{\Lambda^2} \quad (12)$$

with the slope parameter Λ .

At present, only an upper limit exists for the $\gamma e^+ e^-$ decay mode of the η' ($\Gamma(\eta' \rightarrow \gamma e^+ e^-)/\Gamma_{tot} < 9 \cdot 10^{-4}$). With an estimated branching ratio of $3 \cdot 10^{-4}$, as discussed in [55], we expect 45 fully reconstructed η' Dalitz conversion decays per day. Following the discussion for the $\eta' \rightarrow \gamma \pi^+ \pi^-$ decay in section 3.1 we only consider the radiative decay $\eta' \rightarrow \gamma \gamma$ with subsequent conversion of one γ as a possibly important source of background. With fits to the η' signal in each bin of the $e^+ e^-$ invariant mass scale, the differential cross section can be extracted background free, unless there is a background process for the $\eta' \rightarrow \gamma e^+ e^-$ transition. However, since for η decays the $\gamma \gamma$ mode was found to be negligible above very low invariant lepton pair masses [37], and since the ratios $\Gamma(\eta(\eta') \rightarrow \gamma e^+ e^-)/\Gamma(\eta(\eta') \rightarrow \gamma \gamma)$ are approximately the same for η and η' , and

since the photon conversion probability is not changing drastically, it can safely be neglected as a background contribution.

The beam time estimate depends on the desired accuracy for the slope parameter Λ in eq. 12. From the analogous discussion of the η transition form factor in [37], a running time of two months would allow a determination of the slope parameter with a 10% error. A further improvement by a factor of two in accuracy would require a nine months period of data taking. It should be noted, that due to the trigger condition of two charged and one neutral particle in the central detector data taking could be done in parallel with other η' decay studies. For example, the specific trigger requirement for the η' Dalitz conversion decay exactly matches the trigger setup for the $\pi^+\pi^-\gamma$ mode discussed in section 3.1 in terms of particle multiplicities.

4 Experimental facility

4.1 Cooler Synchrotron COSY

COSY is a cooler synchrotron and storage ring operated at the IKP of FZJ. The accelerator complex (see Fig. 22) comprises an isochronous cyclotron (JULIC), used as an injector, a race track shaped cooler synchrotron with a circumference of 184 m, and internal and external target stations [199]. COSY delivers beams of polarized and unpolarized protons and deuterons in the momentum range between 0.3 GeV/c and 3.7 GeV/c. The ring can be filled with up to 10^{11} particles leading to typical luminosities of $10^{31} \text{ cm}^{-2} \text{ s}^{-1}$ when using an internal cluster target. Beams can be phase-space cooled by means of electron cooling at injection energy as well as stochastic cooling at high energies. Typical beam preparation times, including injection, accumulation and acceleration, are of the

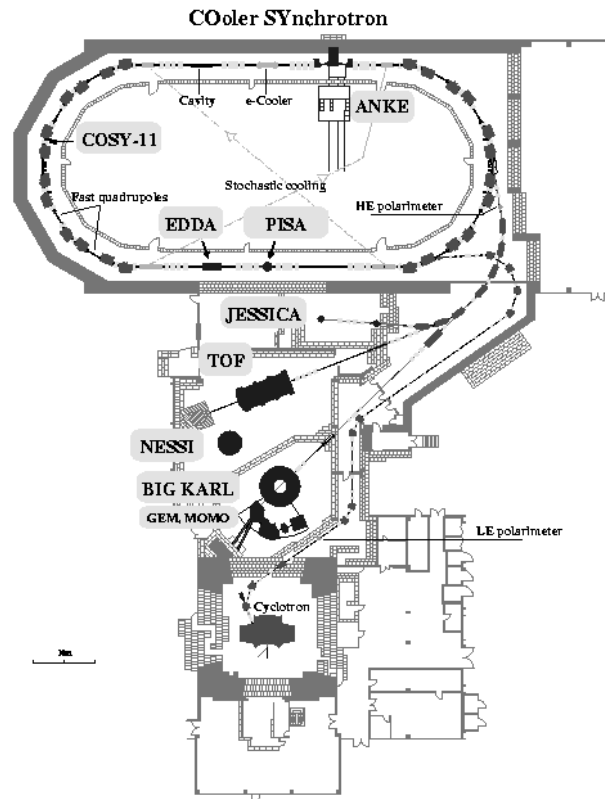


Figure 22: Floorplan of the accelerator complex. The WASA detector will be installed at the place of the old cavity in front of the electron cooler.

order of a few seconds, while the beam lifetime with a cluster target is between several minutes and an hour.

Currently, four internal experiments (ANKE, COSY-11, EDDA, PISA) and three external detector systems (BIG KARL, JESSICA, TOF) are operated by large international collaborations. On the average COSY is running for more than 7000 hours per year. Typically, it delivers beams for experiments with a reliability of 94%.

Implementation of WASA at COSY

The Cooler Synchrotron has two 40 m long straight sections joining the arcs. After removal of the old RF cavity at the beginning of 2004 space for the implementation of WASA at an internal target position in front of the electron cooler is available (see Fig. 22). This location has a number of advantages: most importantly it minimizes both the interference with the existing COSY detectors and the modifications needed to the WASA detector and the accelerator.

Operating WASA with the pellet target with an effective thickness of $2.5 \cdot 10^{15} \text{ cm}^{-2}$ average luminosities of $10^{32} \text{ cm}^{-2} \text{ s}^{-1}$ and beam lifetimes of a couple of minutes are expected [200]. Compared to the present operation at CELSIUS the experimental conditions will be improved due to the different accelerator characteristics: fast magnet ramping, dispersion-free target position, stochastic cooling and a smooth microscopic time structure of the beam.

4.2 The WASA detector

The 4π detector facility WASA [201,202] was designed for studies of production and decays of light mesons at CELSIUS. Pions and eta mesons are produced in proton-proton and proton-deuteron interactions. The highest beam-proton kinetic energy reachable at CELSIUS is 1.5 GeV.

The pellet-target system is integrated in the setup and it provides small spheres of frozen hydrogen and deuterium as internal targets. This allows high luminosity and high detection coverage for meson decay products like photons, electrons and charged pions.

WASA consists of a forward part for measurements of charged target-recoil particles and scattered projectiles, and a central part designed for measurements of the meson decay products. The forward part consists of eleven planes of plastic scintillators and of proportional counter drift tubes. The central part consists of an electromagnetic calorimeter of CsI(Na) crystals surrounding a superconducting solenoid. Inside of the solenoid a cylindrical chamber of drift tubes and a barrel of plastic scintillators are placed. A vertical cross section of the WASA detector is shown in Fig. 23.

4.2.1 Pellet target

The pellet target system was a unique development for the CELSIUS/WASA experiment [203,204]. The main components of the system are shown in Fig. 24. The heart of the setup is the pellet generator where a jet of liquid hydrogen is broken up into droplets with a diameter around $35 \mu\text{m}$ by a vibrating nozzle. The droplets freeze by evaporation in a droplet chamber and form a beam of pellets that enter a 7 cm long vacuum-injection capillary. After collimation, the pellets are directed through a thin 2 m long pipe into the scattering chamber

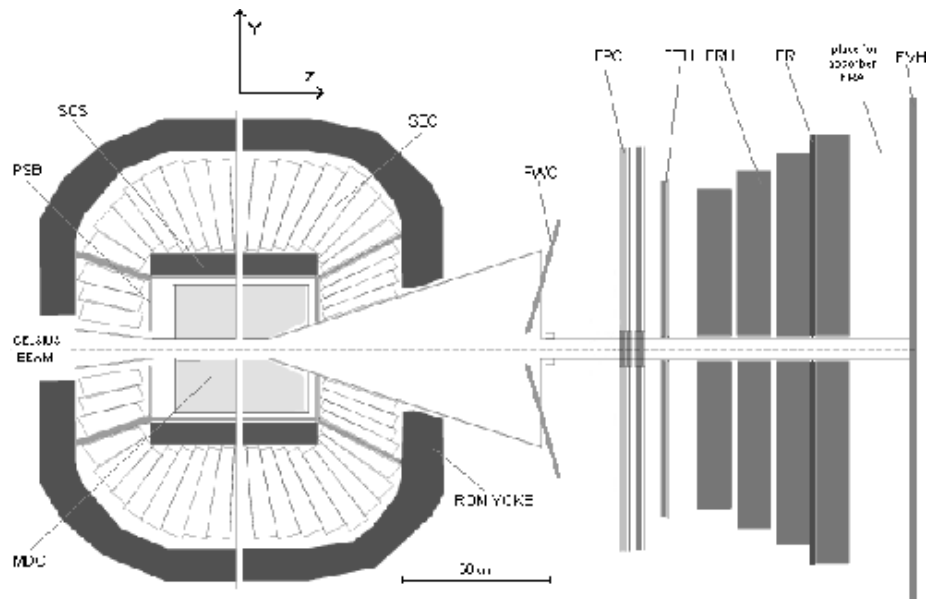


Figure 23: Cross section of the WASA detector. The central detector built around the interaction point (at the left) is surrounded by an iron yoke. The layers of the forward detector are visible on the right-hand side. The individual components are described in the text.

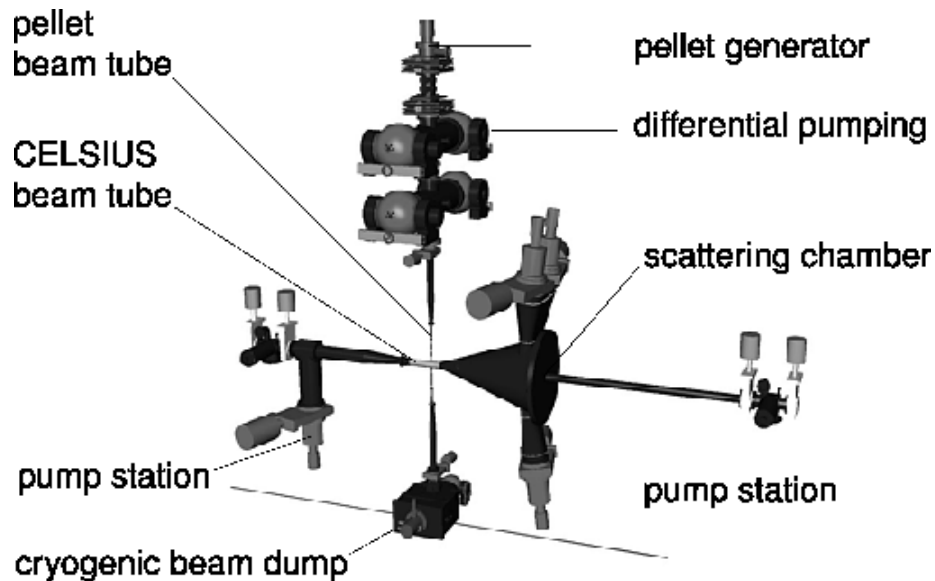


Figure 24: Layout of the pellet target system.

and further down to a pellet beam dump. The inner diameter of the pipe is 5 mm at its entrance to the scattering chamber. This arrangement provides the necessary space to put the 4π detection system around the interaction region.

Pellet target thicknesses of up to $3 \cdot 10^{15}$ atoms/cm² give acceptable half-lives of the circulating ion beam as well as acceptable vacuum conditions. Some of the parameters of the pellet target at the present stage of operation are listed in table 3. The pellet target system operates regularly with pellets of normal hydrogen and deuterium.

Pellet target parameters	Present performance
Pellet diameter	25 - 35 μ m
Pellet frequency	5-12 kHz
Pellet-pellet distance	9-20 mm
Effective target thickness	$> 10^{15}$ atoms/cm ²
Beam diameter	2 - 4 mm

Table 3: Present performance of the pellet target system.

4.2.2 Forward detector

The forward detector (FD) is designed mainly for detection and identification of scattered projectiles and charged recoil particles like protons, deuterons and He nuclei in π and η production reactions. Also neutrons and charged pions can be measured. All FD plastic scintillators may supply information for the first level trigger logic. This part of the setup has already been used in a previous experiment at CELSIUS, WASA/PROMICE, which is described more in detail in [205]. A summary of the most important features of the forward detector (FD) is given in table 4. The individual components are described in some detail in the following.

Forward detector	
Total number of scintillator elements	280
Scattering angle coverage	3° - 17°
Scattering angle resolution	0.2°
Amount of sensitive material [g/cm ²]	50
[radiation lengths]	≈ 1
[nuclear interaction lengths]	≈ 0.6
Thickness of vacuum window (st. steel) [mm]	≈ 0.4
Maximum kinetic energy (T_{stop}) for stopping: π^\pm /proton/deuteron/alpha [MeV]	170/300/400/900
Time resolution	< 3 ns
Energy resolution for:	
stopped particles	$\approx 3\%$
particles with $T_{stop} < T < 2T_{stop}$	4 - 8%
Particle identification	$\Delta E-E$

Table 4: Some features of the Forward Detector.

The Forward Window Counters (FWC)

The FWC is the first detector layer in the FD (along the beam direction) and

consists of 12, 5 mm thick plastic scintillators (Fig. 25). It is mounted tightly on the paraboloidal stainless steel vacuum window. Therefore, the elements are inclined by approximately 10° with respect to the plane perpendicular to the beam direction. The FWC signals are used in the first level trigger logic to reduce the background caused by particles scattered in the downstream beam pipe and in the flange at the entrance to the FD. The signals are also used to select He ejectiles on the trigger level.

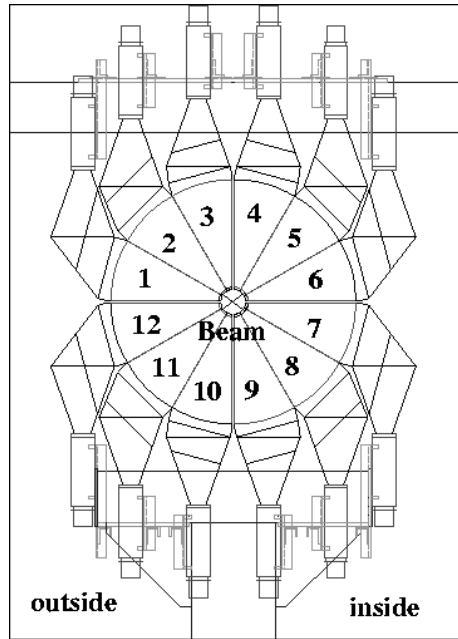


Figure 25: Schematic view of the FWC.

The Forward Proportional Chambers (FPC)

Immediately downstream of the FWC, there is a tracking device. It is composed of 4 modules, each with 4 staggered layers of 122 proportional drift tubes (so called straws) of 8 mm diameter (Fig. 26). The modules are rotated by 45° with respect to each other (in the plane perpendicular to the beam axis). They are used for accurate reconstruction of track coordinates and provide precise angular information of the particles originating from the target region.

The Forward Trigger Hodoscope (FTH)

The FTH, consisting of three layers of 5mm thick plastic scintillators, is placed next to the FPC. There are 24 Archimedian spiral shaped elements in the first two planes and 48 radial elements in the third.

The FTH is mainly used in the first level trigger logic. However, the special geometry, combining all three layers, results in a pixel structure, which is useful for resolving multi-hit ambiguities. In Fig. 27 the structure of the FTH is shown with hits from two passing charged particles.

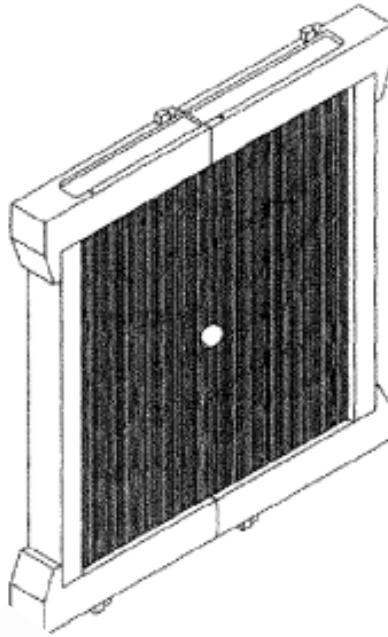


Figure 26: Perspective view of one module of the FTH.

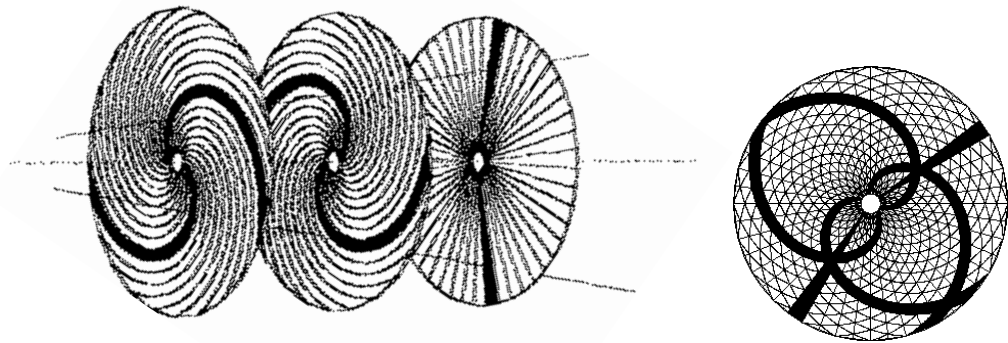


Figure 27: Schematic view of the three forward trigger hodoscope layers.

The Forward Range Hodoscope (FRH)

Behind the FTH, the four layers of the FRH are positioned (Fig. 28). Each plane is made of 24, 11 cm thick, plastic scintillator modules. The FRH, together with FTH, is used for energy determination of charged particles and for particle identification by ΔE -E technique. Fig. 29 shows how protons and deuterons can be identified.

The identity and initial kinetic energy of a charged particle is reconstructed from the pattern of deposited energy in the different detector planes. Fig. 30 shows how the initial kinetic energy of a proton is related to the deposited en-

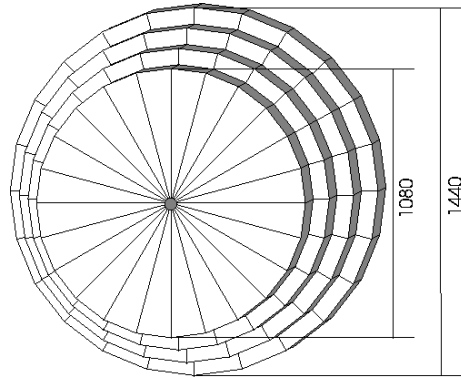


Figure 28: Schematic view of the four forward range hodoscope layers. Dimensions are given in mm.

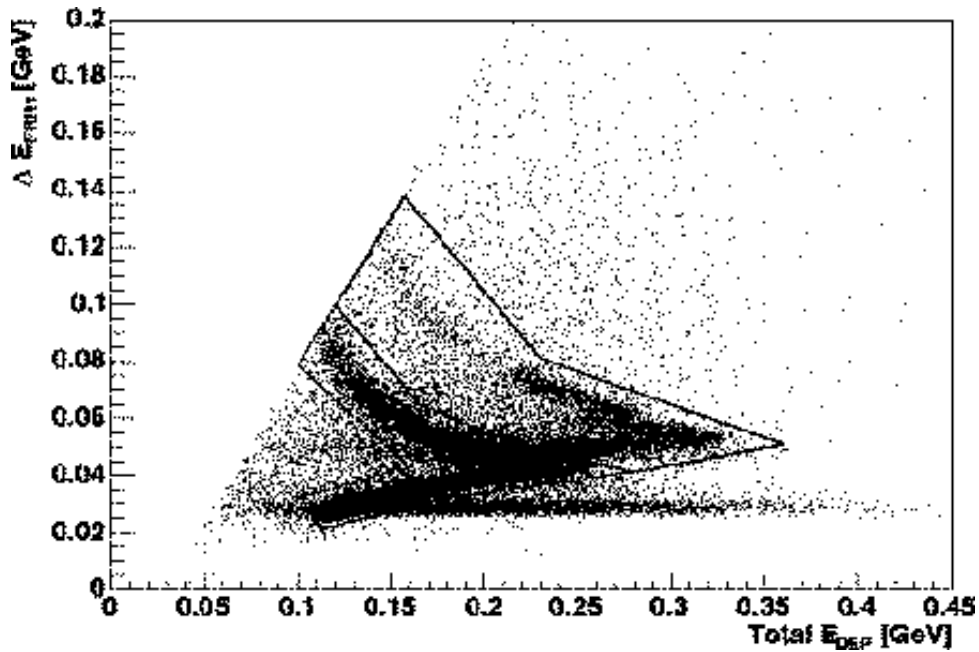


Figure 29: Example of particle identification in the forward detector for data collected at 640 MeV. Energy deposited in the 1st layer of FRH is plotted versus total energy deposited in FTH and FRH. The lines indicate cuts to be used for selecting protons (lower) and deuterons (upper).

ergy in the forward detector scintillators. Even for particles that are stopped in a detector, the total deposited energy is different from the initial kinetic energy. This is because some of the energy is lost in inactive material between the detectors elements, in the scattering chamber windows, etc. Fig. 30 also shows that the variation of the deposited energy is strong enough to be useful for energy reconstruction also for high energy particles not stopping in the detector material. For protons, this can be used in the kinetic energy range

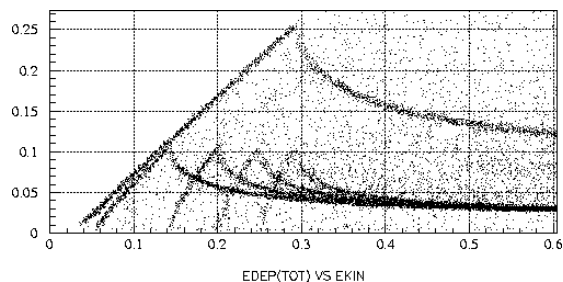


Figure 30: Energy absorbed in the forward detector scintillator material for protons as a function of their initial kinetic energy. The upper curve gives the total energy deposited in the plastic scintillator planes and the lower curves show the energy distributed among the different FRH planes.

300 MeV to 800 MeV and for deuterons in a similar energy range starting from 400 MeV. Identification of punch-through particles can be done using either the veto hodoscope (FVH) or the ΔE information from the last FRH planes.

The Forward Range Interleaving Hodoscope (FRI)

Between the third and fourth layers of the FRH there are two interleaving layers of 5.2 mm thick plastic scintillator bars (Fig. 31). Each layer has 32 bars, oriented horizontally in one and vertically in the other.

The main purpose of this addition to the FRH is to provide a two-dimensional position sensitivity inside the FRH necessary for measurement of scattering angles for neutrons. The efficiency for detection of neutrons of a few hundred MeV kinetic energy by the FRH is around 35 %. In addition, the FRI can help in vertex reconstruction and to discriminate against background tracks due to secondary interactions in the beam pipe and other structural material.

The FRI was recently commissioned; more information about the design and performance of the FRI can be found in [206].

The Forward Veto Hodoscope (FVH)

The last detector layer of the FD is a wall of plastic scintillators (Fig. 32). It consists of 12 horizontal plastic scintillator bars, equipped with photomultipliers on both sides. The hit position along a bar may be reconstructed from signal time information. In the first level trigger the signals are used for rejection (or selection) of particles punching through the FRH.

The Forward Absorber (FRA)

Optionally, a passive absorber layer made of iron can be introduced between the last layer of the FRH and the FVH. The thickness of the absorber can be chosen from 5 mm up to 100 mm. The absorber has been used for stopping the protons from the $pp \rightarrow pp\eta$ reaction at a beam proton energy around 1360 MeV. In this case the faster protons from elastic scattering and from pion production penetrate the FRA and induce signals in the FVH which can be used for veto purposes in the trigger.

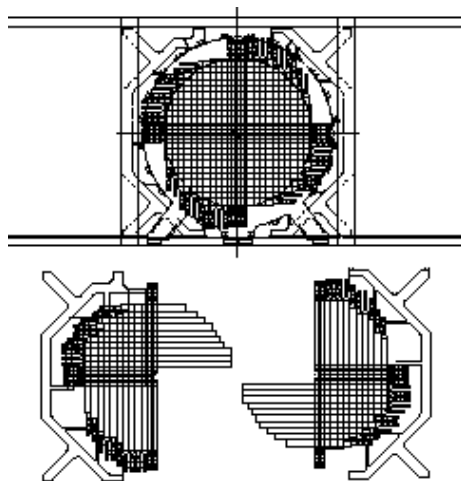


Figure 31: Schematic view of the FRI detector (upper picture) and its two planes with orthogonally oriented scintillator bars (lower picture).

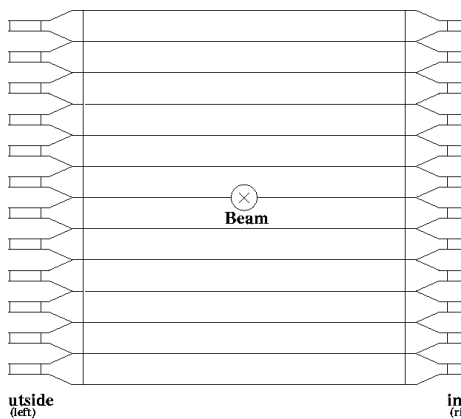


Figure 32: Schematic view of the Forward Veto Hodoscope.

4.2.3 Central detector

The central detector (CD) is built around the interaction point and is designed mainly for detection and identification of the decay products of π^0 and η mesons: photons, electrons and charged pions. It consists of an inner drift chamber (MDC), a solenoid (SCS) providing magnetic field for momentum measurements, thin plastic scintillators in a cylinder geometry (PSB) and a CsI calorimeter (SEC). The amount of structural material is kept minimal to reduce the disturbances on the particles. The beam pipe is made of 1.2 mm thick beryllium and the total thickness of the solenoid corresponds to 0.18 radiation lengths only.

For the design the main requirements were the following:

- it has to handle high particle fluxes at luminosities around $10^{32} \text{ cm}^{-2} \text{ s}^{-1}$.

- it should be able to measure photons with energies from a few MeV up to 800 MeV.
- it should be able to measure, in a magnetic field of about 1 T, the momenta of electrons and positrons in the range $p \approx 20 - 600$ MeV/c with an accuracy $\sigma_p/p < 2\%$.

The momenta of heavier charged particles can also be measured in a similar momentum ranges, but with lower accuracy:

for pions and muons with $p \approx 100 - 600$ MeV/c, $\sigma_p/p < 4\%$

for protons with $p \approx 200 - 800$ MeV/c, $\sigma_p/p < 6\%$

The main components of the Central Detector, shown in Fig. 23, are presented below in some detail.

The Superconducting Solenoid - (SCS)

The SCS provides an axial magnetic field for the momentum measurements for the tracks measured by the MDC. It also protects the CD from low-energy delta electrons produced in the interactions of beam particles with the pellets. The wall thickness of the SCS is minimized in order to allow high accuracy of the energy measurements in the calorimeter. The return path for the magnetic flux is provided by a yoke made out of 5 tons of soft iron with low carbon content. The yoke shields the readout electronics from the magnetic field and serves also as support for the calorimeter crystals. The main parameters of the SCS are given in table 5.

In order to map the magnetic field inside the volume enclosed by the SCS, the magnetic field strength inside the MDC was measured with Hall probes and, in addition, the field distribution was calculated with simulation programs. The calculated values were fitted to the measured ones with an error of $\pm 1\%$ of B_{total} [207]. The magnetic flux density distribution inside of the iron yoke calculated for a current of 667 A is given in Fig. 33. The SCS is described in detail in the Ph.D. thesis of Roger Ruber [208].

Superconducting coil	
Inner/outer radius [mm]	267.8 / 288.8
Superconductor (stabilizer)	NbTi/Cu (pure Al)
Total winding length	465 mm
Maximum central magnetic flux density, B_c	1.3 T
Field uniformity in the MDC	1.22 T $\pm 20\%$
Cooling	Liquid He, 4.5°K
Cryostat	
Material	Aluminium
Inner / outer radius [mm]	245 / 325
Overall length [mm]	555
SCS wall thickness (coil+cryostat) [radl]	0.18

Table 5: Main parameters of the superconducting coil and its cryostat.

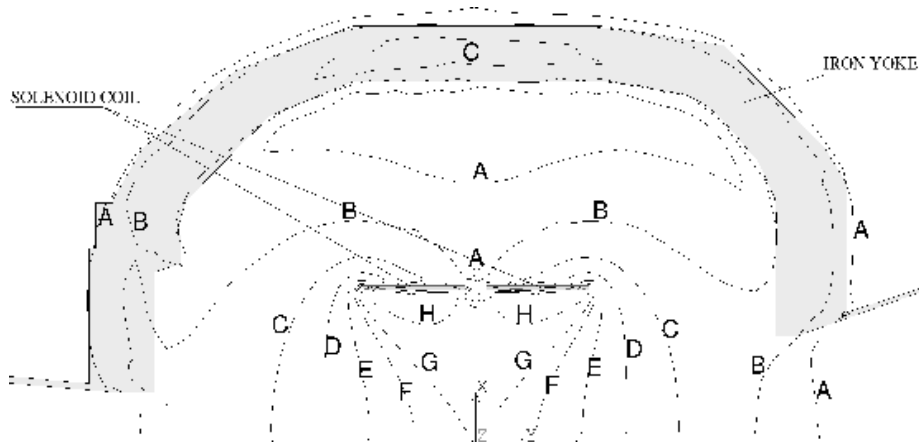


Figure 33: Calculated distribution of the magnetic flux density for a coil current of 667 A [207]. Contour maxima are indicated by lines marked A-H, where: A=0.10T, B=0.25T, C=0.50T, D=0.75T, E=1.00T, F=1.20T, G=1.30T, H=1.50T.

The Mini Drift Chamber - (MDC)

The MDC is placed around the beam pipe and is used for determination of particle momenta and reaction vertex. It is a cylindrical chamber covering scattering angles from 24° to 159° . For large angle scattered protons from elastic proton-proton scattering, a vertex resolution (σ) of 0.2 mm perpendicular and 3 mm along the beam axis can be reached. A detailed description of the MDC can be found in the Ph.D. thesis of Marek Jacewicz [209].

The MDC consists of 1738 drift tubes, so called straws, arranged in 17 cylindrical layers. The diameter of the straws in the 5 inner most layers is 4 mm, 6 mm in the next 6 layers and 8 mm in the outer 6 layers. The straws are made of a thin ($25 \mu\text{m}$) mylar foil coated with $0.1 \mu\text{m}$ aluminum on the inner side only. In the center of each straw there is a $20 \mu\text{m}$ diameter sensing wire made of gold plated tungsten (W(Re)), stretched with a tension of 40 g. The wires are aligned with a precision of $\pm 20 \mu\text{m}$.

This design was chosen in order to cope with the expected high particle flux allowing a maximum deposited energy of approximately $70 \frac{\text{MeV}}{\text{mm}\cdot\text{s}}$ for the straws exposed most at the inner part of the chamber.

The layers are located between radii of 41 and 203 mm. The straws in nine layers are parallel to the beam axis (z-axis) and the other eight layers have small skew angles (6° - 9°) with respect to the z-axis. These “stereo” layers form a hyperboloidal shape.

The straws in the five inner layers are divided unequally by the center of the pellet pipe, while the other layers are symmetrical. The straws in each layer are inter-spaced by small gaps in order to prevent the mechanical deformation by neighboring tubes.

The MDC is fitted inside a cylindrical cover made of 1 mm Al-Be and is placed inside the solenoid (Fig. 34).

The straws in each (half) layer are mounted between ≈ 5 mm thick Al-Be end-plates. The layers are assembled around the Be beam-pipe (Fig. 35) and the

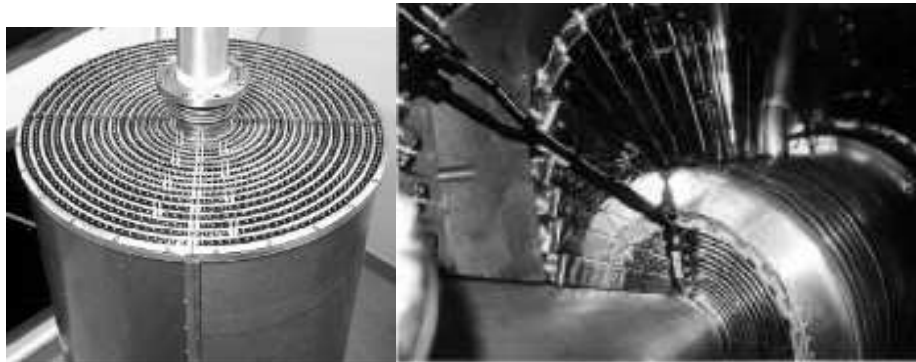


Figure 34: (Left) The fully assembled MDC inside the Al-Be cylinder. (Right) The MDC surrounded by PSB elements.

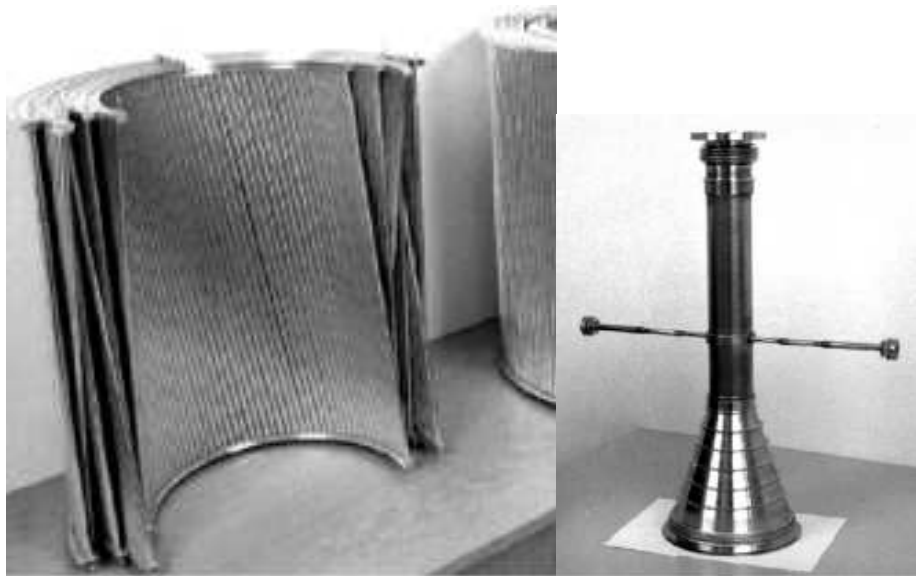


Figure 35: (Left) Drift tubes secured in the end-plates. Note the “stereo” layers interleaved with parallel layers. (Right) Be beam-pipe.

attached pipe for the pellets. The beam-pipe has a diameter of 60 mm and a wall thickness of 1.2 mm. The design drawing of the Be beam pipe is shown in Fig. 36.

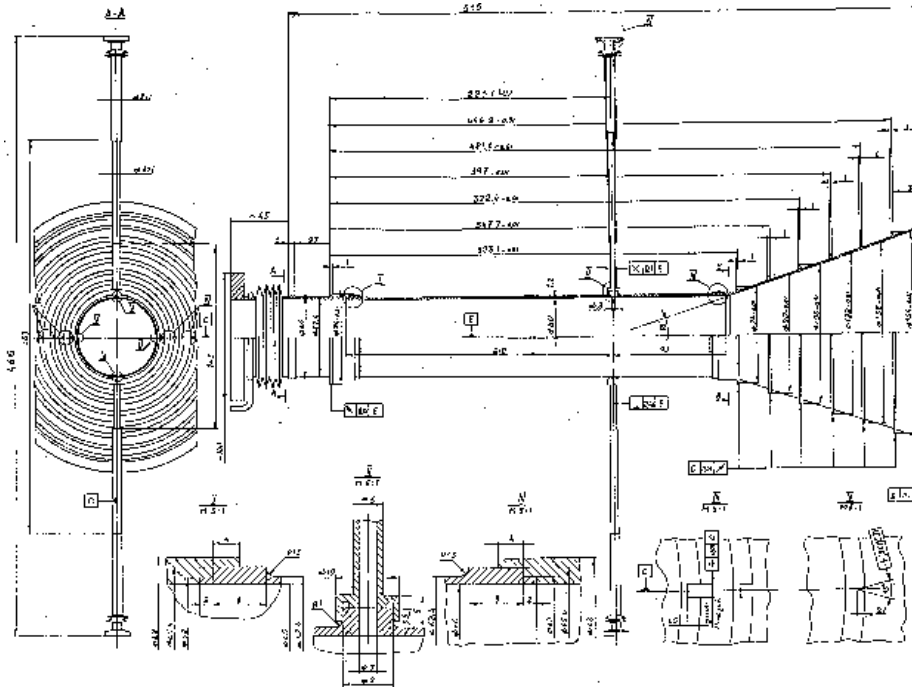


Figure 36: Beryllium beam-pipe including the crossing pellet target tube.

The Plastic Scintillator Barrel - (PSB)

The PSB is located inside the SCS coil and surrounds the MDC. It provides fast signals for the first level trigger logic and, together with the mini drift chamber and the CsI calorimeter, it is employed for charged particle identification by the ΔE -p and ΔE -E methods and serves as a veto for γ identification.

The performance of the PSB has been studied using proton-proton elastic scattering events. Fig. 37 (left plot) shows the result of a Monte Carlo simulation of the angular dependence on the energy deposited in the PSB. Fig. 37 (right plots) shows typical experimental spectra after a correction for nonuniform signal response has been applied.

In the initial experiments the momentum and energy resolution allowed reasonable discrimination between pions and protons, which is illustrated in Fig. 38. For high energy charged particles also SEC information is available and can be used for the identification.

The PSB consists of a cylindrical part and two end caps and contains in total 146 elements shaped as strips of 8mm thickness. In the cylindrical part there are 48(+2) elements of 550 mm length and 38 mm width, forming 2 layers with a small (on average 6 mm) overlap between neighboring elements to avoid that particles pass without registration. The end caps with an outer diameter of approximately 42 cm in the backward and 51 cm in the forward part contain 48 “cake-piece” shaped elements each. The front end cap is flat while the rear cap forms a conical surface. Both end caps have a central hole for the beam pipe (19 cm diameter in the forward and 12 cm diameter in the backward part). The

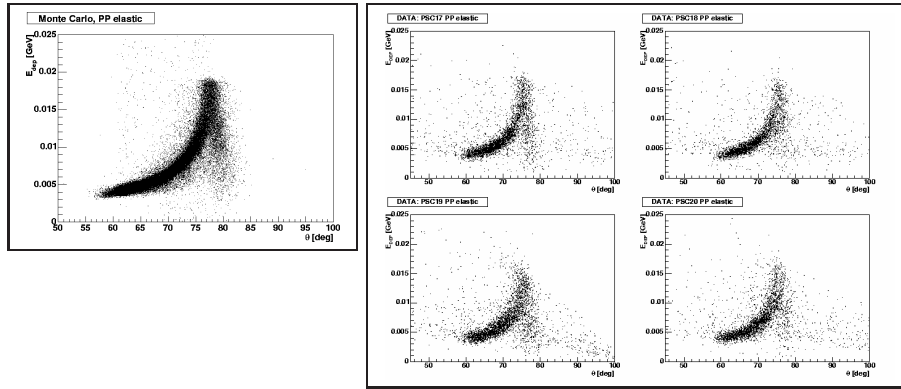


Figure 37: (Left) Angular dependence of the deposited energy in the PSB for simulated elastically scattered protons. The energy deposition increases with increasing polar angle (corresponding to a decrease of the kinetic energy of the proton), until particles begin to stop in the plastic scintillator material (at around $\theta=77^\circ$). (Right) Experimental spectra corrected for light attenuation for four of the PSB central elements.

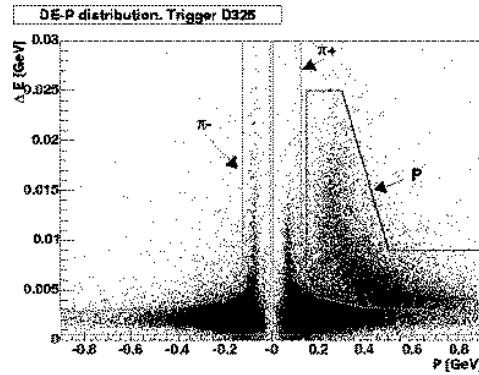


Figure 38: Example of particle identification in the central detector for a raw data sample collected at 1360 MeV. Energy deposited in the PSB is given as a function of signed momentum from the MDC. The regions for protons and pions are marked.

PSB as modeled in the detector simulation program is shown in Fig. 39. One sector of the PSB is shown in Fig. 40 and 41.

Each scintillator is glued to an acrylic light guide coupled to the photomultiplier tube (PMT). The PMTs are placed outside of the iron yoke to shield them from the magnetic field. For this purpose, approximately 50 cm long light guides are used.

The Scintillator Electromagnetic Calorimeter - (SEC)

The CD calorimeter SEC is able to measure photons, electrons and positrons with energies up to 800 MeV. The energy threshold for detection of photons is about 2 MeV. SEC consists of 1012 sodium-doped CsI scintillating crystals

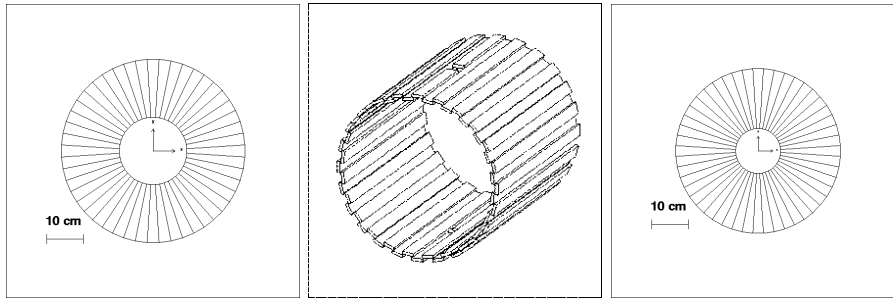


Figure 39: Forward, central and backward parts of the PSB. In the central part, the gaps for the pellet target pipe are visible.

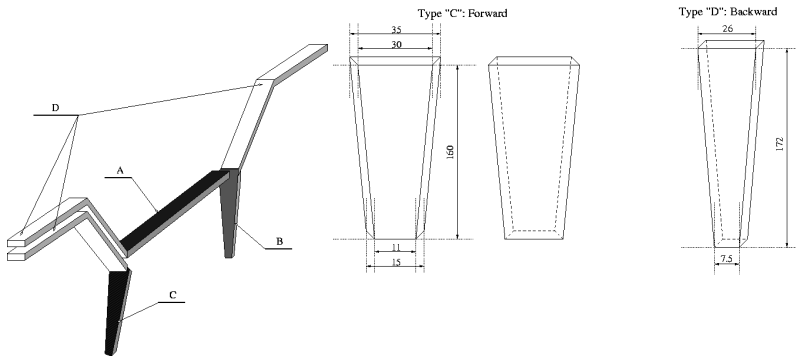


Figure 40: (Left) Layout of one section of the PSB detector. **A** denotes the rectangular counters of the barrel wall and **B** and **C** are trapezoidal elements in the forward and in the backward caps respectively. **D** are bended light guides. (Middle) Two shapes of the trapezoidal forward elements with dimensions marked in mm. (Right) Shape and dimensions in mm of the trapezoidal backward element.

placed between the super-conducting solenoid and the iron yoke. The scattering angles covered by the SEC are between 20° and 169° .

The crystals are shaped as truncated pyramids and are placed in 24 layers along the beam (Fig. 23 and 43). The lengths of the crystals vary from 30 cm (16.2 radiation lengths) in the central part to 25 cm in the forward and 20 cm in the backward part. Fig. 42 shows the angular coverage together with the thickness of SEC. As a measure of the anticipated photon fluxes, the center of mass (CM) system solid angle vs. the laboratory (LAB) scattering angle is shown for some experimental conditions at WASA.

A planar map of the crystals is given in Fig. 44. One can clearly distinguish the three different main parts of the calorimeter: the forward, central and backward parts. The forward part consists of 4 layers with 36 elements each. It covers scattering angles from nearly 20° to 36° . The central part consists of 17 layers each having 48 elements, and covers scattering angles from 36° to 150° . The backward part consists of three layers. Two layers have 24 elements and one layer closest to the CELSIUS beam pipe has only 12 elements. The small spaces between the forward-central and central-backward parts are occupied by PSB

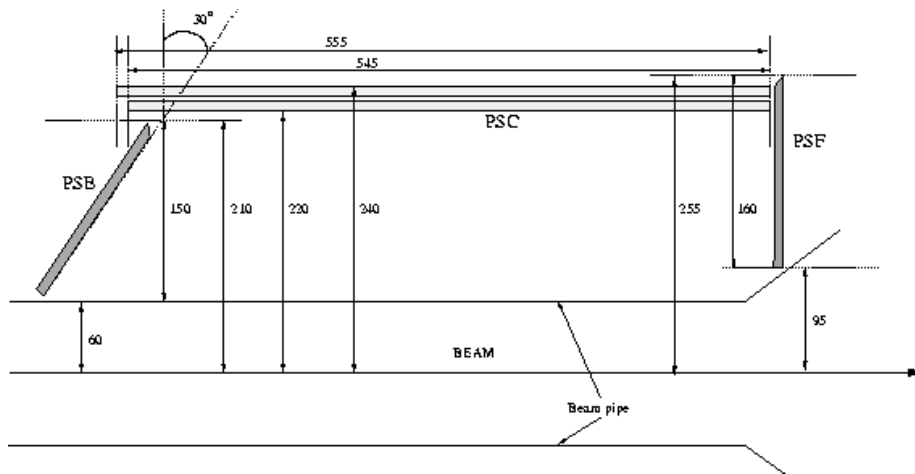


Figure 41: Cross section of the PSB scintillators with dimensions marked in mm. No structural material is shown.

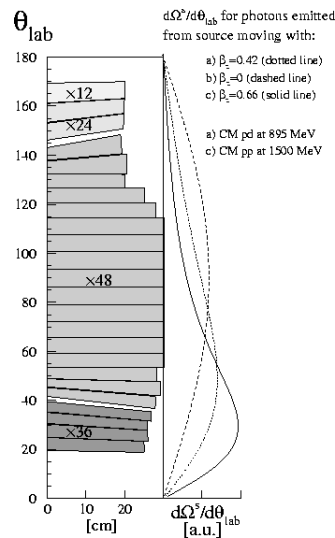


Figure 42: The angular coverage of the SEC. The CM system solid angle vs. the LAB scattering angle is shown for pp and pd interactions at 1500 MeV and 895 MeV.

light guides and mechanical support for the solenoid (back end only). The calorimeter covers nearly 360° in Φ angle. Holes for the pellet pipe (2+2 crystals) and the solenoid chimney (4 crystals) are not shown in the figure. Some design parameters of the calorimeter are given in table 6.

The SEC is composed of sodium-doped CsI scintillating crystals. This type of scintillator material provides a large light yield, has short radiation length and good mechanical properties. CsI(Na) was chosen instead of the more commonly used CsI(Tl) scintillators for the following reasons [210, 211]:

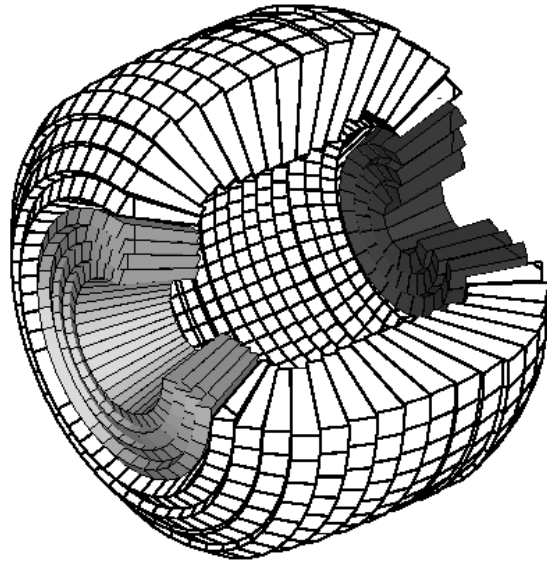


Figure 43: Schematic view of the SEC. It consists of the forward part (shaded area to the left), the central part (not shaded area in the middle) and the backward part (shaded area to the right). The beam is coming from the right side.

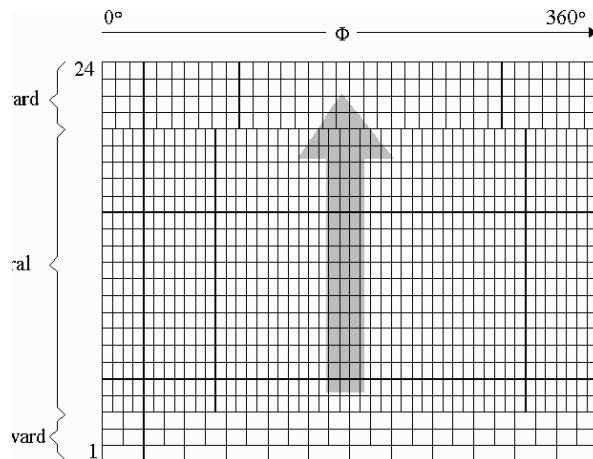


Figure 44: Planar map of the SEC.

- Its emission peak at 420 nm matches well the bi-alkali S11 photocatode of the selected PM tubes, giving good photon statistics and sufficiently fast response.

Scintillator Electromagnetic Calorimeter	
Amount of sensitive material	135 g/cm ²
[radiation lengths]	≈ 16
[nuclear interaction length]	≈ 0.8
Geometric acceptance:	96%
polar angle	≈ 20° – 169°
azimuth angle	≈ 0° – 360°
Max kinetic energy for stopping	
π^\pm /proton/deuteron	190/400/500
Scattering angle resolution	≈ 5°(FWHM)
Time resolution	
charged particles	5 ns(FWHM)
photons	≈40 ns(FWHM)
Energy resolution	
charged particles	≈ 3%(FWHM)
photons	≈ 8%(FWHM)

Table 6: SEC design parameters.

- Its shorter scintillation decay time is preferable in high-rate applications.
- CsI(Na) gives much less afterglow than CsI(Tl).
- CsI(Na) seems more resistant against radiation damage. When irradiated by a proton beam corresponding to 10 years of operation a test crystal did not show any visible change in its structure. The CsI(Tl) test crystal, on the contrary, lost its transparency.

The crystals are connected by plastic light guides, 120 mm to 180 mm long, with the photomultipliers placed the outside of the iron yoke. In Fig. 45, a fully equipped single calorimeter module consisting of a CsI crystal, a light guide, a PM tube and a high voltage unit, enclosed inside a special housing, is shown. The SEC and its performance is described in more detail in the Ph.D. thesis of Inken Koch [183].

The light pulser system (LPS)

The LPS delivers reference light pulses via light fibers to all scintillation counters in order to monitor their gain during the experiment. Since both organic and inorganic scintillators are used, two types of light sources were designed. A xenon flash tube from Hamamatsu is used for the CsI elements of the calorimeter and three LED-based light sources for all plastic scintillators. From those four sources the light signals are transmitted to individual elements via a network of light fibers [212].



Figure 45: A fully equipped module with CsI crystal, light guide, PM tube and housing.

4.3 Modifications

4.3.1 Forward detector (FD)

The FD was designed mainly for measurements of protons of kinetic energies up to 500 MeV. An energy resolution σ_E/E around 3% is obtained at the highest energy. The track coordinates are measured by the FPC straw chambers. At CELSIUS, three modules with 4 layers of straws each, are installed. To improve track coordinate measurements, energy measurements and particle identification for the higher energies anticipated at COSY, the following modifications are planned:

- The first FRH layer will be removed. It gives the few centimeters of extra space, needed for the installation of one more (existing) FPC module. By moving the remaining FRH layers a few centimeters upstream, one gets a better energy measurement performance at the largest scattering angles (17°) covered by the FD.
- Repair of FTH. The FTH and FRH have served at CELSIUS for twelve years and signs of severe aging effects have appeared. Most detectors still work well, but in one of the spiral planes of FTH some elements do not give acceptable signals and the whole plane should be replaced.
- Two new FRH planes should be installed to improve particle energy reconstruction. This would mean that protons of about 350 MeV kinetic energy, instead of 300 MeV at present, would be stopped in the FD (figure 46). The energy resolution at high energy would consequently also be improved. A σ_E/E around 10% could be reached for protons at 900 MeV.
- Downstream of the FRH, we consider the installation of a 10 cm thick water Cherenkov detector, that is composed of ≈ 2 m long and 10 cm wide bars. For protons it would have a range of sensitivity from 500 MeV ($\beta=0.75$) to 1200 MeV ($\beta=0.9$), which well covers the region where the energy determination based on the FRH depositions deteriorates. The combination of the FRH and the Cherenkov information will improve both

the particle identification power and the kinetic energy resolution. As an example, the Cherenkov light output is plotted as a function of kinetic energy for protons and pions from the reaction $pp \rightarrow pp\eta'$ where $\eta' \rightarrow \eta\pi^+\pi^-$ at a beam momentum of 3.3 GeV/c (figure 47). The proton kinetic energy resolution is about 5% for protons above 500 MeV. Studies are underway to obtain more quantitative information on the performance of the proposed Cerenkov detector.

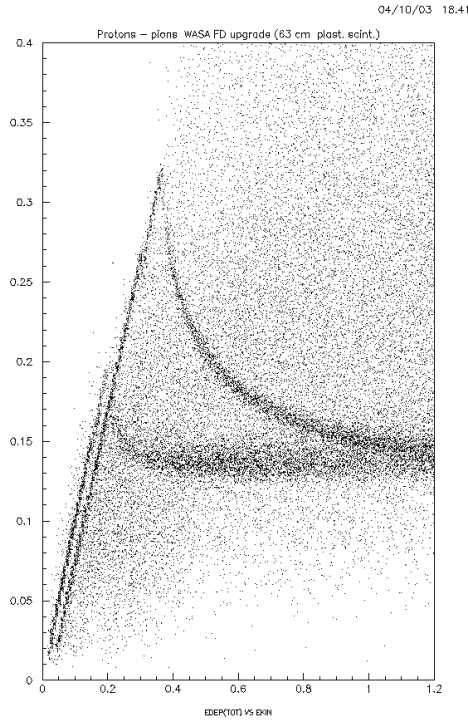


Figure 46: Energy absorbed in the (upgraded) FRH planes for protons (upper curve) and pions (lower curve) as a function of their kinetic energy at the target.

4.3.2 Central detector (CD)

The CD was originally designed for measurements of gammas with energy up to 600 MeV and of electrons and positrons with momenta up to 400 MeV/c. The charged particle momenta are determined by the track curvature in a magnetic field of about 1 Tesla. The maximum lever arm is 160 mm for these measurements and the design accuracy in the position measurements in each of the 17 MDC layers is 100 μm . The accuracy of the field map should be better than 1%. The design momentum resolution for electrons and positrons, scattered at large angles is $< 2\%$ (σ_p/p). With the present implementation of the MDC in the CELSIUS/WASA experiment an optimal resolution, $\sigma_p/p \approx 3\%$ for e^\pm , $\approx 4\%$ for π^\pm and $\approx 8\%$ for protons could be obtained. In real experiments, the momentum resolution has been evaluated for π^\pm and protons and σ_p/p

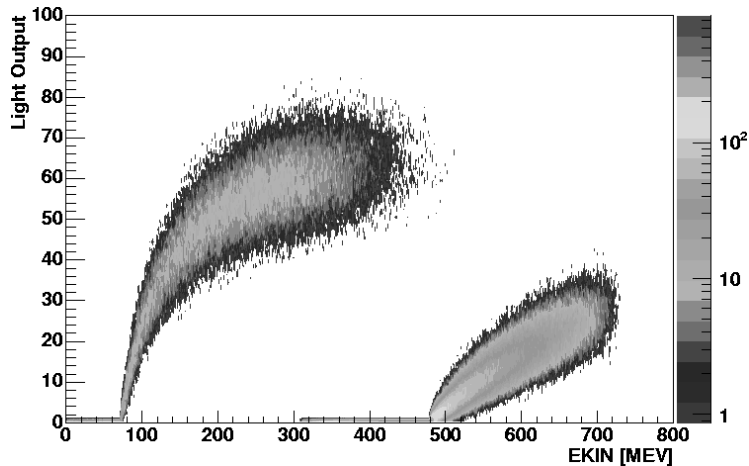


Figure 47: Cherenkov light output for charged particles from the reaction $pp \rightarrow pp\eta'$ at 3.3 GeV/c as a function of kinetic energy.

values of $\approx 4.5\%$ and $\approx 12\%$ were obtained [209]. To improve the momentum measurements for work at higher energies the following actions are planned:

- An increase of the maximum magnetic field to 1.3 Tesla. This puts great demands on some parts of the magnet system, since there will be a 70% increase in the stored energy and in the mechanical forces involved, but it would not require any major hardware upgrades [208]. However, it needs careful tests and "training" of the magnet by expert personnel.
- The MDC electronics have to be upgraded in order to improve the efficiency for detection of pions and electrons and to reach the design time resolution of ≈ 0.5 ns. The extent of this task depends on the actual electrical noise environment at the WASA site at COSY.

The design energy resolution for photons measured in the SE calorimeter is about 5 % (σ_E/E). At present an effective energy resolution of 7-10 % is obtained [183], and the main limitation is a non-linear signal response. This is the product of some different effects and the situation will be improved by modification of PM bases, by usage of new QDCs and, if necessary, by changing some 150 PM tubes.

One source of background in CELSIUS/WASA is interactions in the restgas in the scattering chamber. At present there are three big cryopumps at WASA, two at the forward cone of the scattering chamber and one at the backward cone. The vacuum in the scattering chamber will be improved by adding one more big cryopump in the backward direction. This needs a careful redesign of the backward part of WASA.

Another source of background is due to scattering events originating from the vacuum chamber walls. Most of these events are caused by beam halo particles. It is suggested to put a ring-shaped detector inside of the beampipe just at the entrance to WASA. Signals from this detector should be used in the trigger logic to "veto" events caused by beam halo. Further prestudies will be done to design such a detector and evaluate its anticipated performance in more detail.

4.3.3 Cost estimates

Cost estimate	kEuro
FRH upgrade with two additional layers	200
FTH repair / replacement of one layer	50
FD Cerenkov detector	100
SEC new PM bases / change of PM tubes	50
MDC system refurbishments	130
Additional upstream vacuum pump	40
Upstream internal veto detector	30

Table 7: Cost estimates for some planned detector modifications.

4.3.4 DAQ- and Trigger-System

The WASA DAQ-System was designed more than 10 years ago and implemented with electronics from the same period. Most of the digitizing modules were delivered by the company LeCroy, which is no longer active on the market of nuclear electronics. Furthermore, many parts of the detector electronics have a very low level of integration, leading to a high cabling effort at the detector side, especially for the straws in the MDC and the Forward Detector. In addition, spare parts of the used components cannot be acquired anymore.

Due to the progress in technology the readout speed of the existing system is much slower than possible using a modern, state-of-the-art system. Since the event rate at COSY must be significantly higher than the one currently reached at CELSIUS, this becomes a serious problem. Considering also the maintenance problems and the age of the digitizing modules, it is obvious that successful operation of WASA at COSY can only be achieved by a major upgrade of the existing DAQ system.

Currently, all experiments running at COSY are using the same DAQ system following a uniform approach developed, implemented and maintained by permanent staff of FZ Jülich. In view of the time scale for "WASA at COSY" the upgrade of the WASA DAQ should be based on the third generation of the DAQ at COSY. The main advantages are:

- it implements the desired functionality, including a modern synchronization technique, avoiding the – inherently slow – sequential readout of the digitizing modules,
- it is almost completely developed, thus fitting into the limited time scale,
- it has a good on-site support by the original developers, which is essential for a smooth and successful operation,
- and it is compatible to all existing DAQ systems at COSY.

The current DAQ system

The existing DAQ system of WASA at CELSIUS is mainly based on four FAST-BUS crates containing the digitizing modules (see Fig. 48). The readout is done

by PCs connected to the FASTBUS crates via a proprietary parallel link based on RS485. Since there is no synchronization system, all digitizing modules have to be read out sequentially when a trigger occurs. The readout of the (about) 1500 PMTs is done with LeCroy LRS1881 QDCs. The time information from the straws (2000 channels from the FPC and 1700 channels from the MDC) and the ≈ 500 fast plastic scintillators is digitized using LeCroy LRS1876 TDCs [213]. The trigger system of WASA at CELSIUS is based on dedicated hardware that has been developed by TSL. Due to the high background the trigger system is still evolving to reach higher performance. The first level trigger uses the discriminator outputs of the fast plastic scintillators. It is based on multiplicity and generates the gates for the QDCs and the stop for the TDCs. The second level trigger uses the discriminator outputs from the calorimeter. It is based on cluster multiplicity and energy deposition and generates the FastClear for the digitizing modules.

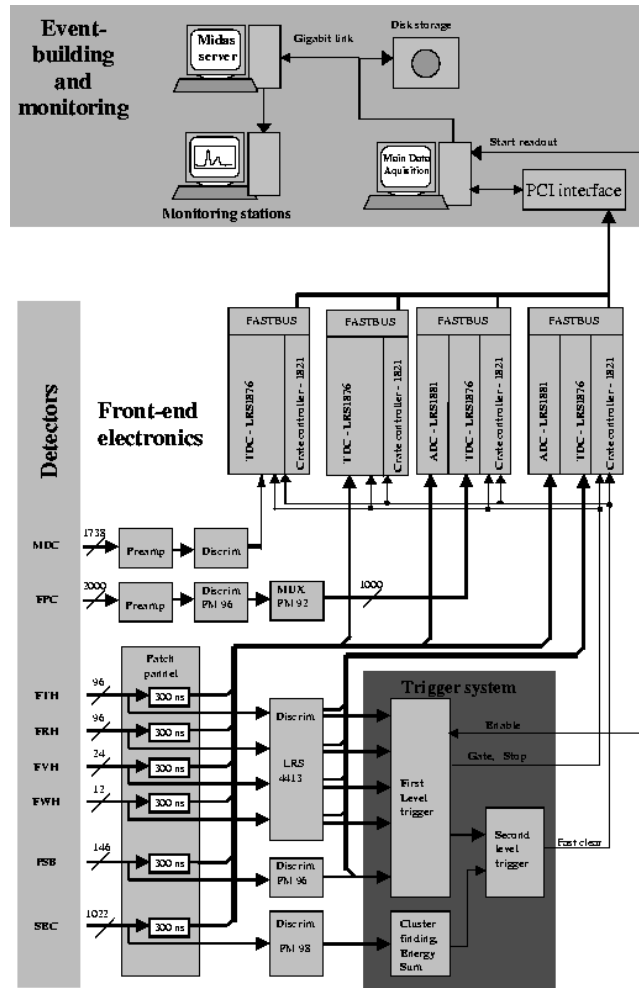


Figure 48: Structure of the existing WASA DAQ and trigger system [213, 214].

The new DAQ system

Starting with the first experiments at COSY permanent staff from ZEL was responsible for a common DAQ system and its further development. In the meantime two evolutionary and elementary steps have been made to adapt it to the rapidly changing technologies [215]. Now, the implementation of a third generation of DAQ has been started aiming for the highest possible event rates [216]. Therefore, state-of-the-art FPGA technologies are combined with fast communication paths to achieve system latencies as low as possible. Commonly used in all three generations is a DAQ software called EMS [215], which guarantees the software compatibility of all implemented systems. EMS follows a well proven client/server architecture and has been developed during a period of more than 10 years (corresponding to a manpower effort of nearly 30 man-years).

As in other DAQ systems (e.g. at CERN) this third generation of DAQ at COSY is based on proprietary solutions in order to guarantee implementations optimized for speed. However, also CAMAC and VME can be integrated despite of the resulting loss of performance. The whole system is designed to run exclusively in a “common stop mode” to avoid many expensive and hard to handle delay units. Here, “common stop mode” means that the trigger is available some 100 ns to 1 μ s after the signal has been digitized. Therefore, the acquisition boards must run in a self-triggering mode digitizing all interesting signals and storing them together with a time stamp. When the – also time-stamped – trigger arrives an FPGA selects the digitized signals inside a predefined time interval.

An essential key component required by this operation mode is a Synchronization System (SYS) to reliably control and synchronize the fast event flow [217]. The SYS delivers a global time base relative to the trigger time. The control of the synchronization system as well as the readout of the digitization modules is done by a farm of embedded industrial PCs. On this farm, EMS-servers controlling the front end modules are implemented. As a future extension also the cancellation of events (software trigger) is considered.

The third generation of DAQ at COSY is based on a bus controller (refer to Fig. 49) connected by a fiber optical link to the PC farm and the synchronization system. The acquisition modules are connected by a high speed LVDS bus. This bus can be implemented as a backplane or as a cable bus covering a distance of 15 meters and serving for control as well as for transmission of event data. The physical layer of the bus complies to the SCSI bus with a maximum transmission speed of 80 or 160 Mbytes/s [218]. In general, acquisition, trigger processing, data reduction, buffer management, and sub-event building can be done by means of FPGAs — either on the acquisition boards or in the bus controller. All these functions are realized without the intervention of a general purpose processor and, thus, lead to the envisaged performance.

As shown in Fig. 50 a new computing layer and a new layer of digitization electronics will be implemented. The readout will be done by a farm of 15 PCs connected via an optical link (a common development of ZEL and the company SIS, with a physical layer identical to Gigabit Ethernet). The overall experiment control and storage is connected via Gigabit Ethernet. The whole system runs under control of the EMS software as used at all other experiments at COSY. The digitization layer consists of crates with readout controllers, QDC and TDC modules and the synchronization system. The event buffering capabilities of the digitization modules in combination with the synchronization system allow the

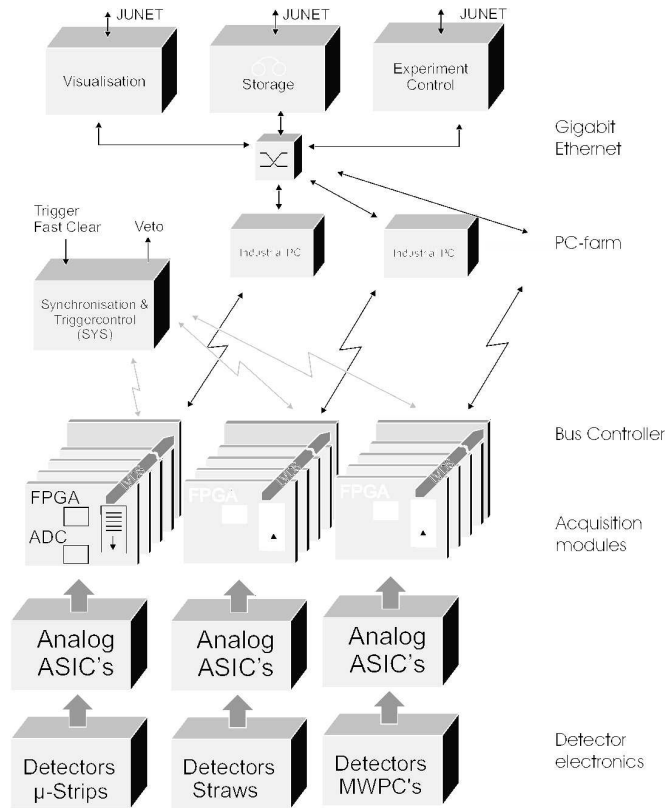


Figure 49: Structure of the third generation DAQ system at COSY.

operation in common stop mode, thus avoiding delay lines. It is expected that with the new system the event rate will be increased at least by a factor of 10. Because of performance requirements and costs the use of commercially available digitizing modules is not possible.

The existing 64 channel TDC module (being used for the proportional chambers of ANKE and the straws at TOF) can be used without modifications for the straws at WASA, provided the discriminator electronics will be changed to a CMP16 based system. It is a 6U board for the LVDS bus based on the F1 chip system developed by ZEL compatible with the third generation of DAQ at COSY [219].

Optionally, also a VME board developed at TSL may be used, although some modifications and a further test phase are necessary [220]. This board has 64 channels, too, and is based on the CERN TDC32. The decision which TDC to use will have only minor impact on the overall cost estimate and project timing and will be done within the next year.

For the calorimeter (pulse duration about $2 \mu\text{s}$) the QDC will be implemented by sampling the analog signal with a 100 MHz FlashADC and subsequent integration in an FPGA. Considering connector requirements and layout restrictions, it is planned to have 16 channels on one 6U base board conforming to the standards of the LVDS bus system developed by ZEL.

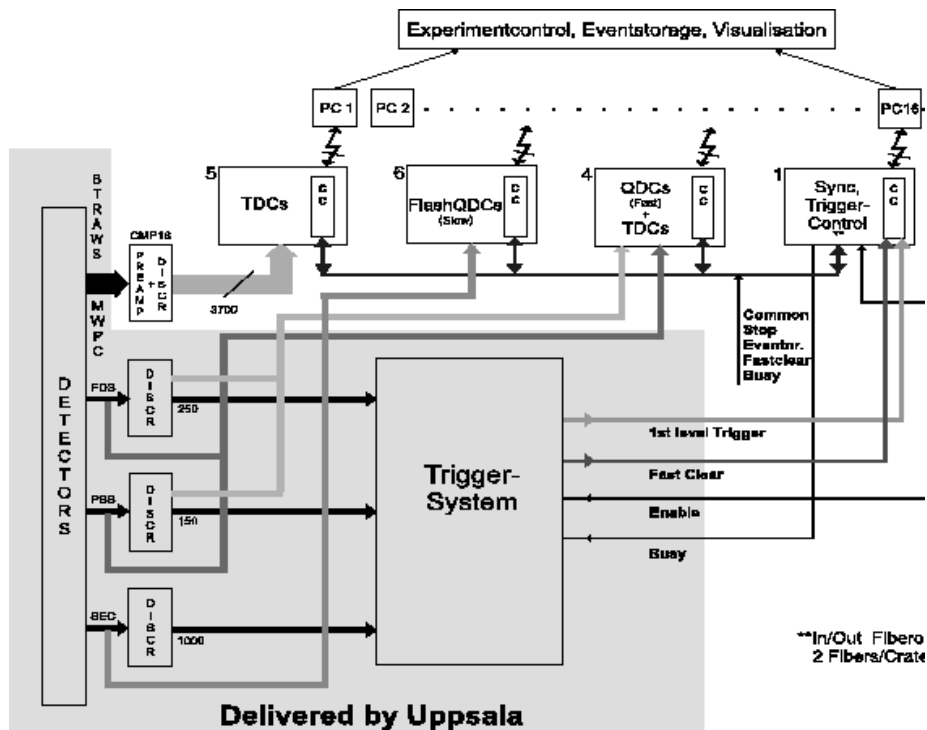


Figure 50: Structure of the new DAQ and trigger system of WASA at COSY.

The latter technique is not possible for the signals from the fast plastic scintillators, because the pulse duration is only ≈ 20 ns. Here, additional shaping or even the use of a QAC chip is required. The technical issues are intensively discussed with people from the University of Giessen (TAPS collaboration), the KFKI Budapest and the TSL. Independent of the final decision, a mezzanine board will be manufactured fitting to the FlashADC board described above and performing the analog preprocessing for 16 channels.

The time stamps required by the free-running mode will be provided by the FPGA on the motherboard for the "slow" QDC using the global time information and by additional discriminators and TDCs for the "fast" QDC.

As indicated in Fig. 50, the discriminators and the trigger electronics from the existing system shall remain. Only with regard to the straws it is intended to replace the discrete preamplifier and discriminator electronics with new modules based on the CMP16 chip. The main advantage will be the increased sensitivity and the compact layout, which allows much shorter cable lengths between straws and preamplifier, thus reducing noise.

A further improvement of the trigger system can be achieved by implementing a third level trigger in the context of the new DAQ system. While this is not possible in the limited time scale of about one year, it should be considered as a future extension. At the moment two basic hardware concepts are discussed:

- Implementation as a processor- or FPGA-farm that operates directly on the DAQ data stream.

Electronics for MDC and FPC based on the CMP16 ASIC		
	3700 channels	95 k€
Digitizing modules		
TDCs (MDC, FPC)	3700 channels	140 k€
QDCs (slow)	1000 channels	100 k€
QDCs (fast)	400 channels	80 k€
add. TDCs	400 channels	16 k€
System components		
	17 Crates (incl. crate controllers, interfaces)	140 k€
	Industrial PC farm (embedded)	30 k€
	Communication equipment	20 k€
	Synchronization system	70 k€
Miscellaneous		
	Racks, infrastructure test and measuring equipment	80 k€
	Experiment control, visualization and storage	20 k€
	Additional cables and connectors	70 k€
	External developments	50 k€
	6% risk reserve	60 k€
Total		1000 k€

Table 8: Cost estimate for the development of a new data acquisition system for WASA at COSY.

- Splitting the data from the digitizing modules into two independent branches, one for the trigger and one going to the DAQ system [221].

In a further future-oriented development project it is planned to integrate the embedded PC functionality in the LVDS bus controller itself using “system on chip” (SOC) technology with a general purpose FPGA and processor on the same chip. However, it is quite uncertain, whether this project will be finished next year. Therefore it has not been considered for the DAQ system of WASA at COSY.

Cost estimate

The cost estimate shown in table 8 does not include manpower, since all developments concerning the new DAQ system and improvements of the existing WASA electronics can be made by existing permanent staff. One exception could be the development of the analog part of the fast QDCs. Most of the existing cables should be reused. However, additional shielded cables are required in some cases and all connectors will be replaced.

5 Project plan

General remarks

The project “WASA at COSY” deals with the relocation of an existing detector system — the Wide Angle Shower Array (WASA) from The Svedberg Laboratory (TSL) at Uppsala university (Sweden) to the Research Center Jülich (Forschungszentrum Jülich, FZJ, Germany), more specifically to an internal target position of COSY (Cooler Synchrotron) at IKP. WASA at COSY will be the experimental activity with the highest priority at the IKP in Jülich for the next several years.

The approach of adapting an existing detector has a number of advantages compared to building a new one: It is faster, provided the detector is available on short notice. Given the necessary lead-time for preparations at COSY, the date that WASA will be available (end of 2005) is regarded as optimal. It is cost-effective if the detector is “in good shape” which is the case for WASA.

However, the movement and setting up of a detector as complex as WASA is not free of charge — even neglecting basic costs such as dismounting, transport, and installation. We anticipate the following investments for necessary repairs and changes to the detector: Adaptation to the higher COSY energy, in particular the forward detectors of WASA. Exchange of electronics for which no spare parts exist and no replacement can be purchased any longer. Replacement of the data acquisition system to improve data taking capabilities and to adapt the WASA-DAQ to COSY standards. These will allow one to carry out the initial experiments described above.

Manpower

Well over one hundred scientists have committed themselves to actively pursue the physics program laid out in this proposal. This includes members of the current WASA at CELSIUS collaboration as well as a wide representation from the COSY users. As the host institute, IKP will have a special role in providing the scientific and technical infrastructure for WASA at COSY. Consequently, IKP will redirect significant manpower (about 10 F.T.E.) to this project, which implies a reduction of the other activities at IKP.

Finances

The financing of this project is not yet finalized. In view of the high priority WASA at COSY has for IKP about one half of the needed investments summarized below could be contributed from the running budget of IKP. This would require a one-time reduction of the number of COSY running hours by 50% for one year in either 2005 or 2006. The remaining investment must be provided by other sources in either Sweden, the EU, the German BMBF, or the Research Center Jülich.

Dismounting, transfer, set-up	100 k€
Preparations at COSY	300 k€
Changes at WASA (“adaptation”)	600 k€
New trigger- and readout electronics	1000 k€
Sum:	2000 k€

Time schedule

June 2005	Termination of CELSIUS operations at TSL
Oct. 2005	Finish dismantling of WASA at CELSIUS
Nov. 2005	Transfer of WASA to Jülich
June 2006	Finish set-up of WASA at COSY
July 2006	Start of commissioning
Jan. 2007	Start of experiments

References

- [1] S. Weinberg, Trans. New York. Acad. Sci. **38**, 185 (1977).
- [2] J. Gasser and H. Leutwyler, Phys. Rep. **87**, 77 (1982).
- [3] G. A. Miller, B. M. Nefkens, and I. Šlaus, Phys. Rept. **194**, 1 (1990).
- [4] D. G. Sutherland, Phys. Lett. **23**, 384 (1966).
- [5] R. Baur, J. Kambor, and D. Wyler, Nucl. Phys. **B 460**, 127 (1996).
- [6] D. J. Gross, S. B. Treiman, and F. Wilczek, Phys. Rev. **D 19**, 2188 (1979).
- [7] B. M. K. Nefkens and J. W. Price, Phys. Scripta **T 99**, 114 (2002).
- [8] R. Kaiser and H. Leutwyler, Eur. Phys. J. **C 17**, 623 (2000).
- [9] T. Feldmann, P. Kroll, and B. Stech, Phys. Rev. **D 58**, 114006 (1998).
- [10] M. Gormley *et al.*, Phys. Rev. **D 2**, 501 (1970).
- [11] J. G. Layter *et al.*, Phys. Rev. **D 7**, 2565 (1973).
- [12] D. Alde *et al.*, Z. Phys. **C 25**, 225 (1984).
- [13] C. Amsler *et al.*, Phys. Lett. **B 346**, 203 (1995).
- [14] C. Amsler, Rev. Mod. Phys. **70**, 1293 (1998).
- [15] A. Abele *et al.*, Phys. Lett. **B 417**, 193 (1998).
- [16] A. Abele *et al.*, Phys. Lett. **B 417**, 197 (1998).
- [17] W. B. Tippens *et al.*, Phys. Rev. Lett. **87**, 192001 (2001).
- [18] J. Kambor, C. Wiesendanger, and D. Wyler, Nucl. Phys. **B 465**, 215 (1996).
- [19] N. Beisert and B. Borasoy, Nucl. Phys. **A 716**, 186 (2003).
- [20] B. Di Micco, in *Mini-Proceedings of the Fourth International Workshop on Chiral Dynamics: Theory and Experiment (CD2003)*, edited by U.-G. Meißner, H.-W. Hammer, and A. Wirzba (eprint, [arXiv:hep-ph/0311212], 2003), p. 93.
- [21] N. Beisert and B. Borasoy, Nucl. Phys. **A 705**, 433 (2002).
- [22] A. H. Fariborz and J. Schechter, Phys. Rev. **D 60**, 034002 (1999).
- [23] A. M. Abdel-Rehim, D. Black, A. H. Fariborz, and J. Schechter, Phys. Rev. **D 67**, 054001 (2003).
- [24] P. Ball, J. M. Frère, and M. Tytgat, Phys. Lett. **B 365**, 367 (1996).
- [25] E. Kou, Phys. Rev. **D 63**, 054027 (2001).
- [26] O. Bär and U.-J. Wiese, Nucl. Phys. **B 609**, 225 (2001).

- [27] B. Borasoy, Eur. Phys. J. **C 34**, 317 (2004).
- [28] J. Wess and B. Zumino, Phys. Lett. **B 37**, 95 (1971).
- [29] E. Witten, Nucl. Phys. **B 223**, 422 (1983).
- [30] M. S. Chanowitz, Phys. Rev. Lett. **35**, 977 (1975).
- [31] M. S. Chanowitz, Phys. Rev. Lett. **44**, 59 (1980).
- [32] M. Benayoun *et al.*, Eur. Phys. J. **C 31**, 525 (2003).
- [33] B. Borasoy and R. Nißler, Eur. Phys. J. **A 19**, 367 (2004).
- [34] B. Borasoy and R. Nißler, Nucl. Phys. **A 740**, 362 (2004).
- [35] M. Acciarri *et al.*, Phys. Lett. **B 418**, 399 (1998).
- [36] A. Abele *et al.*, Phys. Lett. **B 402**, 195 (1997).
- [37] J. Stepaniak *et al.*, Phys. Scripta **T99**, 133 (2002).
- [38] R. I. Dzhelyadin *et al.*, Sov. J. Nucl. Phys. **32**, 520 (1980).
- [39] L. G. Landsberg, Phys. Rept. **128**, 301 (1985).
- [40] M. Hayakawa and T. Kinoshita, Phys. Rev. **D 57**, 465 (1998).
- [41] J. Bijnens, in *Chiral Dynamics: Proceedings*, Vol. 513 of *Lecture Notes in Physics*, edited by A. M. Bernstein, D. Drechsel, and T. Walcher (Springer, Berlin, Germany, 1998), pp. 295–310.
- [42] L. Bergström, Z. Phys. **C 14**, 129 (1982).
- [43] M. J. Savage, M. E. Luke, and M. B. Wise, Phys. Lett. **B 291**, 481 (1992).
- [44] L. Ametller, A. Bramon, and E. Masso, Phys. Rev. **D 48**, 3388 (1993).
- [45] S. Eidelman *et al.*, Phys. Lett. **B 592**, 1 (2004).
- [46] N. Cabibbo, Phys. Rev. Lett. **10**, 531 (1963).
- [47] M. Kobayashi and T. Maskawa, Prog. Theor. Phys. **49**, 652 (1973).
- [48] D.-N. Gao, Mod. Phys. Lett. **A 17**, 1583 (2002).
- [49] C. Q. Geng, J. N. Ng, and T. H. Wu, Mod. Phys. Lett. **A 17**, 1489 (2002).
- [50] A. Lai *et al.*, Eur. Phys. J. **C 30**, 33 (2003).
- [51] C. Jarlskog and H. Pilkuhn, Nucl. Phys. **B 1**, 264 (1967).
- [52] T. Cheng, Phys. Rev. **162**, 1734 (1967).
- [53] J. N. Ng and D. J. Peters, Phys. Rev. **D 47**, 4939 (1993).
- [54] C. Jarlskog and E. Shabalin, Phys. Scripta **T 99**, 23 (2002).
- [55] R. A. Briere *et al.*, Phys. Rev. Lett. **84**, 26 (2000).

- [56] W. Kluge, 2004, private communications.
- [57] F. Piccinini and A. D. Polosa, Phys. Rev. **D 65**, 097508 (2002).
- [58] H. Leutwyler, Phys. Lett. **B 378**, 313 (1996).
- [59] U.-G. Meißner and S. Steininger, Phys. Lett. **B 419**, 403 (1998).
- [60] G. Müller and U.-G. Meißner, Nucl. Phys. **B 556**, 265 (1999).
- [61] N. Fettes and U.-G. Meißner, Phys. Rev. **C 63**, 045201 (2001).
- [62] J. Gasser *et al.*, Eur. Phys. J. **C 26**, 13 (2002).
- [63] U. van Kolck, J. A. Niskanen, and G. A. Miller, Phys. Lett. **B 493**, 65 (2000).
- [64] A. Bernstein, Phys. Lett. **B 442**, 20 (1998).
- [65] J. Niskanen, Few Body Syst. **26**, 241 (1999).
- [66] E. J. Stephenson *et al.*, Phys. Rev. Lett. **91**, 142302 (2003).
- [67] A. K. Opper *et al.*, Phys. Rev. Lett. **91**, 212302 (2003).
- [68] A. Gardestig *et al.*, Phys. Rev. **C 69**, 044606 (2004).
- [69] E. Epelbaum, W. Glöckle, and U.-G. Meißner, Eur. Phys. J. **A 19** 125 (2004); Eur. Phys. J. **A 19**, 401 (2004); [arXiv:nucl-th/0405048], to be publ. in Nucl. Phys. A.
- [70] E. Epelbaum *et al.*, Phys. Rev. **C 66**, 064001 (2002).
- [71] E. Epelbaum *et al.*, Phys. Rev. **C 65**, 044001 (2002).
- [72] E. Epelbaum, U.-G. Meißner, and J. E. Palomar, [arXiv:nucl-th/0407037].
- [73] J. L. Friar, G. L. Payne, and U. van Kolck, [arXiv:nucl-th/0408033].
- [74] C. Amsler and N. A. Tornqvist, Phys. Rept. **389**, 61 (2004).
- [75] S.-K. Choi *et al.*, Phys. Rev. Lett. **91**, 262001 (2003).
- [76] A. Abele *et al.*, Phys. Lett. **B 423**, 175 (1998).
- [77] J. Kuhn *et al.*, Phys. Lett. **B 595**, 109 (2004).
- [78] T. Kunihiro *et al.*, [arXiv:hep-ph/0308291].
- [79] D. Morgan, Phys. Lett. **B 51**, 71 (1974).
- [80] K. L. Au *et al.*, Phys. Rev. **D 35**, 1633 (1987).
- [81] D. Morgan and M. R. Pennington, Phys. Lett. **B 258**, 444 (1991).
- [82] D. Morgan and M. R. Pennington, Phys. Rev. **D 48**, 1185 (1993).
- [83] A. V. Anisovich *et al.*, Eur. Phys. J. **A 12**, 103 (2001).
- [84] S. Narison, Nucl. Phys. Proc. Suppl. **96**, 244 (2001).

- [85] J. D. Weinstein and N. Isgur, Phys. Rev. Lett. **48**, 659 (1982).
- [86] J. D. Weinstein and N. Isgur, Phys. Rev. **D 27**, 588 (1983).
- [87] J. D. Weinstein and N. Isgur, Phys. Rev. **D 41**, 2236 (1990).
- [88] G. Janssen *et al.*, Phys. Rev. **D 52**, 2690 (1995).
- [89] J. A. Oller and E. Oset, Nucl. Phys. **A 620**, 438 (1997), [Erratum-ibid. **A 652**, 407 (1999)].
- [90] N. N. Achasov, [arXiv:hep-ph/0201299].
- [91] R. J. Jaffe, Phys. Rev. **D 15**, 267 (1977).
- [92] J. Vijande *et al.*, in *Proc. Int. Workshop MESON 2002, May 24–28, 2002, Cracow, Poland* (World Scientific Publishing, ISBN 981-238-160-0, 2002), p. 501, [arXiv:hep-ph/0206263].
- [93] F. E. Close and N. A. Törnquist, J. Phys. **G 28**, R249 (2002).
- [94] C. Hanhart, Phys. Rept. **397**, 155 (2004).
- [95] R. A. Arndt, I. I. Strakovsky, and R. L. Workman, Phys. Rev. **C 68**, 042201(R) (2003).
- [96] J. Haidenbauer and G. Krein, Phys. Rev. **C 68**, 052201(R) (2003).
- [97] R. N. Cahn and G. H. Trilling, Phys. Rev. **D 69**, 011501 (2004).
- [98] A. Sibirtsev, J. Haidenbauer, S. Krewald, and U.-G. Meißner, Phys. Lett. **B 599**, 230 (2004); [arXiv:hep-ph/0407011].
- [99] R. L. Jaffe and A. Jain, 2004, [arXiv:hep-ph/0408046].
- [100] H. Högaasen and P. Sorba, Nucl. Phys. **B 145**, 119 (1978).
- [101] R. Jaffe and F. Wilczek, Phys. Rev. Lett. **91**, 232003 (2003).
- [102] D. Melikhov, S. Simula, and B. Stech, Phys. Lett. **B 594**, 265 (2004).
- [103] S. R. Beane, [arXiv:hep-ph/0408066].
- [104] B. L. Ioffe and A. G. Oganesian, [arXiv:hep-ph/0408152].
- [105] D. Melikhov and B. Stech, [arXiv:hep-ph/0409015].
- [106] D. Diakonov, V. Petrov, and M. Polyakov, Z. Phys. **A 359**, 305 (1997).
- [107] N. N. Achasov, S. A. Devyanin, and G. N. Shestakov, Phys. Lett. **B 88**, 367 (1979).
- [108] V. Baru *et al.*, Phys. Lett. **B 586**, 53 (2004).
- [109] S. Weinberg, Phys. Rev. **130**, 776 (1963).
- [110] in *Proc. Workshop on Hadron Physics at COSY, July 7–10, 2003, Bad Honnef, Germany*, edited by A. Gillitzer *et al.* (eprint, [arXiv:hep-ph/0311071], 2003).

- [111] M. Büscher (spokesperson) *et al.*, COSY proposal #140, 2001.
- [112] V. Y. Grishina *et al.*, Phys. Lett. **B 521**, 217 (2001).
- [113] A. E. Kudryavtsev and V. E. Tarasov, JETP Lett. **42**, 410 (2000).
- [114] A. E. Kudryavtsev *et al.*, Phys. Rev. **C 66**, 015207 (2002).
- [115] C. Quentmeier *et al.*, Phys. Lett. **B 515**, 276 (2001).
- [116] P. Moskal *et al.*, J. Phys. **G 28**, 1777 (2002).
- [117] M. Büscher (spokesperson) *et al.*, COSY proposal #55.1, 2001.
- [118] M. Büscher (spokesperson) *et al.*, COSY proposal #97, 2001.
- [119] F. Bellemann *et al.*, Annual Report of the IKP 2001, Berichte des Forschungszentrums Jülich 3978, ISSN 0944-2952, p. 44 (2002).
- [120] M. Büscher, F. P. Sassen, N. N. Achasov, and L. Kondratyuk, in *Proceedings of the 1st Summer School 2002 and Workshop on COSY Physics*, Vol. 16 of *Schriften des Forschungszentrums Jülich, Reihe Materie und Material/Matter and Materials*, edited by K. Brinkmann *et al.* (Forschungszentrum Jülich, Jülich, Germany, 2003), pp. 127–134.
- [121] V. Kleber *et al.*, Phys. Rev. Lett. **91**, 172304 (2003).
- [122] V. Y. Grishina, L. A. Kondratyuk, M. Büscher, and W. Cassing, Eur. Phys. J. **A 21**, 507 (2004).
- [123] A. Sibirtsev *et al.*, [arXiv:nucl-th/0406061], Phys. Lett. B, in print.
- [124] E. Oset, J. A. Oller, and U.-G. Meißner, Eur. Phys. J. **A 12**, 435 (2001).
- [125] P. Fedorets *et al.*, Annual Report of the IKP 2003, <http://www.fz-juelich.de/ikp/publications/AR2003/en/contents.shtml>.
- [126] K. Hagiwara *et al.*, Phys. Rev. **D 66**, 010001 (2002).
- [127] N. Isgur and G. Karl, Phys. Rev. **D 18**, 4187 (1978).
- [128] L. Y. Glozman, Nucl. Phys. **A 663**, 103c (2000).
- [129] U. Löring, B. C. Metsch, and H. R. Petry, Eur. Phys. J. **A 10**, 395 (2001).
- [130] W. Melnitchouk *et al.*, Phys. Rev. **D 67**, 114506 (2003).
- [131] R. Arnold and J. Sakurai, Phys. Rev. **128**, 2808 (1962).
- [132] R. Dalitz, T. Wong, and G. Rajasekaran, Phys. Rev. **153**, 1617 (1967).
- [133] M. Jones, R. H. Dalitz, and R. R. Horgan, Nucl. Phys. **B 129**, 45 (1977).
- [134] N. Kaiser, P. B. Siegel, and W. Weise, Nucl. Phys. **A 594**, 325 (1995).
- [135] N. Kaiser, T. Waas, and W. Weise, Nucl. Phys. **A 612**, 297 (1997).
- [136] E. Oset and A. Ramos, Nucl. Phys. **A 635**, 99 (1998).

- [137] J. A. Oller and U. G. Meissner, Phys. Lett. **B 500**, 263 (2001).
- [138] E. Oset, A. Ramos, and C. Bennhold, Phys. Lett. **B 527**, 99 (2002), [Erratum-ibid. **B 530** (2002) 260].
- [139] D. Jido *et al.*, Nucl. Phys. **A 725**, 181 (2003).
- [140] D. W. Thomas, A. Engler, H. E. Fisk, and R. W. Kraemer, Nucl. Phys. **B 56**, 15 (1973).
- [141] R. J. Hemingway, Nucl. Phys. **B 253**, 742 (1985).
- [142] M. Aguilar-Benitez *et al.*, Ana. Fis. **A 77**, 144 (1981).
- [143] M. Baubillier *et al.*, Z. Phys. **C 23**, 213 (1984).
- [144] J. K. Ahn, Nucl. Phys. **A 721**, 715c (2003).
- [145] J. C. Nacher, E. Oset, H. Toki, and A. Ramos, Phys. Lett. **B 455**, 55 (1999).
- [146] V. Koptev *et al.*, Annual Report of the IKP 2002, <http://www.fz-juelich.de/ikp/publications/AR2002/en/contents.shtml>.
- [147] T. Nakano *et al.*, Phys. Rev. Lett. **91**, 012002 (2003).
- [148] V. V. Barmin *et al.*, [arXiv:hep-ex/0304040].
- [149] S. Stepanyan *et al.*, [arXiv:hep-ex/0307018].
- [150] J. Barth *et al.*, [arXiv:hep-ph/0307083].
- [151] A. E. Aratayn, A. G. Dololenko, and M. A. Kubantsev, [arXiv:hep-ex/0309042].
- [152] V. Kubarovsky *et al.*, [arXiv:hep-ex/0311046].
- [153] A. Airapetian *et al.*, [arXiv:hep-ex/0312044].
- [154] A. Aleev *et al.*, [arXiv:hep-ex/0401024].
- [155] COSY-TOF Collaboration, [arXiv:hep-ex/0403011].
- [156] P. A. Aslanyan *et al.*, [arXiv:hep-ex/0403044].
- [157] ZEUS Collaboration, [arXiv:hep-ex/0403051].
- [158] S. V. Chekanov, [arXiv:hep-ex/0404007].
- [159] M. Abdel-Bary *et al.*, Phys. Lett. **B 595**, 127 (2004).
- [160] S.-L. Zhu, [arXiv:hep-ph/0406204] and references therein.
- [161] J. Z. Bai *et al.*, [arXiv:hep-ex/0402012].
- [162] K. T. Knopfle, [arXiv:hep-ex/0403020].
- [163] C. Pinkenburg, [arXiv:nucl-ex/0404001].

- [164] M. J. Longo, talk at 2004 International Conference on Quarks and Nuclear Physics, Indiana University, May 23, 2004, see <http://www.qnp2004.org>.
- [165] C. Hanhart, J. Haidenbauer, K. Nakayama, and U.-G. Meißner, [arXiv:hep-ph/0407107].
- [166] F. Binon *et al.*, Phys. Lett. **B 140**, 264 (1984).
- [167] J. Gasser and H. Leutwyler, Nucl. Phys. **B 250**, 465 (1985).
- [168] J. Piekarewicz, Phys. Rev. **C 48**, 1555 (1993).
- [169] C.-T. Chan, E. M. Henley, and T. Meissner, Phys. Lett. **B 343**, 7 (1995).
- [170] K. Maltman and T. Goldman, Nucl. Phys. **A 572**, 682 (1994).
- [171] B. Bagchi, A. Lahiri, and S. Niyogi, Phys. Rev. **D 41**, 2871 (1990).
- [172] C. Pauly *et al.*, in *Meson 2004: 8th Workshop On Meson Production, Properties And Interactions* (World Scientific, Singapore, 2004), to be published.
- [173] M. Benayoun *et al.*, Z. Phys. **C 58**, 31 (1993).
- [174] M. Benayoun, P. Leruste, L. Montanet, and J. L. Narjoux, Z. Phys. **C 65**, 399 (1995).
- [175] V. A. Novikov, M. A. Shifman, A. Vainshtein, and V. I. Zakharov, Nucl. Phys. **B 165**, 55 (1980).
- [176] R. Akhoury and J. M. Frère, Phys. Lett. **B 220**, 258 (1989).
- [177] V. Y. Grishina *et al.*, Eur. Phys. J. **A 9**, 277 (2000).
- [178] V. Grishina *et al.*, Annual Report of the IKP 2000.
- [179] P. Fedorets *et al.*, Annual Report of the IKP 2003, <http://www.fz-juelich.de/ikp/publications/AR2003/en/contents.shtml>.
- [180] E. L. Bratkovskaya *et al.*, J. Phys. **G 28**, 2423 (2002).
- [181] L. A. Kondratyuk *et al.*, Phys. Atom. Nucl. **66**, 152 (2003).
- [182] A. E. Kudryavtsev *et al.*, Phys. Atom. Nucl. **66**, 1946 (2003).
- [183] I. Koch, 2004, ph.D. Thesis, Uppsala Universitet, Sweden, pp. 82.
- [184] J. M. Dyring, 1997, ph.D. Thesis, Uppsala Universitet, Sweden.
- [185] G. Fäldt, private communication.
- [186] J. Banaigs *et al.*, Phys. Rev. Lett. **58**, 1922 (1987).
- [187] L. Goldzahl *et al.*, Nucl. Phys. **A 533**, 675 (1991).
- [188] D. Dobrokhotov, G. Faldt, A. Gardestig, and C. Wilkin, Phys. Rev. Lett. **83**, 5246 (1999).
- [189] A. Magiera (spokesperson) *et al.*, COSY proposal #59, 1997.

- [190] V. Hejny (spokesperson) *et al.*, COSY proposal #83, 1999.
- [191] in *Proc. 5th ANKE workshop on Strangeness Production on Nucleons and Nuclei, Krzyze, Poland, Sept.8-10, 2003*, edited by M. Büscher *et al.* (Berichte des Forschungszentrums Jülich, Jül-4109, ISSN 0944-2952, 2003).
- [192] R. Abegg *et al.*, Phys. Rev. **D 53**, 11 (1996).
- [193] W. A. van den Bosch, Study of the Possibility to Measure $\eta \rightarrow e^+e^-e^+e^-$ Using WASA, WASA Report 96-7, 1996.
- [194] J. Stepaniak, Dilepton pair production in proton proton interactions as a background for $\eta \rightarrow e^+e^-$ decay, WASA Memo 98-8, 1998.
- [195] A. I. Titov, B. Kämpfer, and E. L. Bratkovskaya, Phys. Rev. **C 51**, 227 (1995).
- [196] M. Zétényi and G. Wolf, Phys. Rev. **C 67**, 044002 (2003).
- [197] K. Shekhter *et al.*, Phys. Rev. **C 68**, 014904 (2003).
- [198] W. K. Wilson *et al.*, Phys. Rev. **C 57**, 1865 (1998).
- [199] R. Maier, Nucl. Instr. Meth. **A 390**, 1 (1997).
- [200] A. Lehrach and D. Prasuhn, Annual Report of the IKP 2003, <http://www.fz-juelich.de/ikp/publications/AR2003/en/contents.shtml>.
- [201] CELSIUS/WASA Homepage, <http://www.tsl.uu.se/wasa>.
- [202] J. Zabierowski *et al.*, Phys. Scripta **T99**, 159 (2002).
- [203] B. Trostell, Nucl. Instr. and Meth. **A 362**, 41 (1995).
- [204] C. Ekström *et al.*, Nucl. Instr. and Meth. **A 371**, 572 (1996).
- [205] H. Calén *et al.*, Nucl. Instr. and Meth. **A 379**, 57 (1996).
- [206] C. Pauly, ph.D. Thesis, Universität Hamburg, Germany, in preparation.
- [207] R. J. M. Y. Ruber, Comparing Measured and Calculated Magnetic Field, 2001, WASA Memo 01-03.
- [208] R. J. M. Y. Ruber, 1999, ph.D. Thesis, Uppsala University, Sweden.
- [209] M. Jacewicz, 2004, ph.D. Thesis, Uppsala University, Sweden.
- [210] R. J. M. Y. Ruber, Radiation hardness test of CsI for a calorimeter at CELSIUS, 1990, WASA report 2, Uppsala University.
- [211] U. Schuberth, 1995, Uppsala Dissertations from the Faculty of Science and Technology 5.
- [212] J. Zabierowski *et al.*, Nucl. Instr. Meth. **A 338**, 577 (1994).
- [213] K. Fransson, Phys. Scripta **T99**, 176 (2002).

- [214] P. Marciniewski, 2001, ph.D. Thesis, Uppsala Universitet, Sweden.
- [215] M. Drochner, W. Erven, P. Wüstner, and K. Zvoll, IEEE Trans. Nucl. Sci. **45**, 4 (1998).
- [216] P. Wüstner *et al.*, proc. 13th IEEE Real Time Conference, Montreal, Canada, May 2003.
- [217] W. Erven *et al.*, DAQ Synchronisations-Modul, 2003, internal report, ZEL, Forschungszentrum Jülich.
- [218] W. Erven and K. Zvoll, 80Mbyte Bus, 2003, internal report, ZEL, Forschungszentrum Jülich.
- [219] W. Erven *et al.*, TOF Auslesesystem mit dem TDC-F1, 2004, internal report, ZEL, Forschungszentrum Jülich.
- [220] L. Gustafsson, A small guide of the new WASA-TDC, 2003, internal report, ISV, Uppsala University.
- [221] P. Marciniewski, A proposition for a Trigger and Data Acquisition System for the WASA@COSY experiment, 2004, internal report, TSL, Uppsala University.